NAVAL POSTGRADUATE SCHOOL
MONTEREY, CALIFORNIA

THESIS

SURVEY OF PDP DATA FROM PMG DELTA II

by

Chia-Hwa Chi

June 1995

Thesis Advisor: Richard C. Olsen

Approved for public release; distribution is unlimited.

19960122 115

DTIC QUALITY INSPECTED 1

DISCLAIMER NOTICE

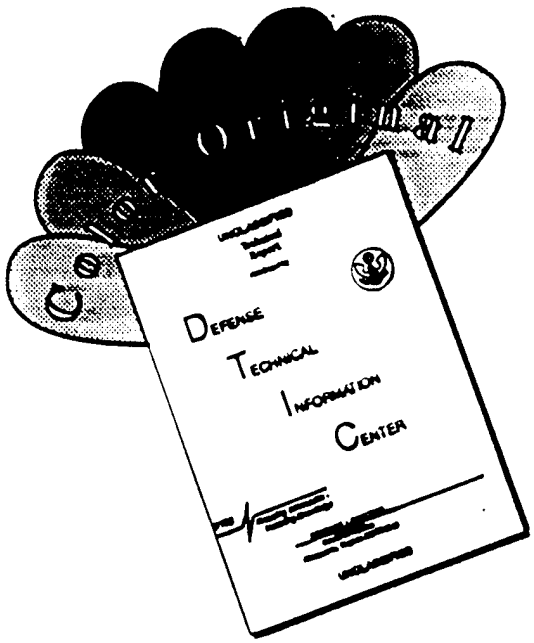

THIS DOCUMENT IS BEST QUALITY AVAILABLE. THE COPY FURNISHED TO DTIC CONTAINED A SIGNIFICANT NUMBER OF COLOR PAGES WHICH DO NOT REPRODUCE LEGIBLY ON BLACK AND WHITE MICROFICHE.

REPORT DOCUMENTATION PAGE

Form Approved
OMB No. 0704

Public reporting burden for this collection of information is estimated to average 1 hour per response, including the time for reviewing instruction, searching existing data sources, gathering and maintaining the data needed, and completing and reviewing the collection of information. Send comments regarding this burden estimate or any other aspect of this collection of information, including suggestions for reducing this burden, to Washington headquarters Services, Directorate for Information Operations and Reports, 1215 Jefferson Davis Highway, Suite 1204, Arlington, VA 22202-4302, and to the Office of Management and Budget, Paperwork Reduction Project (0704-0188) Washington DC 20503.

1. AGENCY USE ONLY *(Leave blank)*	2. REPORT DATE	3. REPORT TYPE AND DATES COVERED
	June 1995	Master's Thesis

4. TITLE AND SUBTITLE
SURVEY OF PDP DATA FROM PMG DELTA II

5. FUNDING NUMBERS

6. AUTHOR(S)
CHI, Chia-hwa

7. PERFORMING ORGANIZATION NAME(S) AND ADDRESS(ES)
Naval Postgraduate School
Monterey CA 93943-5000

8. PERFORMING ORGANIZATION REPORT NUMBER

9. SPONSORING/MONITORING AGENCY NAME(S) AND ADDRESS(ES)

10. SPONSORING/MONITORING AGENCY REPORT NUMBER

11. SUPPLEMENTARY NOTES
The views expressed in this thesis are those of the author and do not reflect the official policy or position of the Department of Defense or the U.S. Government.

12a. DISTRIBUTION/AVAILABILITY STATEMENT
Approved for public release;
Distribution unlimited.

12b. DISTRIBUTION CODE

13. ABSTRACT *(maximum 200 words)*

The Plasma Motor Generator (PMG) experiment was launched on 26 June 1993. The purpose was to verify the ability of the Hollow Cathode plasma contactor to provide a low impedance contact between the spacecraft and the ambient plasma. This thesis uses the data from Plasma Diagnostics Package (PDP) to study the effects of different modes on the rocket body. The electron data normally show a warm, or hot power law distribution with a characteristic energy of 10 's eV. There is a consistent peak in the ion data at ~10 eV, which is also a peak in phase space density (distribution function). The average potential difference due to the varying bias (+65 and +0V) between rocket and ambient plasma is ~ -4 V. Subtle changes in the spectrum occur when the Far End Package (FEP) hollow cathode is switched off. Attempts were made to estimate the potential of the Delta rocket body. The variations in the data due to environmental (orbital) effects, and the rapid sequencing of the PMG, made it difficult to analyze the data. The most of the measurements are interpreted as generated locally. The non-Maxwellian character of the electron distributions suggest a heating process has occurred. These processes may be due to collisions between gas or plasma emitted from the experiment and the ambient neutral oxygen, due to the high orbital energy of the system.

14. SUBJECT TERMS
Plasma Motor Generator, hollow cathode, tether, plasma diagnostics package, far end package, near end package.

15. NUMBER OF PAGES
132

16. PRICE CODE

17. SECURITY CLASSIFICATION OF REPORT	18. SECURITY CLASSIFICATION OF THIS PAGE	19. SECURITY CLASSIFICATION OF ABSTRACT	20. LIMITATION OF ABSTRACT
Unclassified	Unclassified	Unclassified	UL

NSN 7540-01-280-5500

Standard Form 298 (Rev. 2-89)
Prescribed by ANSI Std. 239-18

Approved for public release: distribution is unlimited.

SURVEY OF PDP DATA FROM PMG DELTA II

by

CHI, Chia-hwa

Commander, Republic of China Navy

B. S., Chinese Naval Academy, 1981

Submitted in partial fulfillment of the

requirements for the degree of

MASTER OF SCIENCE IN APPLIED PHYSICS

from the

NAVAL POSTGRADUATE SCHOOL

June 1995

Author:

Chi, Chia-hwa

Approved by: 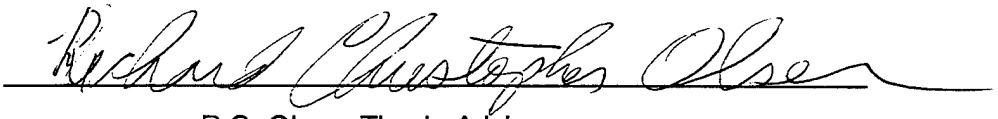

R.C. Olsen, Thesis Advisor

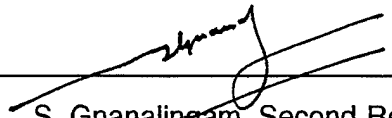

S. Gnanalingam, Second Reader

William B. Colson, Chairman,

Department of Physics

ABSTRACT

The Plasma Motor Generator (PMG) experiment was launched on 26 June 1993. The purpose was to verify the ability of the Hollow Cathode plasma contactor to provide a low impedance contact between the spacecraft and the ambient plasma. This thesis uses the data from Plasma Diagnostics Package (PDP) to study the effects of different modes on the rocket body.

The electron data normally show a warm, or hot power law distribution with a characteristic energy of 10's eV. There is a consistent peak in the ion data at ~10 eV, which is also a peak in phase space density (distribution function). The average potential difference due to the varying bias (+65 and +0V) between rocket and ambient plasma is ~-4 V. Subtle changes in the spectrum occur when the Far End Package (FEP) hollow cathode is switched off.

Attempts were made to estimate the potential of the Delta rocket body. The variations in the data due to environmental (orbital) effects, and the rapid sequencing of the PMG, made it difficult to analyze the data. The most of the measurements are interpreted as generated locally. The non-Maxwellian character of the electron distributions suggest a heating process has occurred. These processes may be due to collisions between gas or plasma emitted from the experiment and the ambient neutral oxygen, due to the high orbital energy of the system.

TABLE OF CONTENTS

I. INTRODUCTION 1

II. BACKGROUND 3

A. TETHER 3

B. ENVIRONMENT 5

1. The Ionosphere 5

2. The Magnetic Field 5

C. TETHER ELECTRODYNAMICS 6

D. HOLLOW CATHODE 6

E. THE PMG MISSION 7

1. PMG Circuit 9

2. Hollow Cathode 10

3. Plasma Diagnostics Package 10

F. LIOUVILLE'S THEOREM 11

III. OBSERVATION 15

A. METHOD OF ANALYSIS 15

B. OVERVIEW, THE EFFECT OF ENVIRONMENT 17

C. ION PEAKS (POSITIVE BIAS) 18

D. ION PEAKS (NEGATIVE BIAS) 19

E. HIGH CURRENT MODE 21

F. THE EFFECT OF HOLLOW CATHODE ON/OFF 21

G. ION OBSERVATIONS PRIOR TO DEPLOYMENT 22

IV. SUMMARY AND ANALYSIS 23

V. CONCLUSION 25

APPENDIX 63

LIST OF REFERENCES 109

INITIAL DISTRIBUTION LIST 111

ACKNOWLEDGEMENT

The author expresses his appreciation to Professor R. C. Olsen, for his scholarly advice, expertise in graphical computer analysis, infinite patience, and guidance made this work possible.

The PMG experiment was headed by Jim McCoy of NASA/JSC. The PDP instrument was built by Roy Torbert of the University of New Hampshire. Thanks go to NASA/LeRC for supporting the PDP sensor, and the UNH staff for their assistance. The concept of ionization due to orbital interactions with the ambient neutrals is due to McCoy, who in turn credits Mario Grossi and Bob Estes.

Professor Olsen acknowledges the financial support of NASA/JSC.

I. INTRODUCTION

Tether satellites provide an opportunity for exciting capabilities not possible with single satellites. In particular satellites connected by conducting wires, or electrodynamic tether, provide new possibility for communications, radar, power and control (Thompson, 1988). Electrodynamic tethers must make clear electrical contact with the ambient plasma, in order to conduct the substantial currents applications. This requirement causes a need for so-call "plasma contactors", designed to provide low impedance connections to the ambient plasma. One of the most effective candidates are hollow cathode gas discharge systems.

The NASA Plasma Motor Generator (PMG) experiment was developed to test the ability of hollow cathodes to provide a low impedance contact between the spacecraft and the ambient plasma. Tests in Low Earth Orbit (LEO) were designed to operate both as an orbit-boosting electrical motor and as a generator that converts orbital energy into electricity. Figure 1 illustrates the electrodynamic motor/generator principle investigated by the PMG experiment. Previous studies on the PMG experiment have shown evidence of the viability of hollow cathode plasma source to provide significantly lower impedance electrical paths between the spacecraft and the ambient ionosphere. The conducted currents with the plasma contactor "on" were typically measured with values much greater than with the plasma contactor "off". (Chang, 1994)

Charged particle measurements make it possible to further study the interactions between satellite and the environments. In this thesis, the author studied electrostatic analyzer and mass spectrometer measurements to determine the interactions of the tether system with the environment. Data were studied to determine the effects of tether bias modes, hollow cathode operations modes, and environmental effects (ambient plasma density).

The data used in this thesis are from the Plasma Diagnostics Package (PDP), which provided 1-2 orbits of useful data. This is the first comprehensive look at the

PDP data. These data were analyzed interactively and in detail for this thesis. Chapter II describes the background of the PMG experiment. Chapter III describes the method used to analyze the data. Utilizing the raw PMG data, the PDP spectrograms, and line plots were generated to observe and interpret the behavior of charged particles in LEO regions. Chapter IV presents the summary and analysis of the observations. Chapter V are the conclusions and recommendations.

II. BACKGROUND

A. TETHER

The electrodynamic tether is, at its basic level, a wire moving through a magnetic field. The concept of using tethers in space was first documented by Tsiolkovsky in 1895, the Russian school teacher and pioneer of astronautics, reflected in the form of a tower reaching from the Earth's equator to beyond geostationary altitudes. He postulated that upon ascending such a "Heavenly Tower", the effects of gravity would gradually diminish until they disappeared completely. This grandiose idea has received further attention in the modern space era for the purpose of lifting payloads into space, and concepts have been developed under the title "space elevator", and "orbital tower", with some scaled down but still ambitious variations proposed in the 60's and 70's (Thompson, 1988; Bekey, 1986). A long wire in space, anchored (or not) at the ends with satellites, is a stable system, due to gravity gradient effects (Bekey, 1986). As such, an electrodynamic tether offers intriguing possibilities as both a motor and generator. (Grossi, 1986)

Drell et al (1965) proposed tethers as "Alfven Engines", utilizing tether electrodynamics for propulsion and power generation. They related the new ideas to some observations associated with the Echo 1 satellite. Space tethers were promoted as a concept in the early 1970's by Mario Grossi with the encouragement of Hannes Alfven. The first tether in space experiments began in 1966 as part of the Gemini program. The effects on the motion of the tethered system were examined using the Gemini XI and XII spacecraft together with the spent stage of the Atlas-Agena D launch vehicle. Figure 2 shows the simple connection of Gemini spacecraft/target vehicle tethered configuration.

The Gemini XI flight was launched on September 12, 1966. On Gemini XI, a spin-up maneuver was successfully conducted with no evidence of significant cable-

dynamics effects. This confirmed that cable dynamics were not critical in the rotational behavior (i.e. a spin-stabilized configuration was shown to be feasible). The procedure for spinning up the tethered spacecraft/target vehicle system consisted of backing the spacecraft away from the target vehicle until the tether was almost taut, then firing the translational thrusters to provide thrust on the spacecraft normal to the line between the vehicles. The spin-up moment on the system was supplied entirely by the spacecraft translation-control system.

The Gemini XII flight experiment was launched on 11 November, 1966. Gemini XII studied the feasibility of gravity gradient stabilization. The system was initialized by various translational and attitude thrustering maneuvers by the spacecraft. This was followed by an active stabilization of the target vehicle using the target-vehicle attitude control system. The gravity-gradient stabilization orientation was successfully demonstrated in Gemini XII. (Bekey, 1986)

The next major tether experiment was TSS-1, launched in July 1992 on STS-46. The major components of the Tethered Satellite System are: the deployer system, the tether, the satellite; the carriers on which the system is mounted, and science instruments. The TSS-1 experiment worked reasonably well, until ~175 m out, when the cable snagged. The relatively short deployment restricted the $\vec{V}\times\vec{B}$ induced potential drop to ~40 V, and the resulting currents only reached ~15 mA (AW & ST, August 10, 1992). The mission was successful, however, in demonstrating successful (dynamic) control of the satellite, alleviating many fears about the mechanical behavior of the tethers.

B. ENVIRONMENT

1. THE IONOSPHERE

Tethered satellite systems operate in the ionosphere, a region of mixed neutral and ionized gas. The density of electrons in the ionosphere changes with the amount of radiation received from the Sun. During daylight the density of electrons increase and, likewise, during no daylight; the density of electron decreases. The nature of the ionosphere is neutral overall (i.e., there are equal numbers of ions and free electrons). The variation of electron density with altitude led to subdividing the ionosphere into the D, E, and F regions (as seen in Figure 3). From Figure 3, it can be seen that electron density at various altitudes during day and night will vary. Figure 4, from Katz et al (1995) shows the model ionosphere density for the PMG orbit.

The ionosphere extends from 85 km to approximately 1,000 km, and is not composed entirely, or even primarily, of ions and free electrons. Neutral air particles far outnumber charged particles and, even at the most dense layers of the ionosphere, there are rarely more than one million electron-ion pairs in a cubic centimeter. Figure 5 shows the neutral density versus the altitude (Heinz and Olsen, 1994).

2. THE MAGNETIC FIELD

Charged particle motion and tether electrodynamics are both strongly affected by the Earth's magnetic field. There is a significant magnetic field along the Earth's surface, similar to that of a bar magnet, also known as a dipole field. Figure 6 shows the general shape of the dipole field. Note that the lines emerge from the Earth in the southern hemisphere, so that the pole located in Antarctica should really be called the geomagnetic north pole. But it was felt that this confused everybody and it is called the GM South Pole. This magnetic field decreases as the distance from the Earth increases.

C. TETHER ELECTRODYNAMICS

The physics of the system is simple. The orbital motion of the deployed system results in an electrical field of the order of 200 V/km along the tether. The resulting potential difference between the ends of the tether will nominally cause the far ends to float positive and negative, with respect to the plasma at the ends of the tether. Hence, charges of the appropriate sign will flow to the orbiter and satellites, and a net current will flow through the tether. Figure 7 shows the electrodynamic tether system with electrodynamic drag. Typical ionospheric values, for an orbiting system, result in induced voltage of several kilovolts for a 5-10 km system.

In order for a complete circuit to exist, current must flow through the plasma. It is difficult for the highly magnetized plasma to conduct such currents, and it is believed that closure of the complete circuit may occur via currents along magnetic field lines down into the E-region where collisions allow currents to flow perpendicular to the magnetic field.

D. HOLLOW CATHODE

The hollow cathode, as designed for space applications, has its origin in work done in ion engine technology at TRW by Sellen (1965), and NASA/LeRC by Rawlin and Pawlik (1968), and at Hughes (Ward and King, 1987). Figure 8 shows an early design, due to Rawlin and Pawlik (1968). The primary change since that time has been the transition from rolled foil inserts to porous tungsten inserts, impregnated with barium carbonate (Ba CO_3).

This design was implemented for Solar Electric Rocket Test II (SERT-II), which flew in the 1970's, and demonstrated the viability of the technology (Kerslake, 1971). The 0.25 A (nominal) beams produced by the ion thrusters of SERT-II were effectively current and charge neutralized by external hollow cathodes, producing early evidence of their effectiveness as plasma contactors.

Olsen (1985) showed similar effectiveness in ion engine and charge control applications for data from geo-synchronous orbit.(figure 18 in Olsen 1985), ATS-6 experiments in eclipse, for example, showed that the hollow cathode could 'ground' the satellite, eliminating the substantial (Kilo Volt) potential typically found in that environment. One reason for relatively low currents in the TSS-1 mission may have been relatively high impedances at the satellite-plasma boundaries. One way to deal with this problem is to put plasma sources on the satellites. Gas discharge plasma generators, such as hollow cathodes, can provide an electrical bridge to the more diffuse ionospheric plasma. Such devices have been termed 'Plasma Contactors'. Hasting (1987) and Park and Katz (1987) have developed the basic theory of hollow cathodes in such applications. Park et al (1993) and Vannaroni et al (1992) present experimental results from laboratory work. A major purpose of the PMG experiment was to test this technology, as applied to a tether system.

E. THE PMG MISSION

The hardware of the PMG experiment consisted of four major subsystems, 1.) the Far End Package (FEP), 2.) Near End Package (NEP), 3.) Electronics interface box (SEDS), and 4.) Plasma Diagnostics Package (PDP). This assembly was attached and carried aboard the second stage of an Air Force Delta-II rocket. The rocket was launched at 13:27 GMT on June 26, 1993. After a third stage separation and a second stage fuel depletion-burn, the PMG system was left in an elliptical orbit, approximately 193 x 869 km, at a 25.7 degree inclination. The FEP was spring-ejected from the Delta-II second stage at approximately 2000 seconds Mission Elapsed Time (MET), at a rate of 2 - 3 m/sec, trailing a 500 m conducting wire from the PMG tether deployer assembly. Within minutes, the two-body tether system stabilized in a gravity-gradient configuration with the FEP above the Delta-II second stage. A summary of key events during the flight sequence is shown in Table I.

Table I. PMG Mission Timeline

EVENT	*EVENT ID*	*PMGT (sec)*	*GMT (hh:mm:ss)*
Launch	1	-1600	13:27:00
End second stage depletion burn	2	-46	13:52:54
PMG power on	3	0	13:53:40
Electrometer calibration (64 sec)	4	251	13:57:51
FEP start sequence	5	317	14:03:08
NEP start sequence	6	329	14:03:20
Start continuous current read (242 sec)	7	364	13:59:44
Begin FEP/tether deployment	8	400	14:00:20
End continuous current read	9	606	14:05:50
High current mode (44 sec)	10	607	14:05:51
First standard data frame (61 sec)	11	651	14:04:31
Day → night (spacecraft)	12	1170	14:13:10
Geographic equator (asc)	13	2147	14:29:28
Apogee (868 km)	14	2469	14:34:49
Magnetic equator cross (asc)	15	2545	14:36:05
High current mode (44 sec)	16	2853	14:41:13
High current mode (44 sec)	17	3194	14:46:54
Night → day (spacecraft)	18	3259	14:47:59
High current mode (44 sec)	19	3654	14:54:34
Geographic equator cross (dec)	20	5054	15:17:54
Perigee (194 km)	21	5314	15:22:14
Geomagnetic equator cross (des)	22	5416	15:23:56
Day → night (spacecraft)	23	6887	15:48:27
Geographic equator cross (asc)	24	7850	16:04:19
Apogee (868 km)	25	8190	16:10:10
Magnetic equator cross (asc)	26	8320	16:12:20
Night → day (spacecraft)	27	8970	16:23:10
High current mode (44 sec)	28	9031	16:24:11
High current mode (44 sec)	29	9313	16:28:53
Last electrometer data frame	30	9652	16:34:32
Electrometer calibration (33 sec)	31	9655	16:34:35
High current mode (through LOS)	32	9688	16:35:46
Geographic equator cross (dec)	33	10,761	16:53:39
Magnetic equator cross (dec)	35	11,158	16:59:16
Day → night (spacecraft)	34	12,600	17:23:36
Geographic equator cross (asc)	36	13,552	17:39:10
Magnetic equator cross (asc)	37	14,033	17:47:20
Loss of telemetry	38	14,415	17:54:33

Figure 9 shows the altitude of the rocket. Note that perigee was in the middle of the day, so the day-night effect reinforces the altitude effects on local plasma density.

1. PMG CIRCUIT

The PMG circuit diagram, shown in Figure 10, was designed to measure currents and potentials in the tether, as a function of bias voltage. The NEP electrometer provided tether current measurements for all combinations of bias voltage (+65, +35, +0, -0, -65, -130 V.) and load resistances (2.2MΩ, 0Ω, 100Ω, 200Ω, 500Ω). For several short intervals (e.g. 2853 - 2897 seconds PMGT), the power supply was bypassed, so that larger currents (e.g. ~1A) could flow. This was termed high current mode and these times are noted in Table I. Unfortunately, the electrometer did not function properly during these intervals. The PDP data are valid at these times.

Primary results from the current measurements were obtained by Chang (1994). Figure 11 illustrates the standard data frame sequence. Each voltage, resistance sweep took approximately 10 seconds. The bias voltages was varied at 10 second intervals, with the load resistance stepped at 2 second intervals. The 2 second dwell at 2.2 MΩ produces a tether potential measurement; subsequent measurements provide current at 500 Ω, 200 Ω, 100 Ω, and 0 Ω load resistance. There is ~160 Ω resistance in the tether and circuitry, besides the load resistance. In addition to the sequence of events illustrated here, the FEP hollow cathode was shut off for 10 seconds in every 90 seconds.

Figure 12 shows the deployment data. The current drops sharply once the FEP separates from the Delta second stage. The initial sequence of variations is not clearly understood, but it is apparent that the system quickly settles down to ~0.075 A, with a modulation of ~5 to 10 mA. The large drops at 450 and 550 seconds PMGT are due to the cycling of the FEP hollow cathode.

Figure 13 shows the currents measured at +65 V bias, and -130 V bias, for zero load resistance over the entire mission. Note that the currents in the negative

direction are uniformly larger in magnitude than the positive currents, even though the net potential in that direction is less than the net potential for +65 V bias. This is because the large surface area of the Delta rocket body provides a very efficient collector of electrons. The downward spikes in the +65 V trace are again due to the FEP cycling. Apparently, when the FEP hollow cathode is off, the FEP cannot collect a significant electron current. Katz et al (1995), have explained much of the physics behind these results, though their current estimates are slightly high.

Figure 14 shows the contrast for hollow cathode "on" vs "off". When the hollow cathode was on, the measured potential across the 2.2 MΩ load resistance was approximately 20 V higher than when hollow cathode was off. This implies a substantial plasma impedance at the FEP, when the hollow cathode is off (~1MΩ).

2. HOLLOW CATHODE

The hollow cathode system configuration is illustrated in Figure 15. There were two hollow cathodes on the PMG system, one at each end, the hollow cathode design used for PMG provides a supply of Xenon gas within a hollow electron emitter cathode heated to approximately 1,300°. A strong voltage gradient between the cathode and corresponding anode plate establishes a plasma discharge to create a partially ionized gas. The free expansion of this ionized gas plume from the hollow cathode into the surrounding ionosphere creates a region of increased plasma conductivity extending many meters into the ambient plasma.

3. PLASMA DIAGNOSTICS PACKAGE

The Plasma Diagnostics Package (PDP) provided two primary sensors for analysis, a mass analyzing ion detector, and an electron detector. Both are based on "top-hat" electrostatic analyzer designs. The ion analyzer was modified to allow coarse discrimination between Oxygen and Xenon. The objective was to separate the locally generated plasma, and ambient plasma detected at the rocket. The sensor

views were combined to cope with limited data rates. There are five particle detector pads in PDP, namely PD0, PD1, PD2, PD3, and PD4. PD0 and PD1 are the electron detectors, viewing up and down. The remaining pads are the ion detectors. PD2 and PD3 are used for Xenon, and PD4 for Oxygen.

The PDP data consists of 256 bytes of data in each frame. The 256 bytes of data consists of 120 bytes of detector accumulator counts from the first sweep, followed by another 120 bytes of accumulator counts from the second sweep, followed by 6 analog monitor bytes from the first sweep, followed by 6 more analog monitor bytes from the second sweep, follow by 1 status byte, 1 frame counter byte and 2 frame sync bytes. Each 120 bytes of detector data consists of an entire 24 step energy sweep. Therefore in every frame there are two complete energy sweeps. Each step has five detector accumulator bytes, one for each particle detector pad. Table II shows step number versus particle energy for the detectors.

F. LIOUVILLE'S THEOREM

One brief 'theoretical' element is needed to provide a basis for the charged particle analysis, this is Liouville's theorem, or phase-space invariant. Liouville's theorem discusses the density of particles in the "phase" space; whose coordinates are the position and velocity of a particle. Each particle is represented by a point in phase space. The fundamental equation with $f(\vec{r}, \vec{v}, t)$ has to satisfy is the Boltzmann equation:

$$\frac{\partial f}{\partial t} + \vec{v}\cdot\nabla f + \frac{F}{m}\cdot\frac{\partial f}{\partial \vec{v}} = \left(\frac{\partial f}{\partial t}\right)_c \qquad (1)$$

Where F is the force acting on the particles; the right hand side represents any residual contribution, due to collision, to the rate of change of f. Since we shall be dealing only with the density of the particles, we shall not have enough information to calculate the detailed forces; but only the average force. Thus, collision effects and other fluctuation effects will be missing. With the Lorentz force, Equation 1 will be cast

Table II. Energy Sweep Table

FRAME/STEP	ELECTRON ENERGY (eV)	ION ENERGY (eV)
23	2.36	2.02
22	2.85	2.86
0	4.10	4.19
21	6.15	6.07
1	6.94	6.94
20	8.71	7.98
2	9.55	9.60
19	11.38	10.97
3	13.27	12.46
18	15.85	14.96
4	19.50	17.03
17	22.25	19.52
5	27.30	23.27
16	30.90	26.48
6	36.80	31.30
15	43.65	35.80
7	51.15	42.80
14	60.15	48.70
8	70.40	57.70
13	85.75	66.30
9	99.50	75.20
12	160.00	90.10
10	252.00	102.00
11	393.50	121.90

into the form:

$$\frac{\partial f}{\partial t} + \frac{\partial f}{\partial \vec{r}} + \frac{q}{m}(\vec{E} + \vec{v}\times\vec{B})\cdot\frac{\partial f}{\partial \vec{v}} = 0 \qquad (2)$$

This equation expresses the conservation of particles in space, and it is this form that will usually be referred to as Liouville's theorem. (Gartenhaus, 1964)

Generally speaking, we can interpret this theorem as: A group of points in phase space, representing the position and velocity coordinates of a group of particles. retain the same phase-space density as it moves with time. (Cheng, 1984)

III. OBSERVATION

The purpose of this chapter is to present an analysis of the data gathered by the PDP during the PMG experiment. The first section discusses the methods of analysis. The remaining sections discuss behavioral characteristics of charged particles given varying experimental and environmental factors.

A. METHOD OF ANALYSIS

The analysis began with the creation of survey spectrograms from the raw PDP data from the PMG experiment. A typical example of such spectrograms is shown in Figure 16. The data shown were taken at local night from 1770 to 2013 second PMGT. Figure 16 is vertically separated into five sections. The top three sections (PD2 - PD4) display ion information and the remaining two sections (PD0, PD1) display electron information. This figure indicates the count rate of electrons and ions in the detector versus time (seconds) and energy (eV). The horizontal axis defines time, and the vertical axis gives the energy of the charged particles. The count rate is indicated by color scale variations from black to red, with black corresponding to minimum counts, and red to maximum counts. Where the spectrograms show white spaces either zero counts were recorded or no data exists.

Four cycles of the PMG system are presented in Figure 16. At the beginning of the spectrogram interval (1770 second PMGT), the PMG system is in negative bias mode. The electron data appear to be saturated at this time. By 1790 second PMGT, the bias has switched to positive bias, and a diffuse electron background is observed. The system remains at positive bias until 1810 second PMGT. Early in the mission, the ion data are clearly defined during positive bias mode. The ion data show peaks in the 10~20 eV energy range during positive bias intervals. These peaks go away during negative bias. No clear peaks were found in electron data.

During the process of analysis, the author found that there were discrepancies in the PDP timing, as compared to the PMG mission timeline shown in Table I. Comparing the frame counter with the raw data from PDP, it was determined that gaps exist in the PDP data. These are presumably due to telemetry drop-acts. There was less redundancy in the PDP data scheme than in the PMG current measurement. Corrections were made by checking the PDP data frame by frame, and comparing with the data from PMG. This was fairly straightforward for small data gaps (less than one frame). Comparison with data from special intervals, such as the high current mode operations, made it possible to confirm the timing.

Line plots were created for count rate and phase space density, the distribution function was calculated as:

$$f = \frac{count\ \ rate}{E^2}$$

where E is the energy channel of the detector. Since absolute calibration was not available, additional terms such as the geometric factor have been left out. Therefore the distribution function is in arbitrary units throughout this work.

Figure 17 illustrates the PMG data in line plots from 1787 second PMGT at +65 V bias (The rocket was in eclipse, at 770 km altitude). The upper left window presents the ion count rate versus energy, with the solid line representing the data from PD2, the "+" for PD3, and the "*" for PD4. The lower left window presents electron count rate versus energy, with the solid line representing data from PD0, and diamond signs for PD1 data. The upper and lower right windows presenting distribution function versus energy plots for ions and electrons respectively, using the same symbols to indicate the pad. The time in seconds is given above the lower left hand figure (have 1787 second). The value given in parenthesis is the corrected (true) time, which can be used for comparison to the PMG data. Figure 18 shows another example, taken 5 seconds later, at 1800 second PMGT. Comparing Figure 18 with Figure 17, the electron count rate has decreased with time, and the ion peak has shifted to lower

energy. However, the spectra are otherwise similar. Note that the vertical axes are logarithmic. In this format Maxwellian distributions will appear as straight lines in the distribution function plots. Peaks in the ion data are most easily identified in the count rate plots. However, we will be using the distribution function plots to look for shifts in potential, that is, to make use of Liouville's theorem.

Figure 17 and 18 shows a number of characteristics of the data which persist throughout the PDP data sets. First, the electron count rate is almost flat as a function of energy. Such a distribution is not Maxwellian, but rather follows a power law. The ion data show a characteristic peak in count rate and phase space density which indicate an accelerated distribution. The width is a few eV, indicating a relatively low energy plasma, but still substantially hotter than the natural plasma of the ionosphere. It is tempting to assign the ions measured in the peak the role of ionospheric plasma, accelerated to the Delta rocket body by the (negative) potential on that body. In both cases, a -20 V potential is implied. An alternative is to consider the possibility of a source region near the vehicle, at a potential +20 V with respect to the vehicle.

B. OVERVIEW, THE EFFECT OF ENVIRONMENT

Environmental effects were an important factor in the PMG experiment. Most are considered to be due to variations in ambient plasma density (as seen in Figure 4). The substantial variations in operational mode make it difficult to understand spectrograms on longer time scales. An overview figure was created, however for data taken at positive bias. The data were scanned frame by frame, and Figure 19 was constructed from the selected positive bias data. There are some fine scale features due to variations in bias which were not eliminated. There is a precipitous decrease in the ion flux at 0.6 hours, which appears to be instrumental in nature, as though a high voltage supply had failed. Peaks remain visible (in daylight) at ~10 eV. There is a substantial increase in ion flux at 1.0 and 2.5 hours, apparently associated with night-day transitions. In the electron data, there is a persistent peak at 20 - 30 eV

from 1.0 to 2.0 hours.

Figure 20 shows data from early in the mission, at 1368s (0.38 hours). During the period, a peculiar peak was found in the electron data during positive bias operations (see spectrograms in Appendix). The peak is apparent in the PD0 measurements (the solid line)of the electron count rate plot. The peak is at ~30 eV. The distribution function plot shows a modest peak, or inflection as well. The energy of these peaks decreased monotonically with time during each tether bias sequence. Figure 21 shows the observations 10 seconds later. The peak has dropped to ~20 eV, and there is now a distinct local maximum in the distribution function at this energy. This features was not obviously present in the daylight data which followed.

Figure 22 shows the PMG data from ~1.25 hours, shortly after the transition from night to day. At this time, the first (local) maximum in the electron density is encountered (as seen in Figure 4). There is a peak in the ion data at 20 eV. There is a very small peak in the electron as well, but the distribution function is monotonically decreasing. The daylight data from 1.0 - 2.5 hours all show this enhancement in the electron flux at 20 - 30 eV. There are particularly strong electron fluxes at 1.67 hours, during the interval of peak. Figure 23 illustrates the data from ~1.67 hours. The electron data show a large peak in count rate at 20 eV, but the distribution function is still monotonically decreasing. The distribution function has a characteristic energy of 10 - 20 eV, which is 2 orders of magnitude larger than the ambient electron temperature. There is a persistent peak at 10 eV in the ions. Finally Figure 24 compares the electron distribution function at perigee and apogee.

C. ION PEAKS (POSITIVE BIAS)

Variations in the ion data with PMG bias mode could be followed in the PDP data. Figure 25 illustrates a typical example of these data from PD2. The solid line shows the 0 V bias data, the dashed line shows the ion data for +65 V bias. The bold line shows a background level of one count per accumulated. The peak shifts by ~4 V

as the bias is changed. These change were measured for the first 2,000 seconds of the mission. Analysis of the data after 2,120 PMGT is neglected, because the data in the ion detector could no longer be analyzed in this way (as seen in Figure 19). The results are given in Table III. From Table III, it can be seen that there is a difference of ~-4 v during daytime. During the nighttime the magnitudes of the potential increase, as do the magnitudes of the deltas.

D. ION PEAK (NEGATIVE BIAS)

Curiously, the ion data showed clear spectra late in this mission, for negative bias (note again, Figure 19 is for positive bias data only). Figure 26 is a spectrogram with such "ion peaks". Compared to the "normal" data shown in Figure 16, the ion fluxes during negative bias are much lower (This may be due to changes in the instrument). There are clear peaks, however as can be seen in the PD2 and PD3 data at 8600, 8660, 8720, 8780, and 8900s. In each pair of peaks, the first, lower peak, is at -65 V bias, the higher peak at -130 V bias. The data at ~8600 seconds PMGT are shown in line plot form in Figure 27. The peak at 25 eV comes at -65 V bias (8613s), the peak at 66 eV corresponds to -130 V bias (8624s). Converting the count rate to distribution function, as shown in Figure 28, gives a different perspective on the ion peak. The lower energy peak (8613s) becomes a monotonically decreasing function, and could simply be interpreted as a warm, but non-Maxwellian distribution. The higher peak (8624s) becomes noisy below 50 eV, and can either be interpreted as flat below that energy in phase space density, or as a broadly peaked distribution from 50 - 80 eV. A second example shows similar data (as seen in Figure 29, Figure 30), again with broad peaks in count rate. Note that, the relative height of the peaks has changed. Normally, they are about the same. The data taken at -130 V bias again show evidence of a peak in distribution function. Only one clear line spectra was found in PD3 for these bias conditions (the fluxes are usually very low in PD3). Figures 31 and 32 show the data in PD2 and PD3 at 8025 second PMGT.

Table III. The Potential Difference Between Bias

PMGT (sec)	+ 65v bias	0v bias	Difference (v)
653	-11.0v	- 6.9v	-4.1v
711	-11.0v	- 6.9v	-4.1v
772	-11.0v	- 6.9v	-4.1v
830	-11.0v	- 6.9v	-4.1v
893	-12.5v	- 8.0v	-4.5v
951	-12.5v	- 8.0v	-4.5v
1015	-11.0v	- 8.0v	-3.0v
1075	- 9.6v	- 6.9v	-2.7v
1133	-11.0v	- 6.9v	-4.1v
1191	-11.0v	- 6.9v	-4.1v
1249	-11.0v	- 6.9v	-4.1v
1310	-11.0v	- 6.9v	-4.1v
1365	-12.5v	- 8.0v	-4.5v
1429	-11.0v	- 8.0v	-3.0v
1487	-12.5v	- 8.0v	-4.5v
1547	-12.5v	- 8.0v	-4.5v
1603	-15.0v	- 8.0v	-7.0v
1661	-17.0v	- 8.0v	-9.0v
1721	-17.0v	- 8.0v	-9.0v
1779	-15.0v	- 9.6v	-5.4v
1840	-17.0v	- 9.6v	-7.4v
1901	-17.0v	- 9.6v	-7.4v
1956	-17.0v	-11.0v	-6.0v
2017	-17.0v	-11.0v	-6.0v
2075	-17.0v	- 9.6v	-7.4v

The persistence (or lack thereof) of the peak in the distribution plots is significant. A peak in count rate will occur for a Maxwellian distribution, naturally for an electrostatic analyzer. Persistence of the peak in the distribution function would imply an accelerated distribution, as found in charging peaks.

Examination of the data showed that the energies of the peaks remained relatively constant, at 66 V for -130 V bias. The peaks, observed for -65 V bias, varied more in energy, from 11 to 26.5 V.

E. HIGH CURRENT MODE

For several short intervals, the power supply was bypassed, and nominally substantial currents were allowed to flow. As noted the electrometer did not work properly at these times. Figure 33 shows the PDP data for one such interval (~3670s), shortly after the first "dawn", as the electron density is rising. The data are similar to those seen for all positive bias measurements, and in particular, the positive bias data taken just before this time are very similar. The lack of in the ion data is normal during this part of the orbit.

F. THE EFFECT OF HOLLOW CATHODE ON/OFF

One of the more interesting results from the analysis of the PMG current data was the sharp decrease in tether current observed when the FEP hollow cathode was cycled off (Chang, 1994). This effect is most easily considered immediately after deployment. Figure 34 shows the measurements from 330 to 570 seconds PMGT. The FEP hollow cathode cycles off at 450 and 550s, for a 10 second interval. There are changes in both the electrons and ions, but the shifts in the electron data are more straightforward to analyze. Figure 35 shows the electron count rate versus energy at 450 seconds PMGT, with the solid line for hollow cathode in the turned "off" position, and dashed lines for the hollow cathode on data. There is a clear increase in the electron flux from 10 - 20 eV, as seen in the spectrogram.

The distribution function plots (not shown) are almost indistinguishable. A search of the data set for further examples was difficult. Fortunately, the High Current mode was switched on full time after 9688 seconds PMGT. The FEP hollow cathode cycling was again very clear in the data (see also, spectrograms in Appendix). Figure 36 is an example from this period, which shows the largest shift found due to the FEP hollow cathode cycling. The upper curve is at PMGT 10,955 second when the hollow cathode was turned "off", and the lower two curves show the hollow cathode in the "on" position. These data might be interpreted as a change in potential. If the lower curves are shifted upwards in energy by 1 eV, they overlap the hollow cathode "off" data. By Liouville's theorem, this implies a 1 V shift in the rocket body potential.

G. ION OBSERVATIONS PRIOR TO DEPLOYMENT

One other feature of the PDP data is visible in the spectrogram, Figure 34. The hollow cathode ignited prior to separation of the FEP. The ignition sequences were designed to start 70 - 80 seconds before deployment. There is some uncertainty about the exact timing, but comparison with the PMG current measurements suggests that deployment coincides with the increase in electron flux at 345s, seen in Figure 34. The ion data show substantial fluxes before this. Figures 37 and 38 show the initial ion and electron data. The electron flux is initially low, and the distribution function resembles what might be expected for ionospheric plasma. The ion data are peaked at 20 - 40 eV, and again show evidence of a peak in the distribution function. In Figure 38, the electron flux has started to increase, white the ion energies have decreased. It is tempting to attribute these ions directly to the hollow cathode. Note that the discharge voltage for the hollow cathode is initially about 9 eV (Chang, 1994). The plasma potential in the discharge is normally close to the anode potential.

IV. SUMMARY AND ANALYSIS

During the PMG experiment, the PDP provided approximately 2 orbits of useful data, as shown in this thesis. The data from the ion detectors was questionable to some extent, and the (apparent) failure at 2000 second PMGT limited the usefulness of those data. However, the PDP data did provide a lot of opportunities for in-depth research. To summarize the observations as follow:

1. The environmental effects play an important role in PMG experiment. The electron flux in daylight is much greater than nighttime. Because of the orbital design, the rocket passed through perigee only at local noon, and, apogee at night. Therefore, a question raised is: What portion of the effects seen here are caused by day/night effects, and which are caused by altitude effects?

2. There was a persistent peak in the ion data from both the xenon and oxygen channels at ~10 eV, during 0 or positive bias. Variations in the bias (+65 V and +0V), caused the peak to shift in energy by ~ -4 V. The biggest shift observed was -9 V at 1661 second PMGT.

3. Ion peaks were also observed at negative bias. The peak observed at -130 V bias was constant in energy at 66 eV. The ion peak observed for -65 V bias, varied more in energy, from 11 to 26.5 V. These peaks were only found in the xenon data, although there was evidence of non-zero ion flux in the oxygen data (PD4) at the same time.

4. The electron flux increased during times when the FEP hollow cathode switched off. Again, these are intervals during which only very small currents are flowing through the tether. These observations may reflect an increase in the NEP potential of 0.1 to 1.0 V. The highest shift occurred at 10955 second PMGT, ~ 1 V.

From the observations stated above, the ion and electron distributions we have observed are in general inconsistent with ionospheric origins. The warm electron

distributions indicate a source of substantially heated distributions. With these, we observe ion distributions which indicate acceleration. It is not clear that the ions observed in the ion peaks are accelerated ionospheric distributions. In particular, the peaks observed during negative bias contradict such an interpretation. It appears that these must be a substantial, local, source of heated plasma, generally at a potential of +10 to +20 V with respect to the Delta rocket body.

The orbital energy at the system, at 7km/s, gives the xenon a kinetic energy of 33 eV in the ambient (atomic oxygen) frame of reference (Oxygen has a kinetic energy at 7.6 eV at 7 km/s). The ionization potentials for these atoms are 13.6 eV for oxygen, and 12.1 eV for xenon. The 33 eV kinetic energy of the xenon is more than sufficient to produce ions in collisions with the ambient oxygen atoms. This would not be unlike the ionization processes in the shock region preceding a comet. The plasma potential in this region must however be at +10 to +20 V with respect to the Delta rocket body, almost independent of the voltages applied to the tether system.

A positive potential of such a magnitude would be possible for relatively cool ions and hot electrons, since the escaping electrons will leave behind a positive space charge, resulting in enhanced positive potential.

IV. CONCLUSION

In this thesis, we attempted to estimate the potential of the Delta rocket body, but the variations in the data due to environmental (orbital) effects, and the rapid sequencing of the PMG, made it difficult to analyze the data. Instead, it was found that the plasma observed by the PDP were locally generated. The distributions have substantial characteristic energy. The non-Maxwellian character of the electron distributions suggests a heating process has occurred. The large increases in ion flux at dawn (Figure 19) are unexplained.

If there is another space experiment related to PMG in the future, it is recommended that an electron sensor with a much smaller geometric factor would be helpful to collect data, and an increase in the number of energy steps with a shorter sweep period is needed. Alternatively, fewer modes should be used on the tether, and longer intervals should be used. These changes would provide or present a better picture of the rocket-space environment interaction.

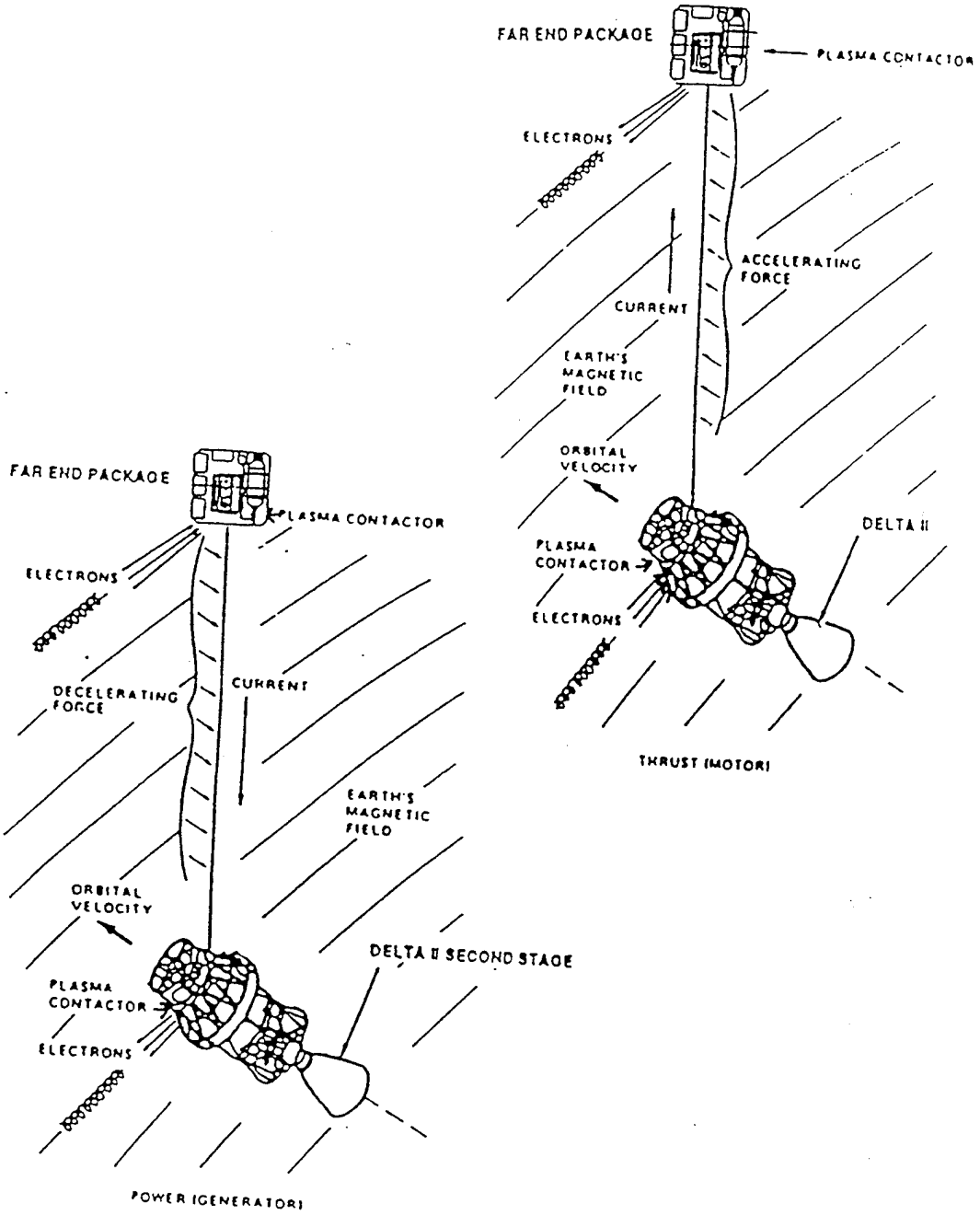

Figure 1. PMG Electrodynamic Motor/Generator Principle

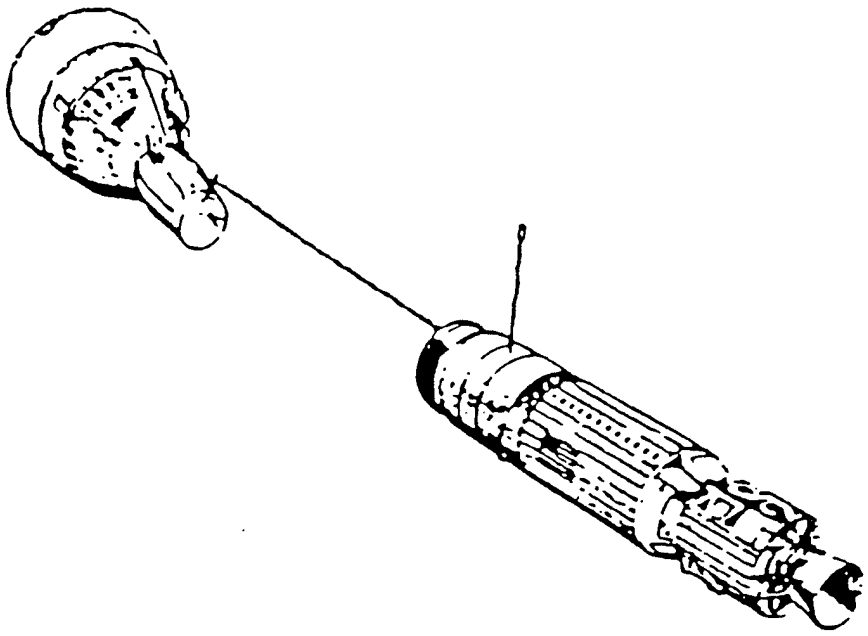

Figure 2. Gemini Spacecraft Tethered Configuration

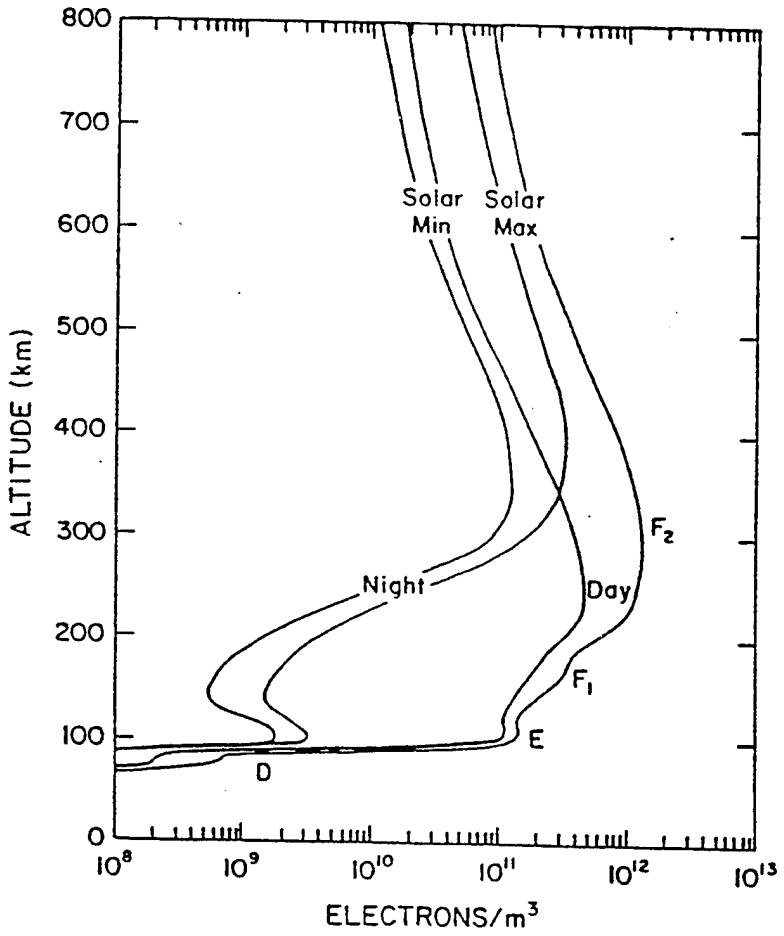

Figure 3. Plasma Density with Altitude in the Ionosphere

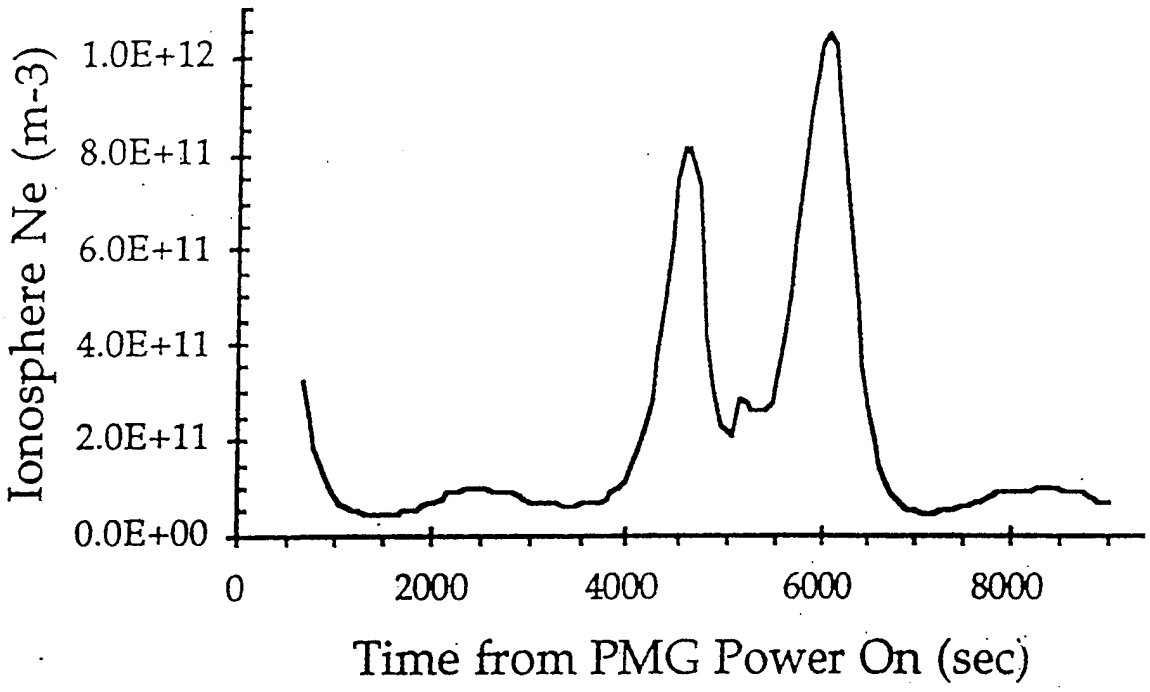

Figure 4. Ionosphere Density Model (Katz, 1995)

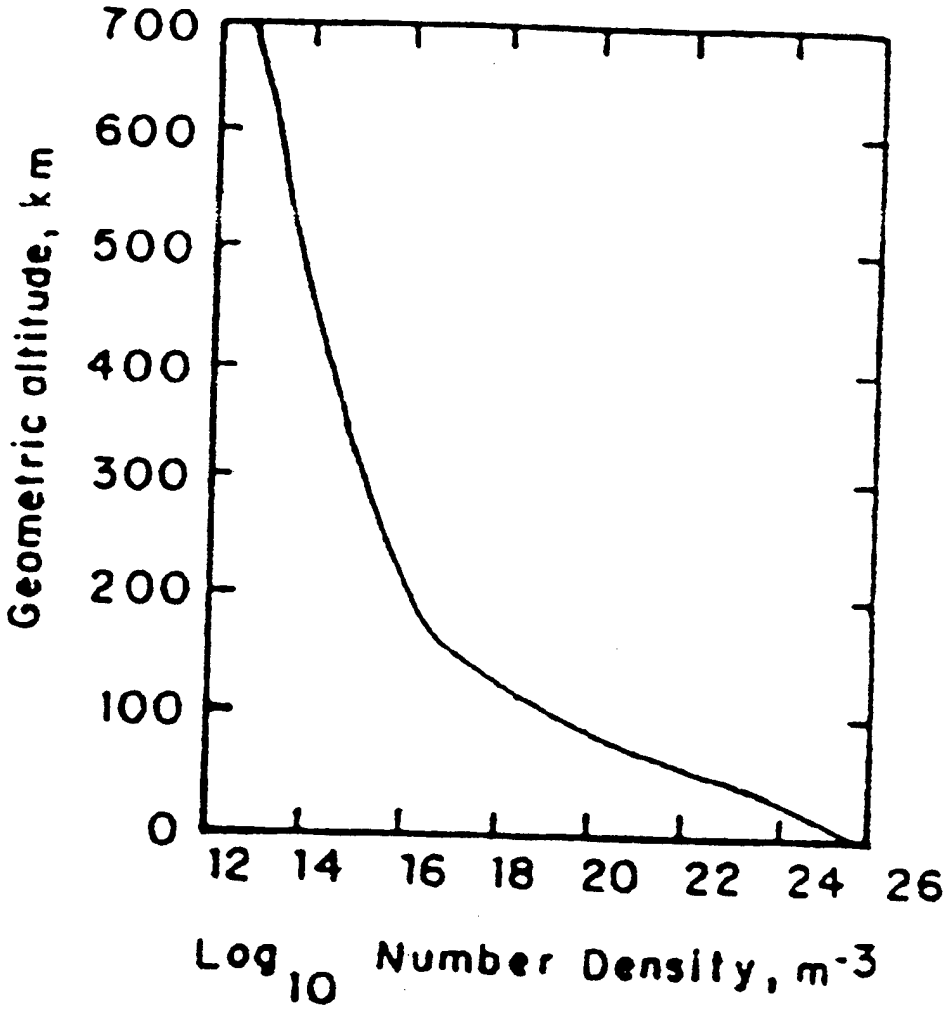

Figure 5. The Neutral Density with Altitude in the Ionosphere

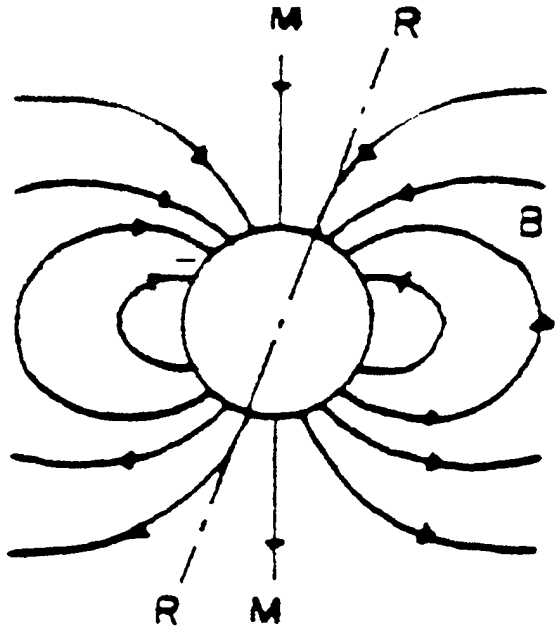

Figure 6. Earth's Dipole Field

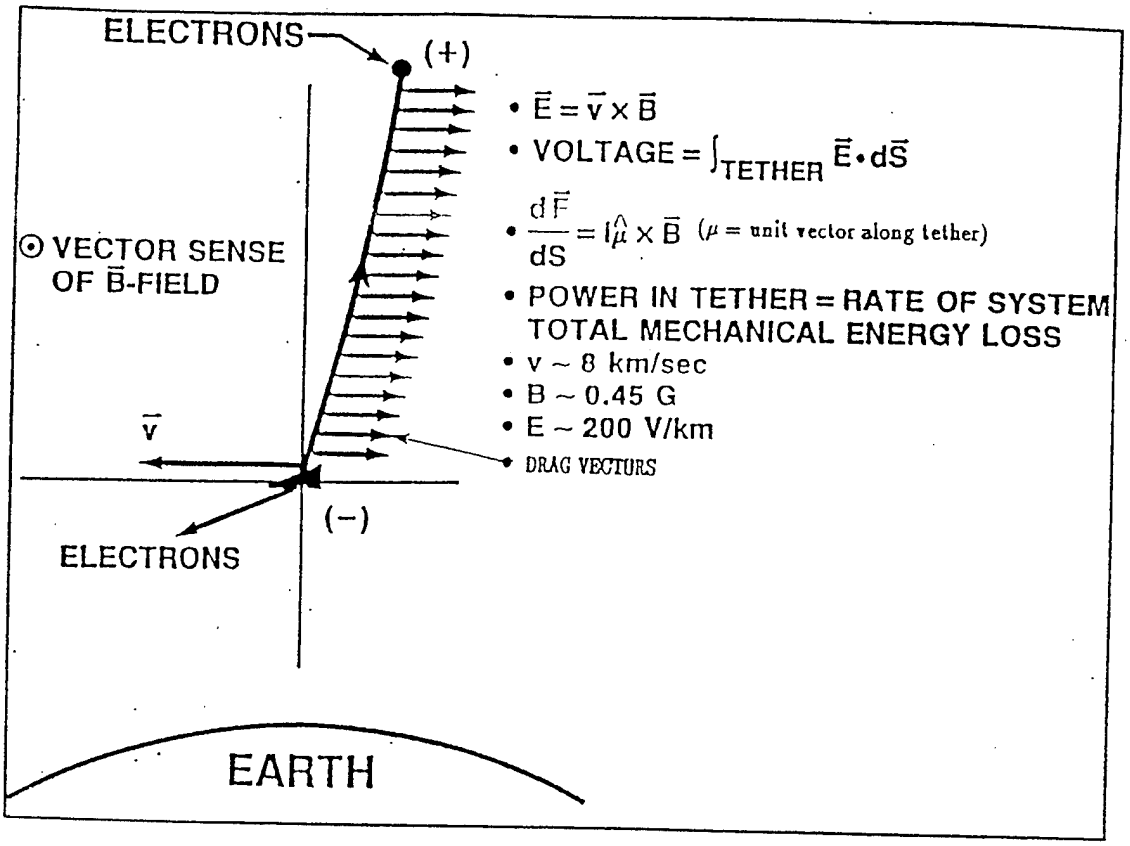

Figure 7. Electrodynamic Tether System (Yoon, 1988)

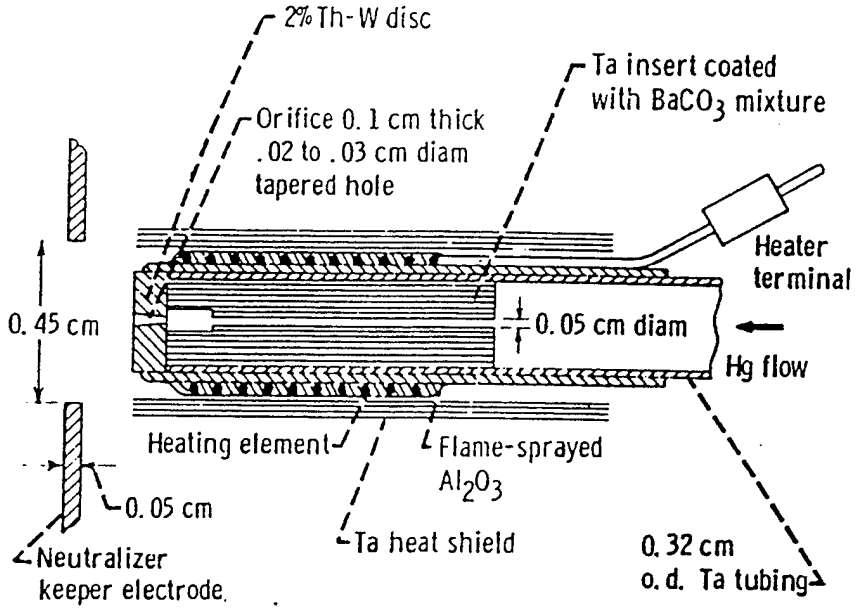

Figure 8. Plasma-bridge Neutralizer Cathode

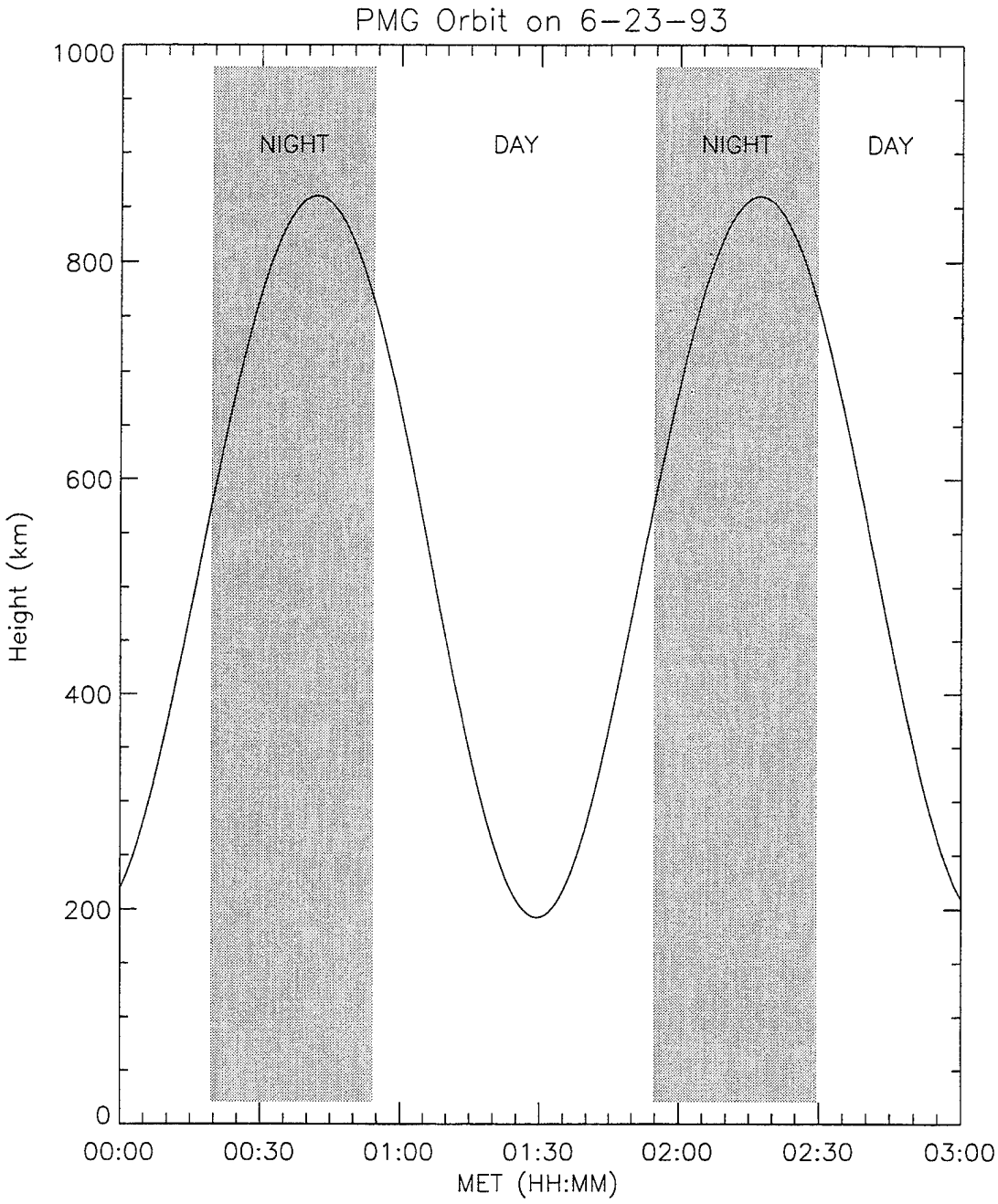

Figure 9. Altitude of Orbiter

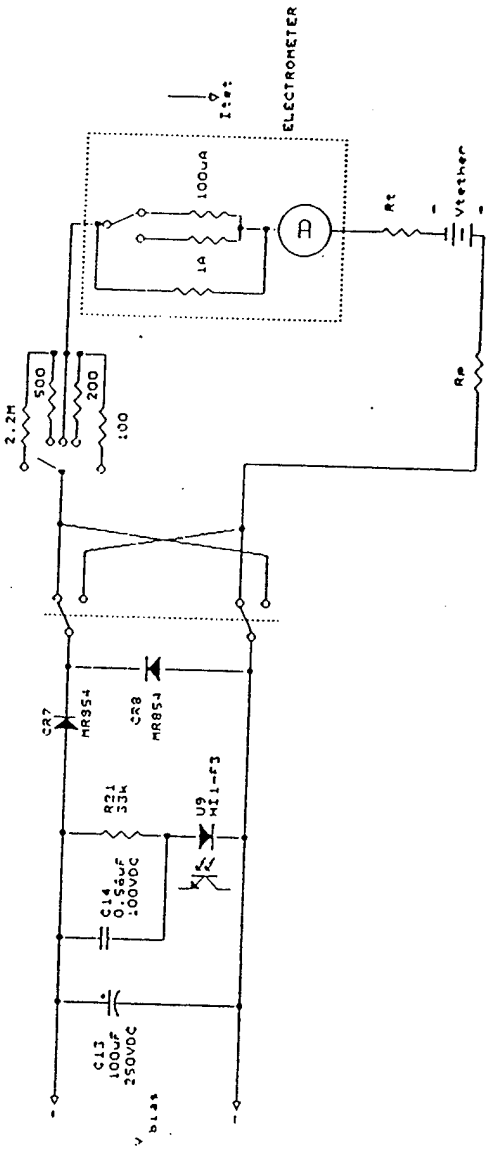

Figure 10. PMG Circuit Diagram

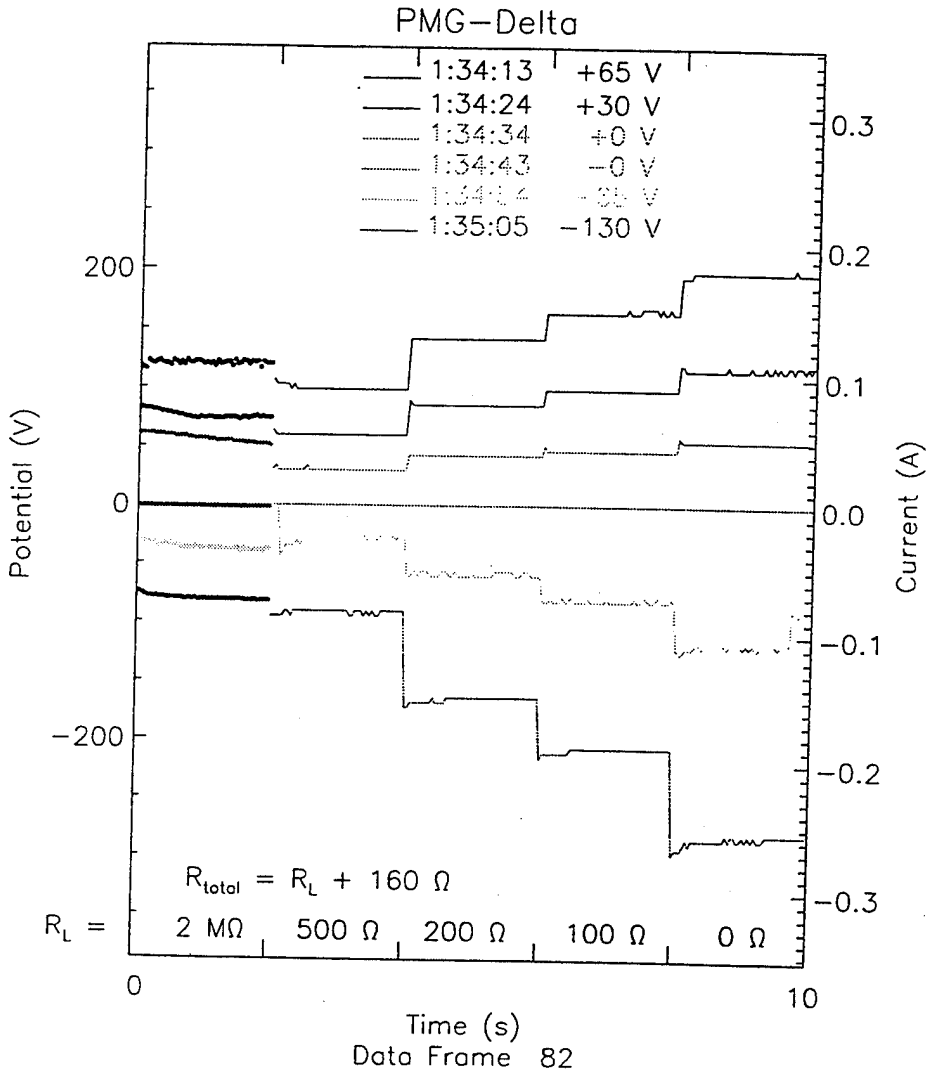

Figure 11. Standard Data Frame Sequence (Chang, 1994)

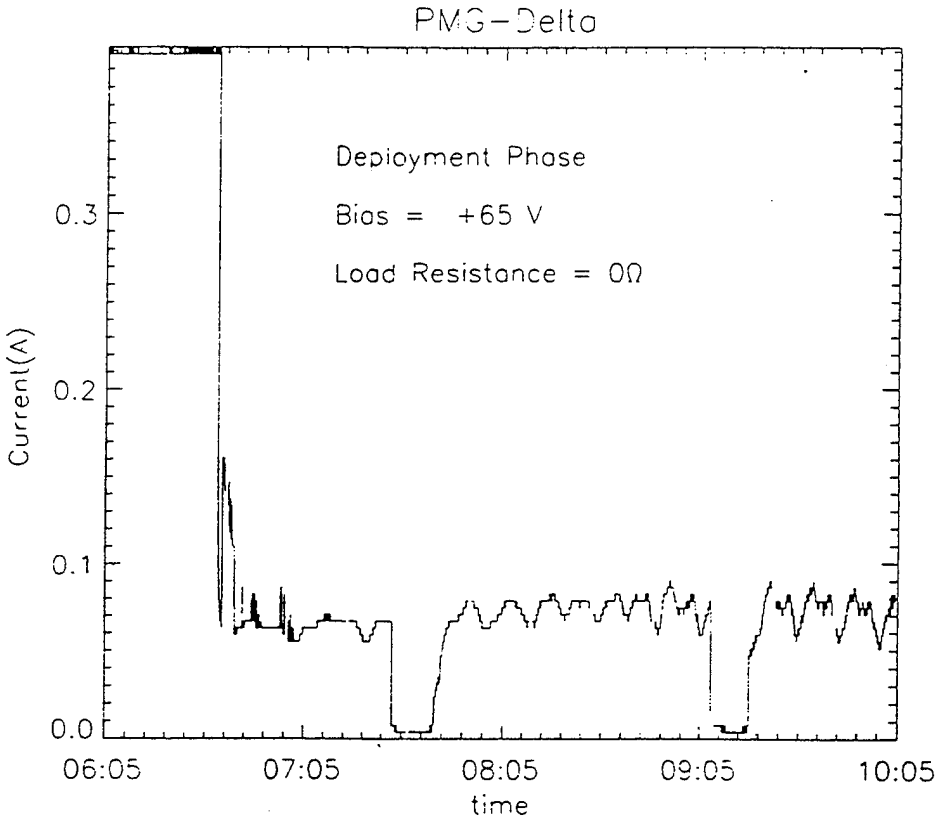

Figure 12. PMG-Delta Deployment Phase

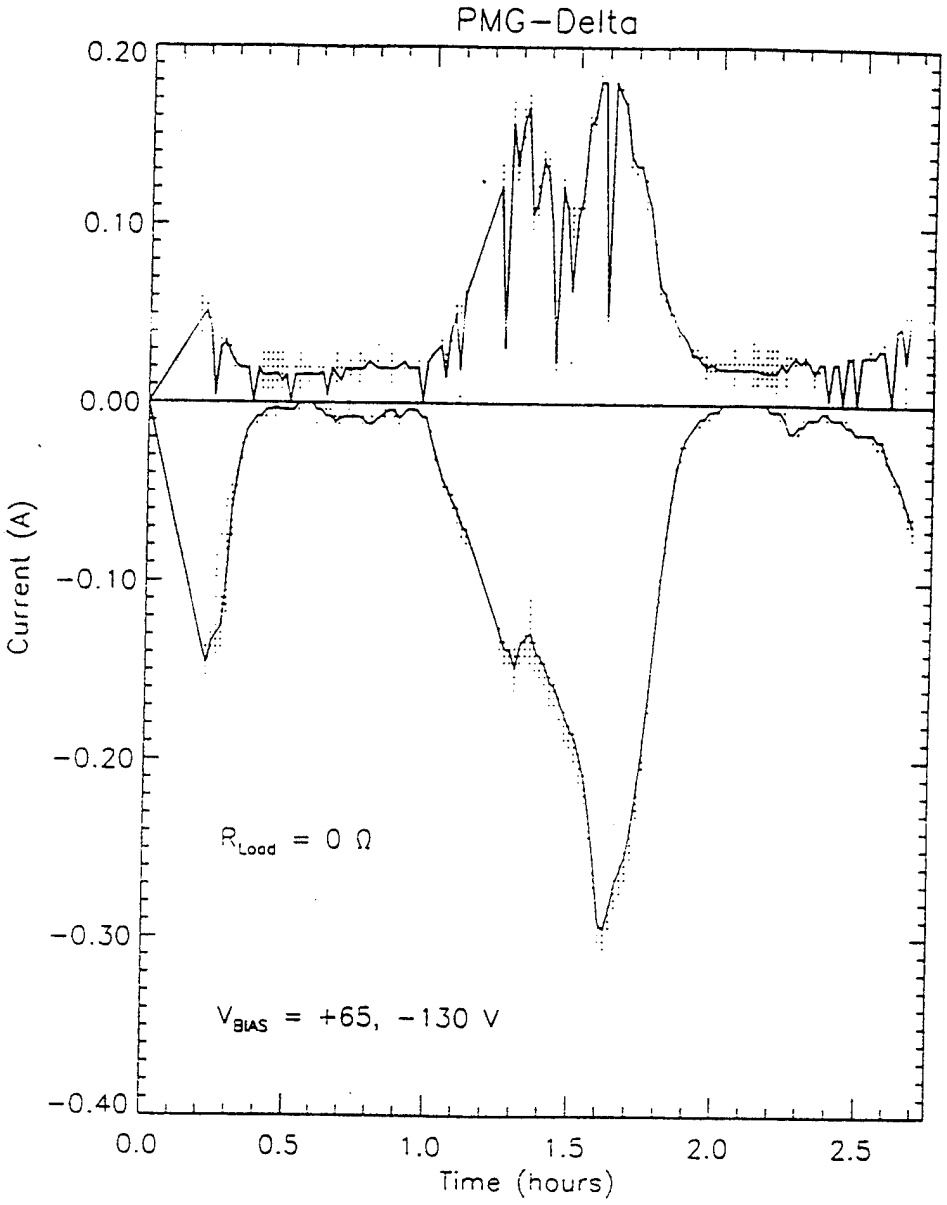

Figure 13. Current Summary

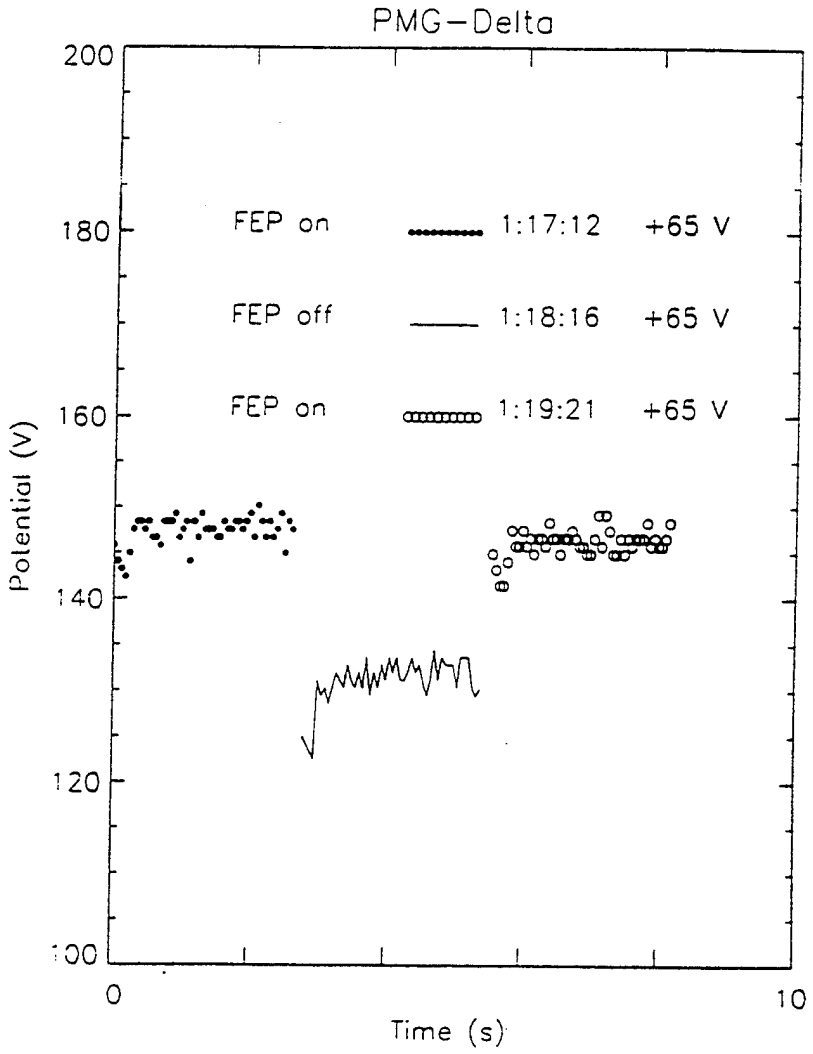

Figure 14. Potential Change with Hollow Cathode Working Condition (Chang, 1994)

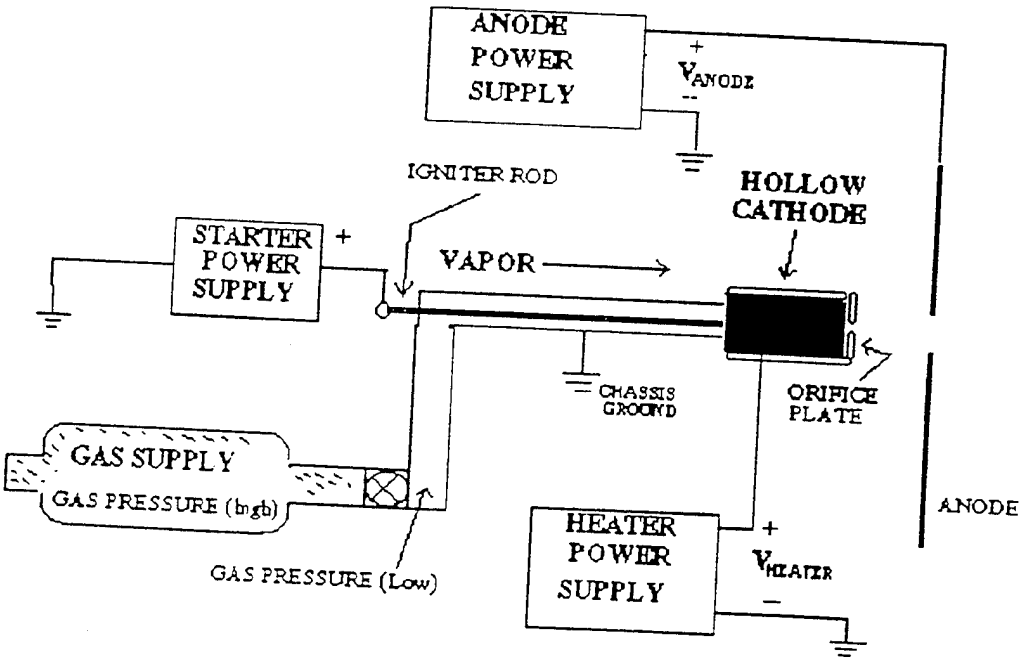

Figure 15. Schematic of PMG HC Subsystem

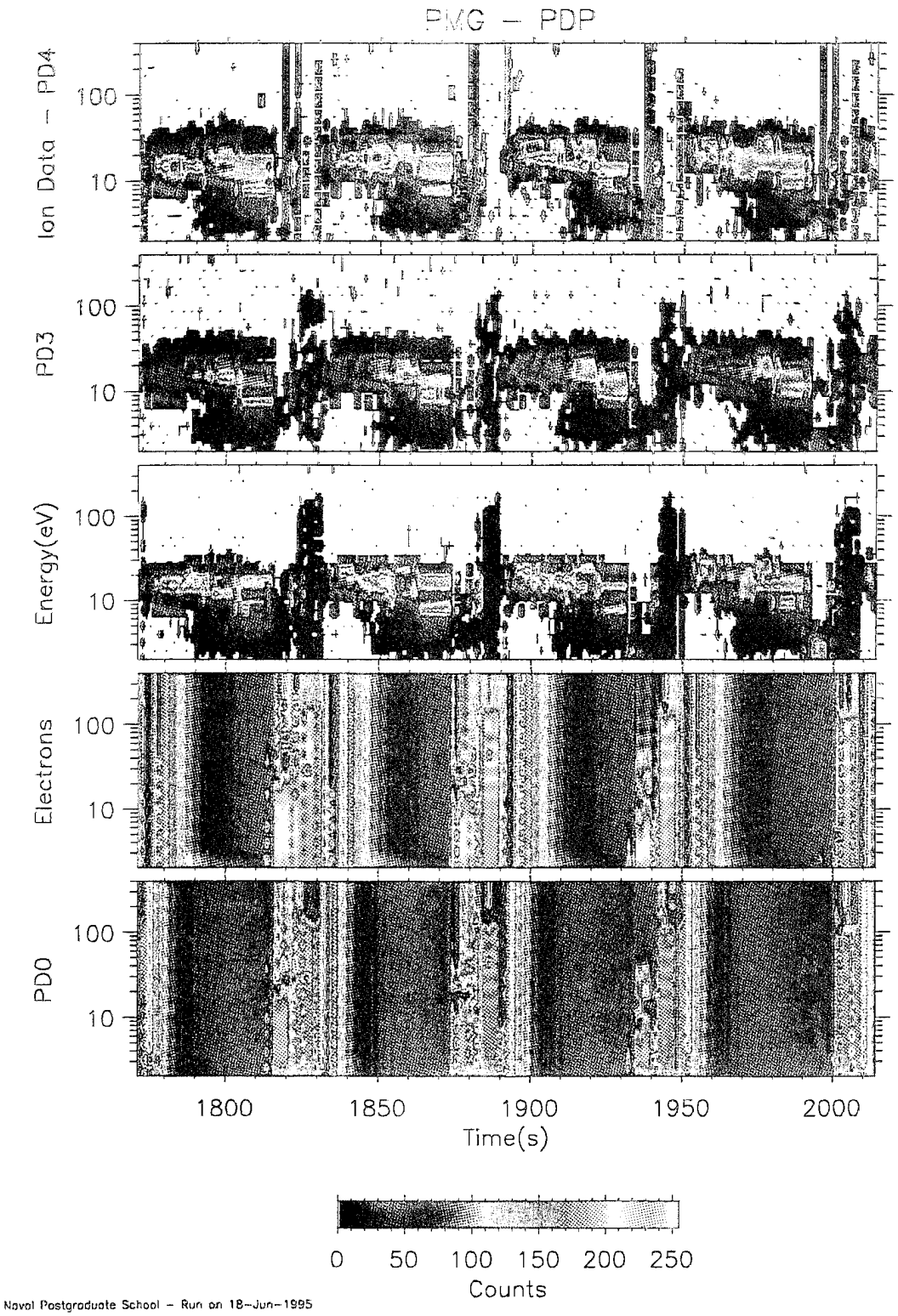

Figure 16. PDP Spectrogram from 1770 to 2013 Seconds PMGT

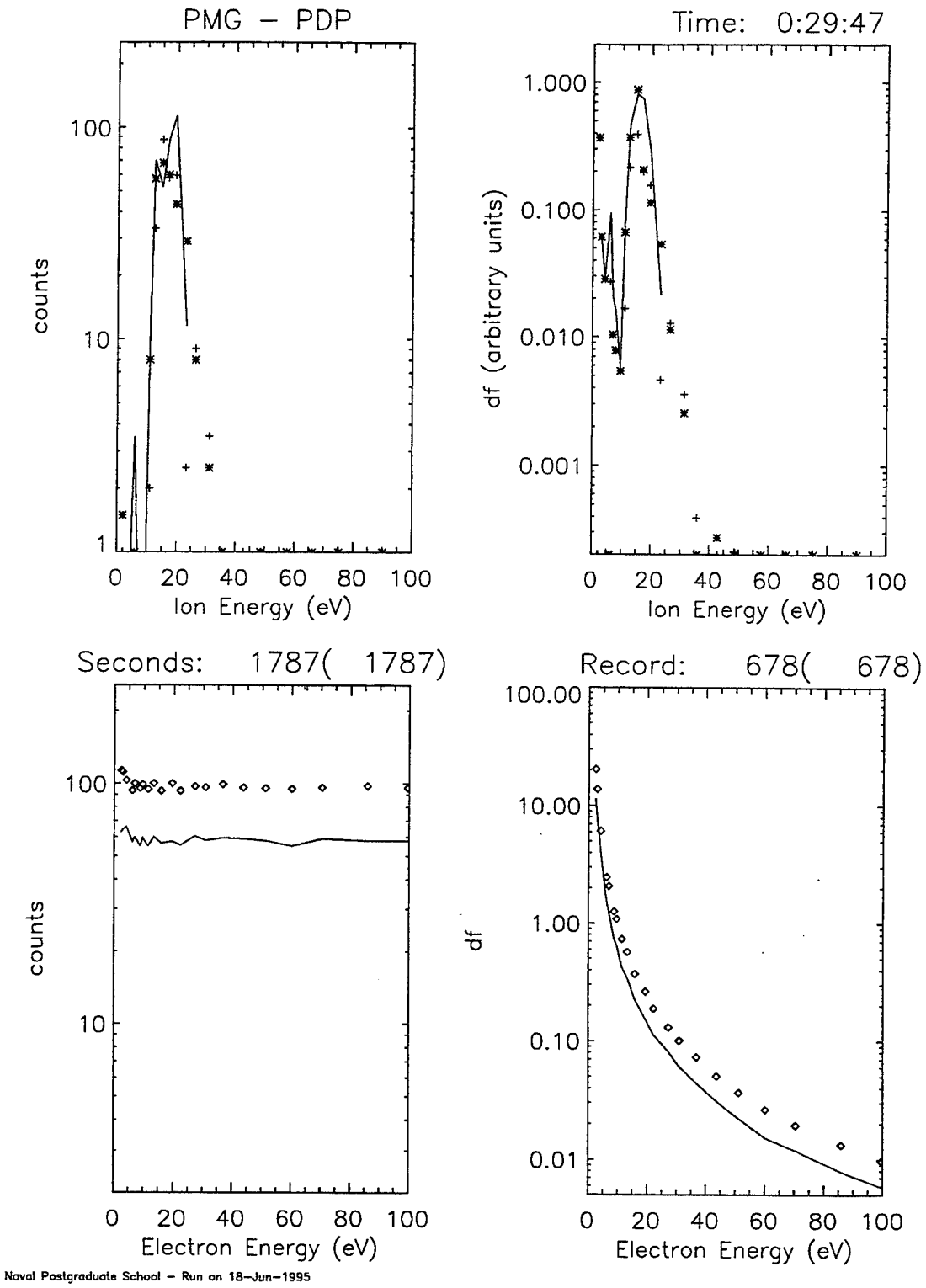

Figure 17. Line Plot of PDP Data (1787s PMGT)

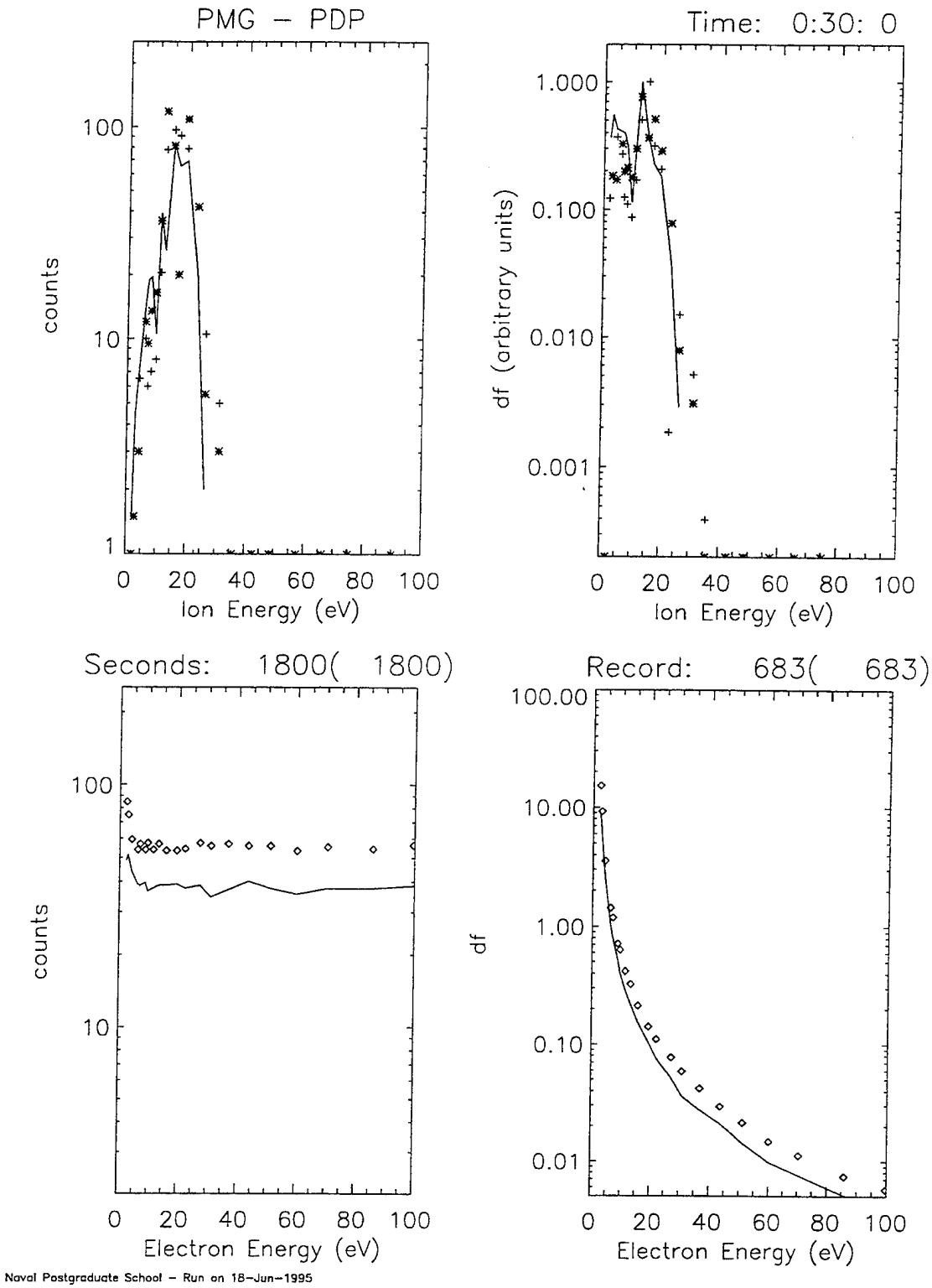

Figure 18. Line Plot of PDP Data (1800s PMGT)

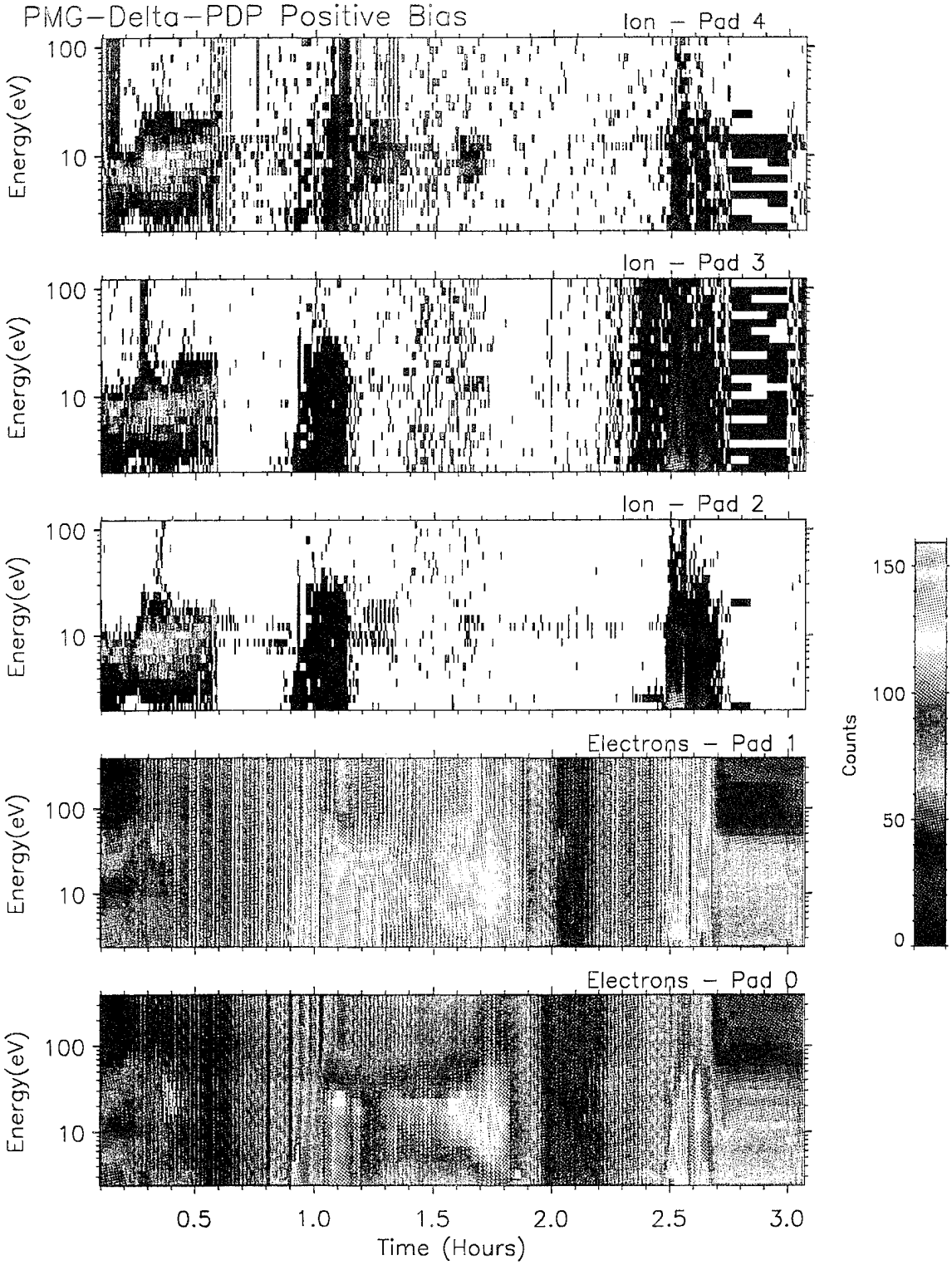

Figure 19. The Overview of Spectrogram from PDP

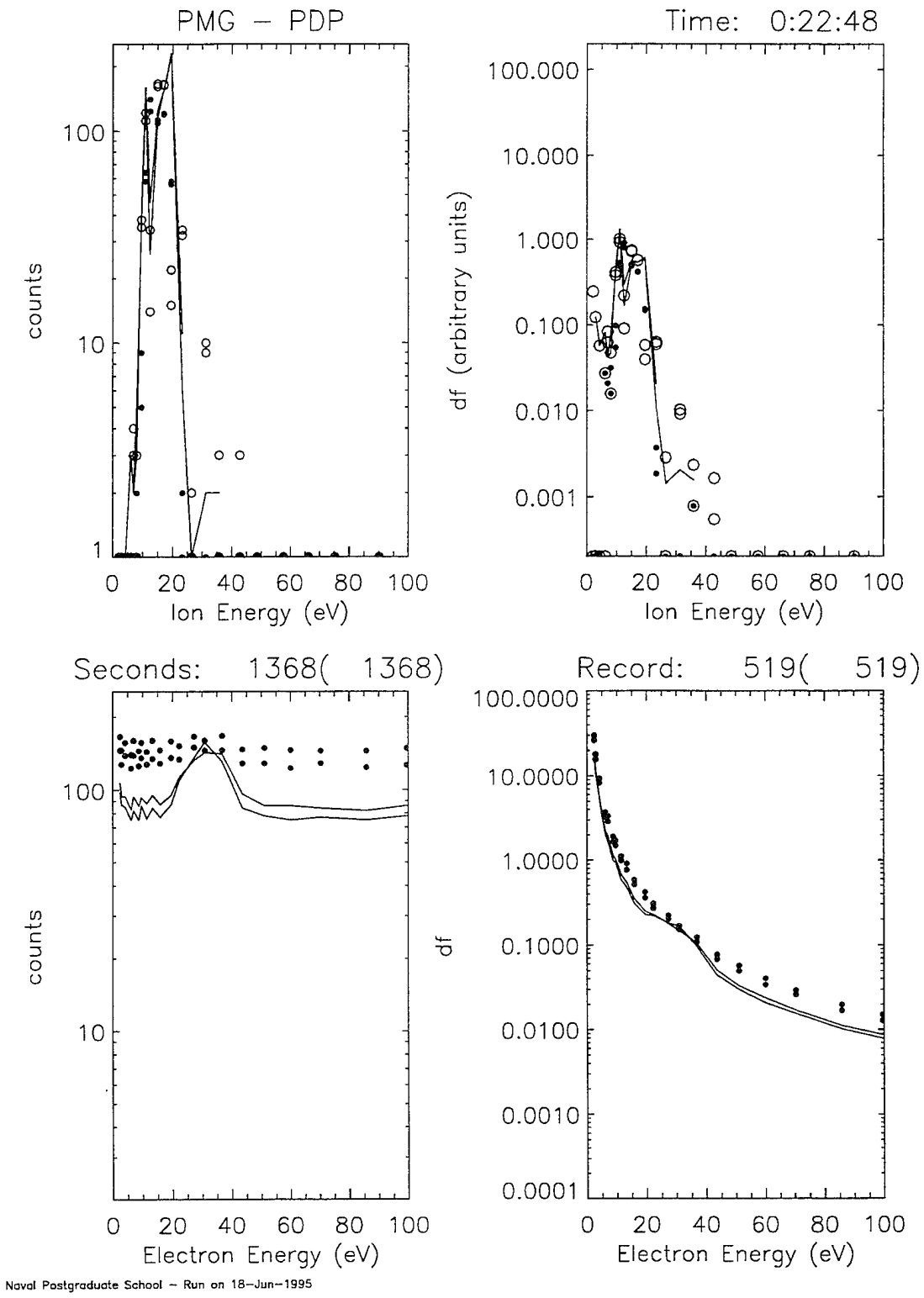

Figure 20. Line Plot of PDP Data (1368s PMGT)

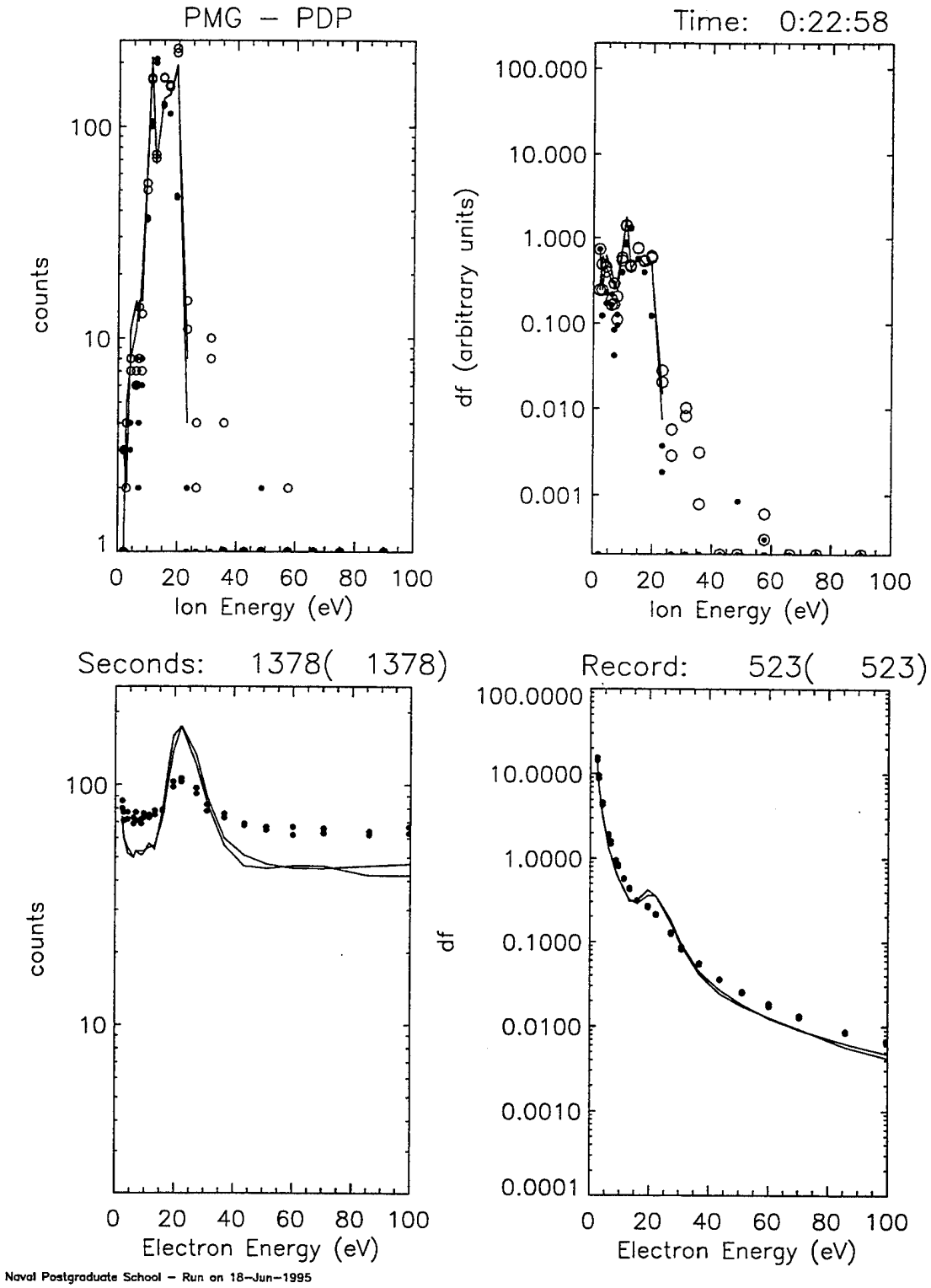

Figure 21. Line Plot of PDP Data (1378s PMGT)

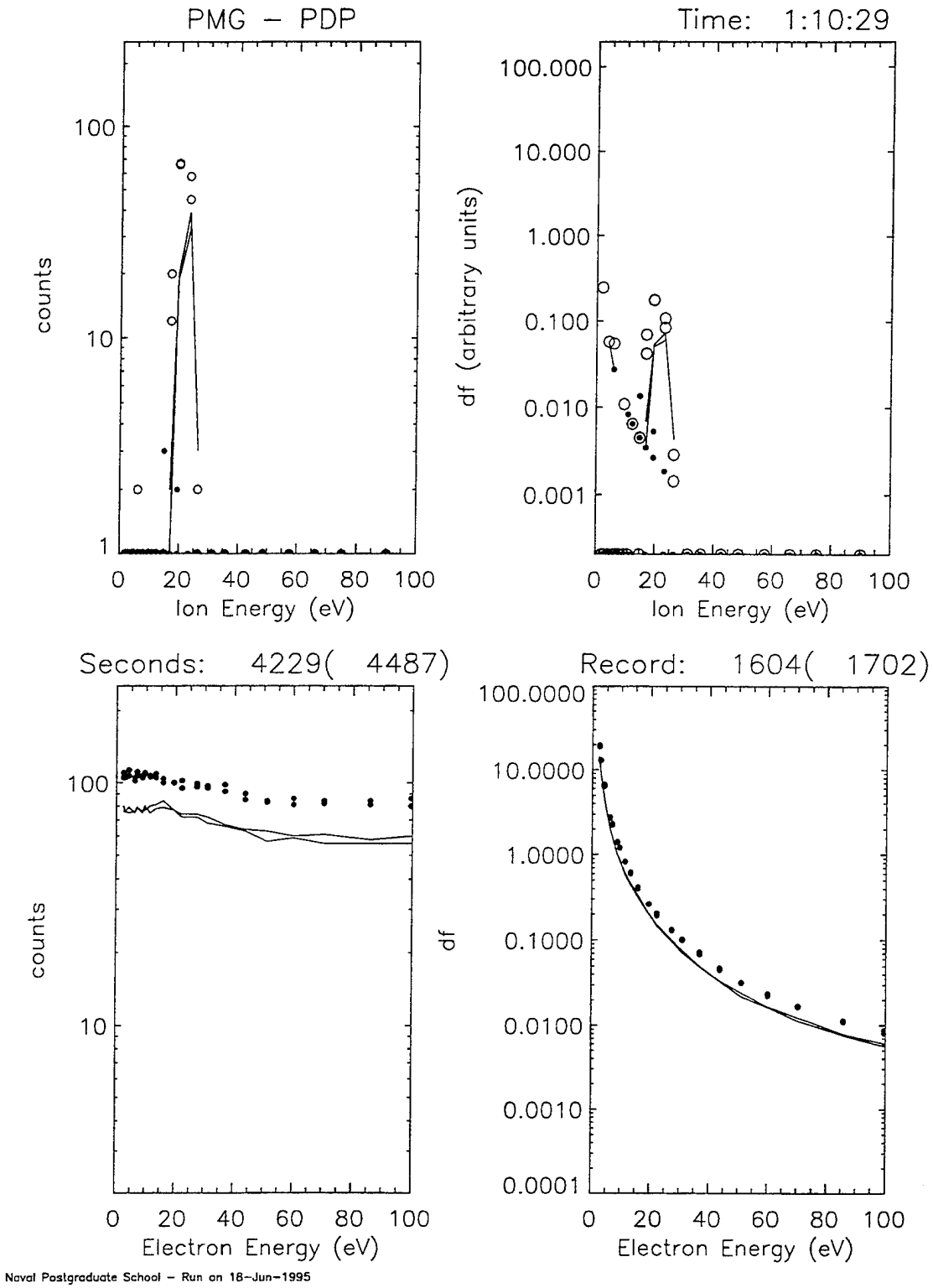

Figure 22. Line Plot of PDP Data (4487s PMGT)

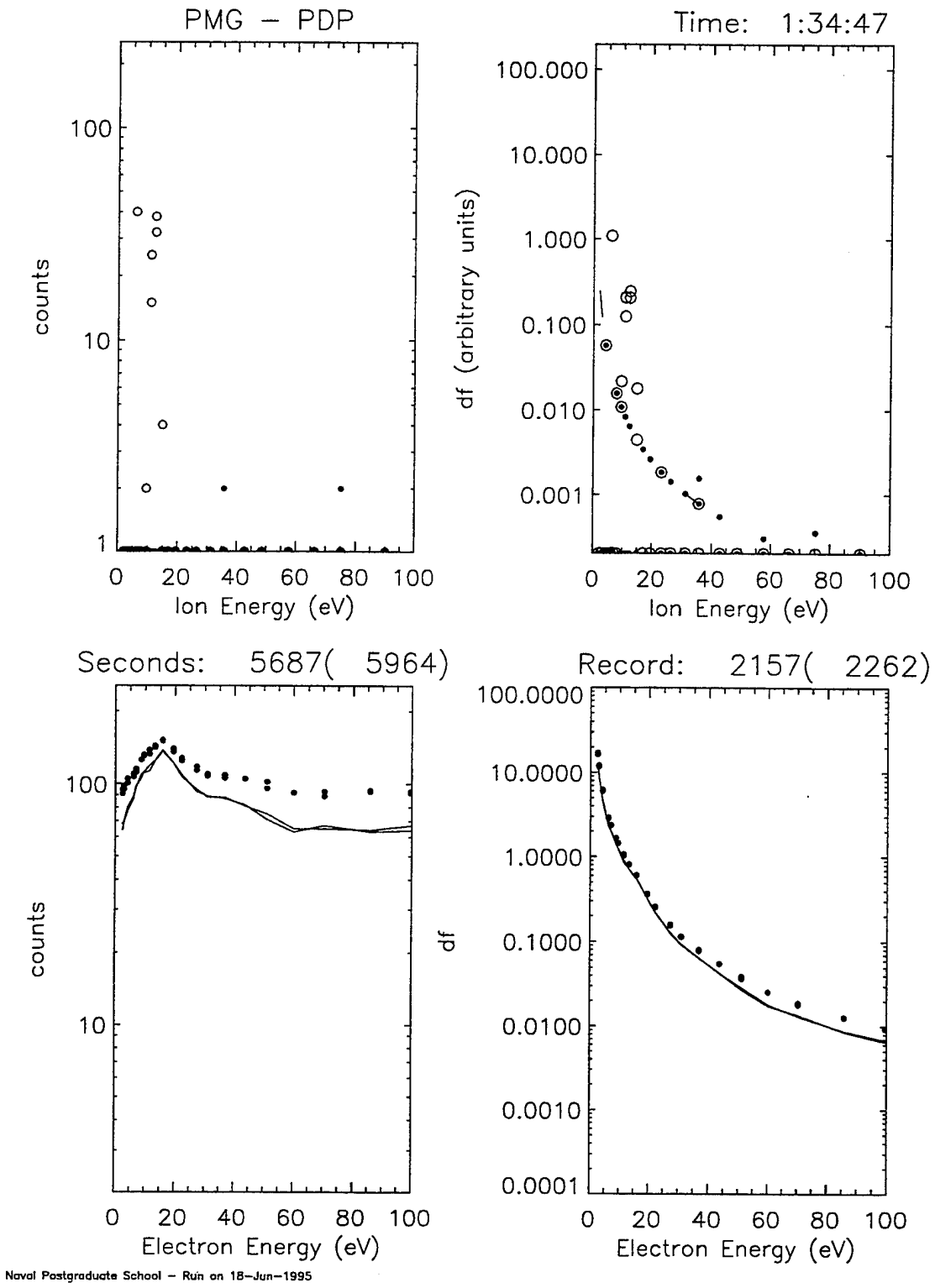

Figure 23. Line Plot of PDP Data (5964s PMGT)

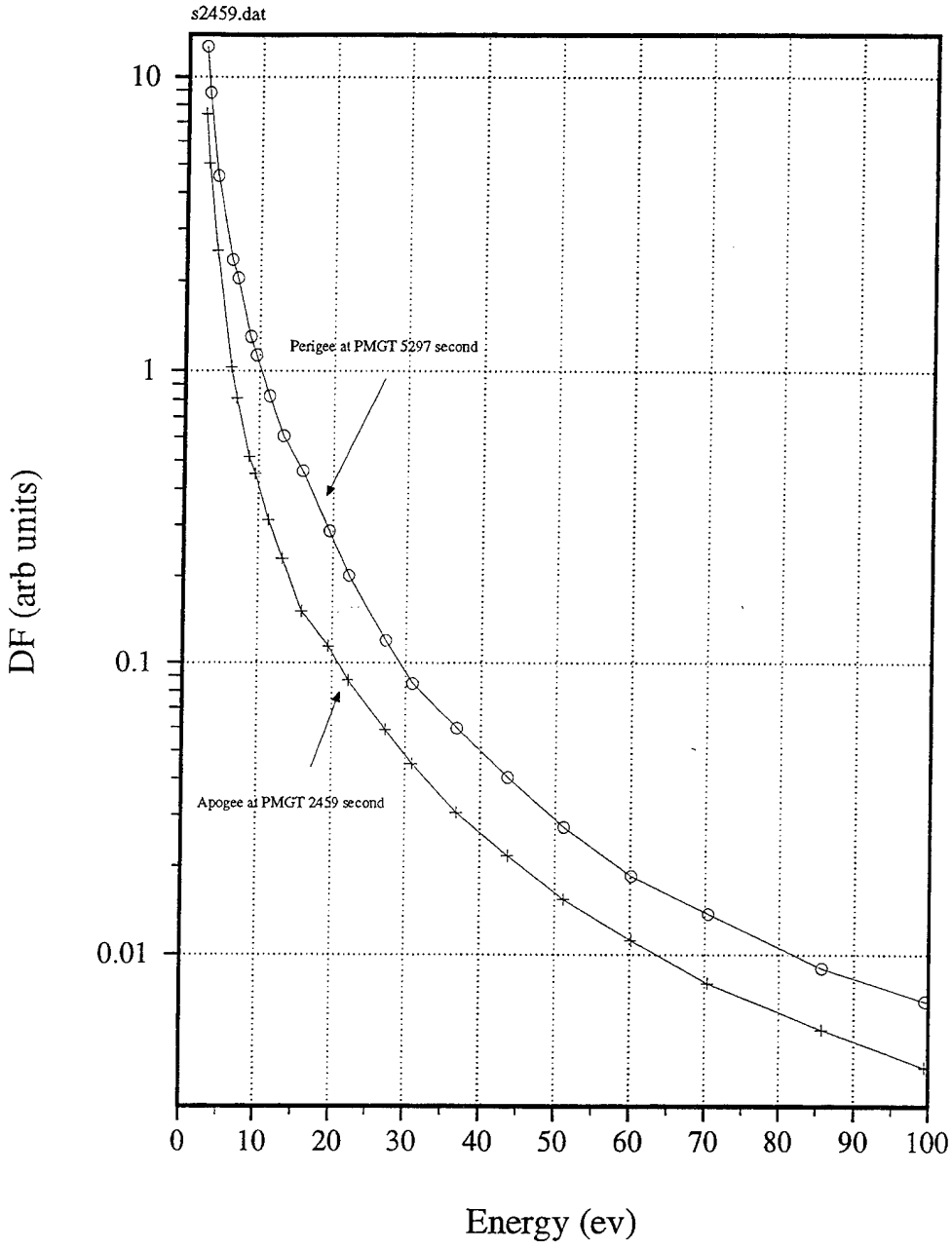

Figure 24. The Electron Spectrum at Perigee and Apogee

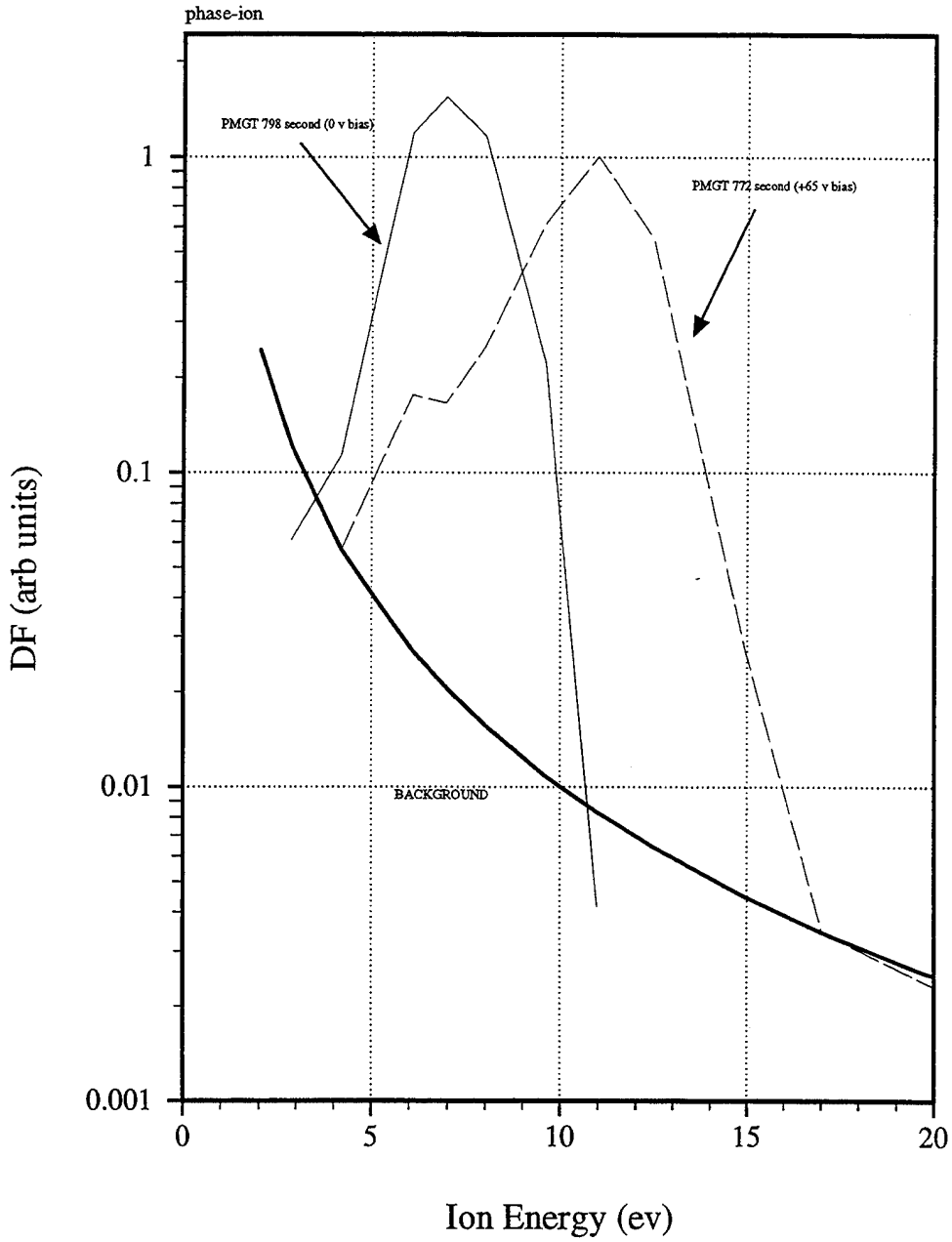

Figure 25. The Effect of Varying Bias

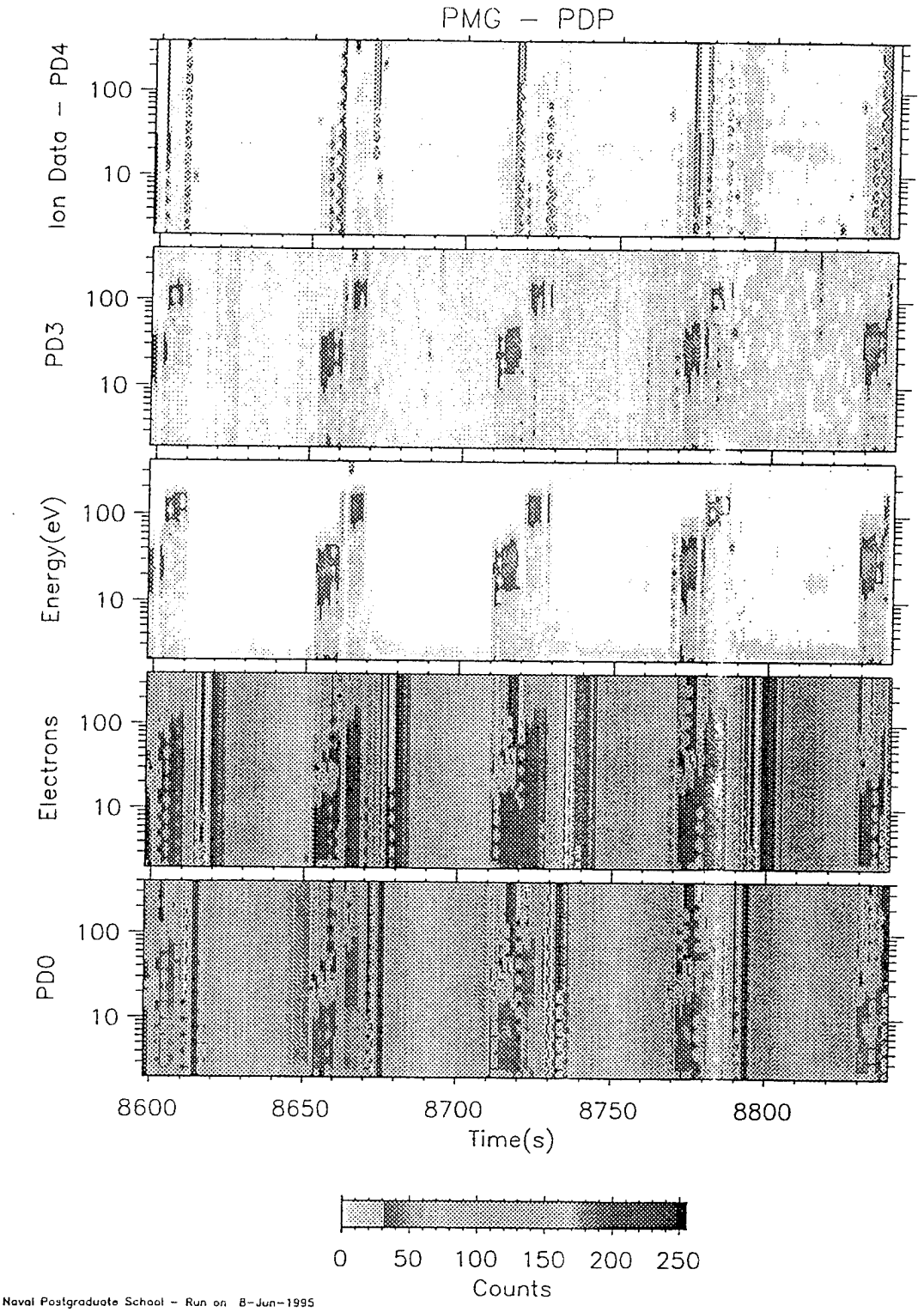

Figure 26. PDP Spectrogram from 8598 to 8840 Seconds PMGT

PD 2

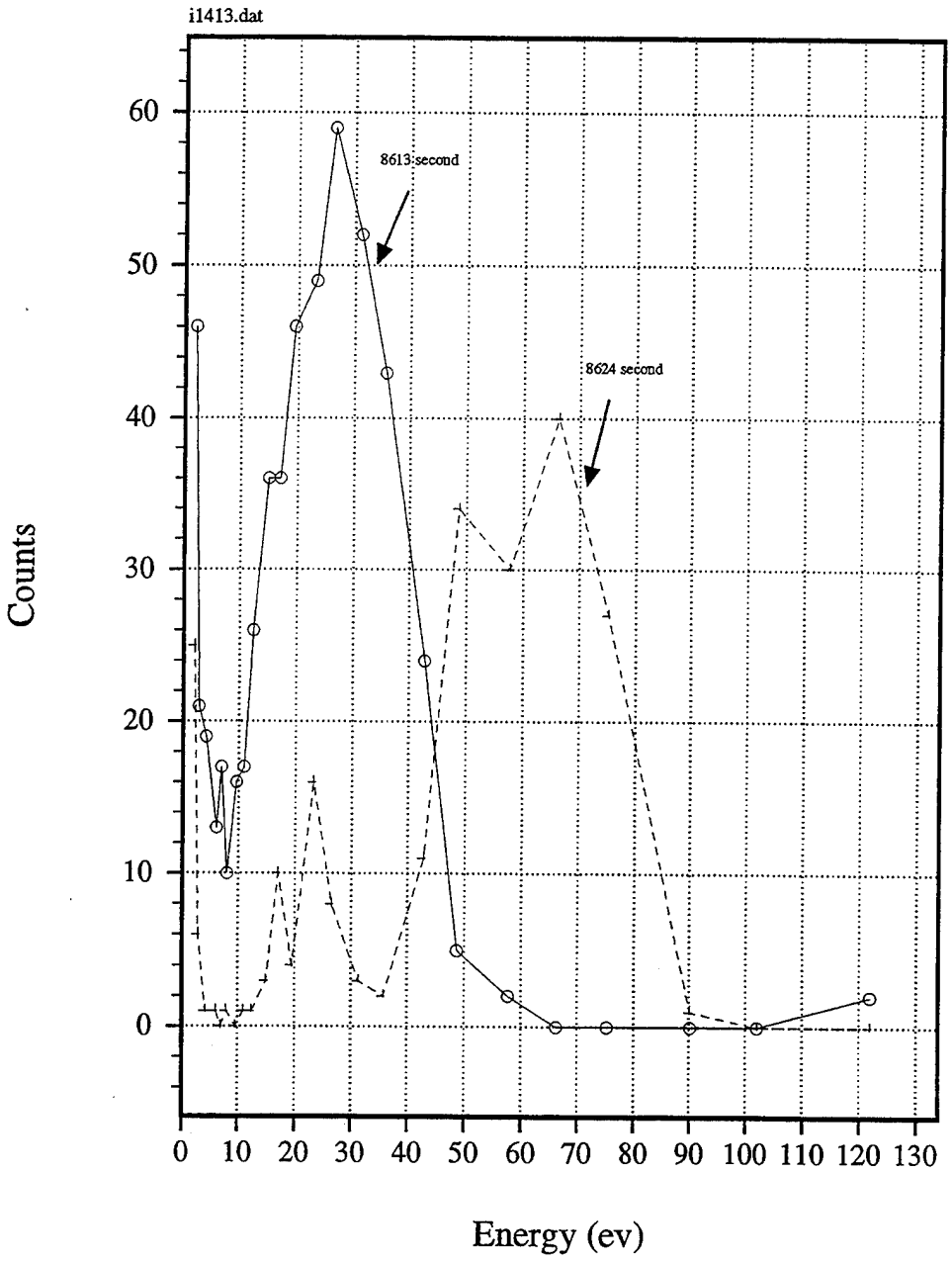

Figure 27. Ion Count Rate, -65 V and -130 V Bias

PD 2

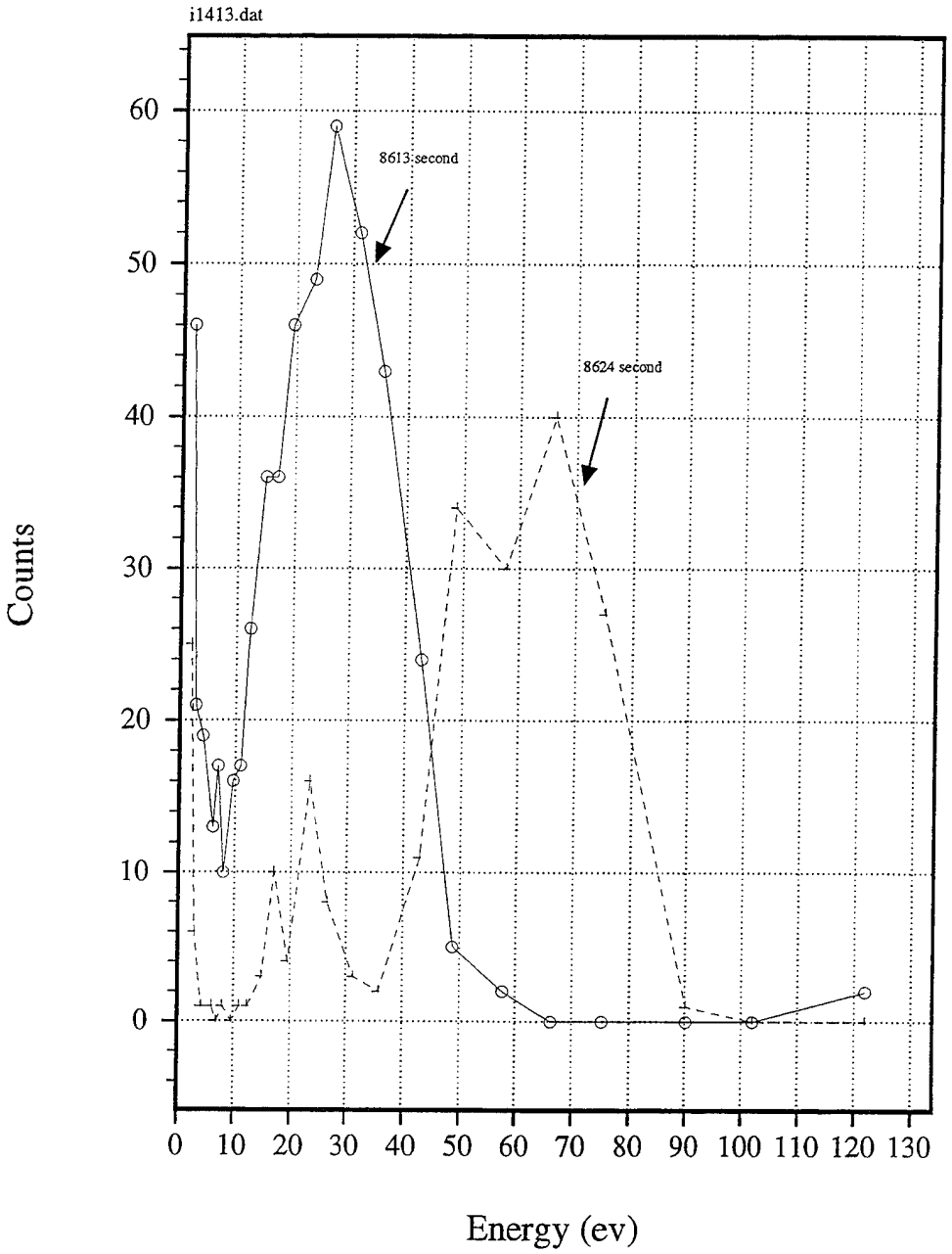

Figure 28. Ion Distribution Function for Negative Bias Mode

PD 2

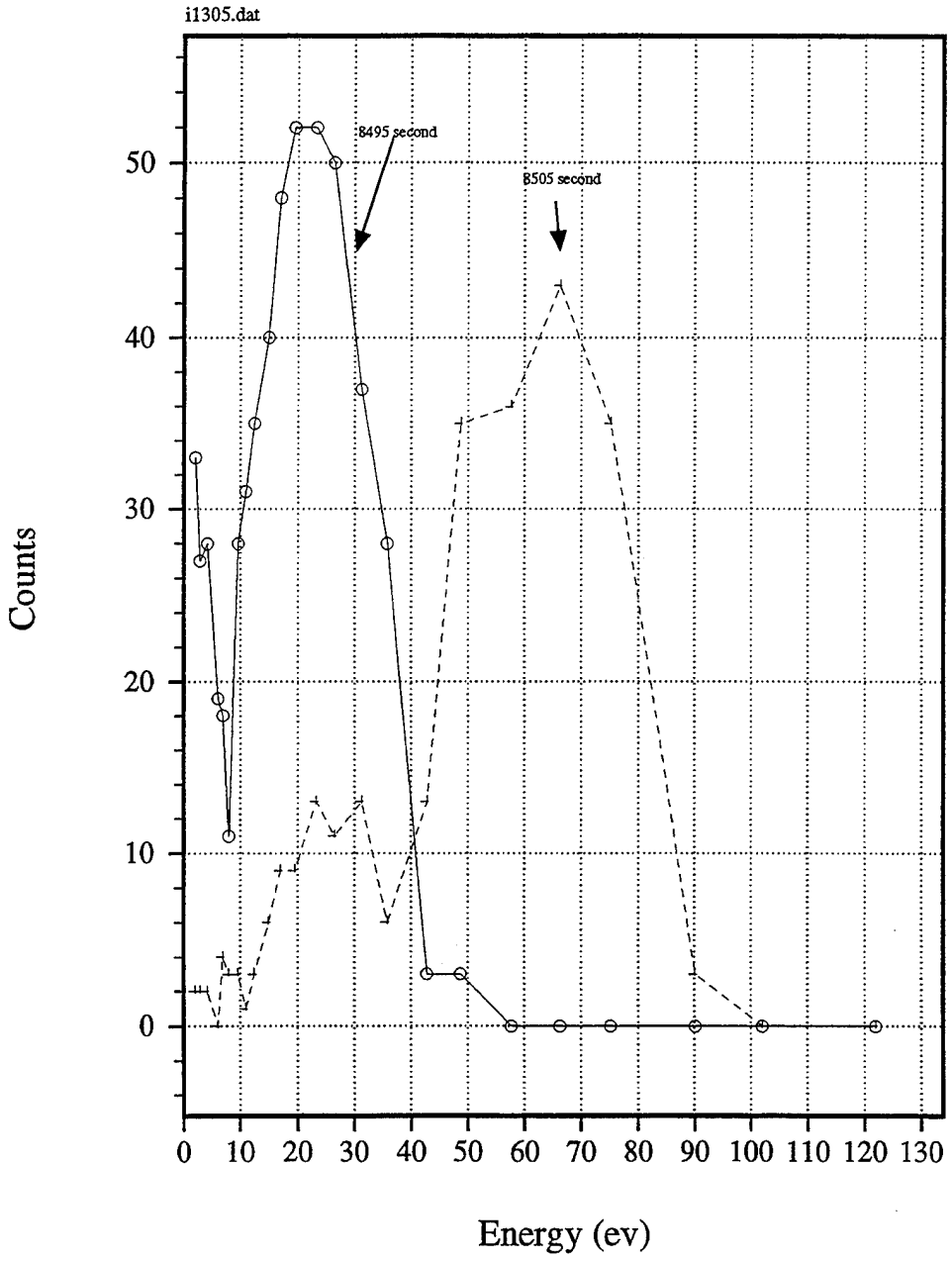

Figure 29. Ion Count Rate, -65 V and -130 V Bias

PD 2

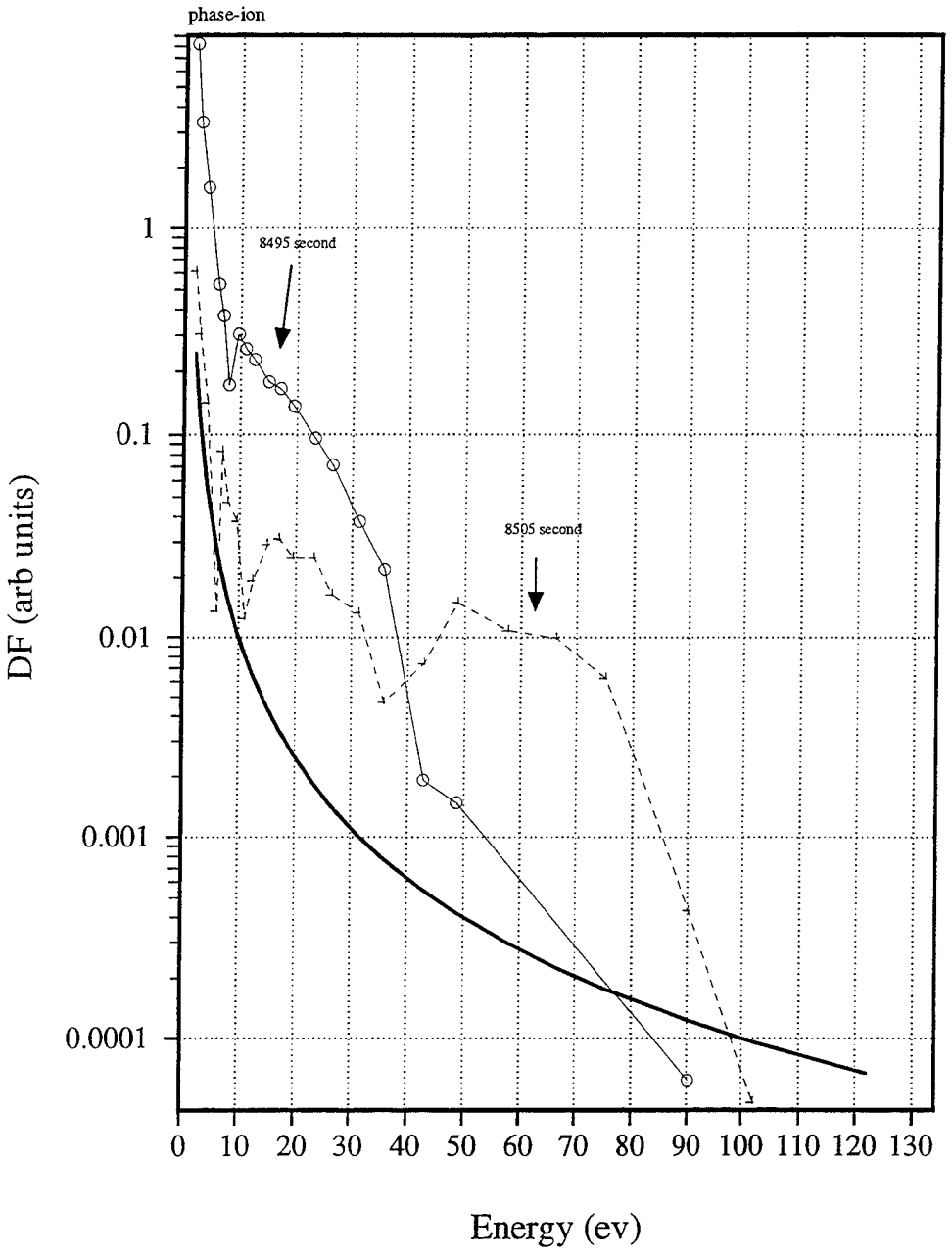

Figure 30. Ion Distribution Function for Negative Bias Mode

PD 2

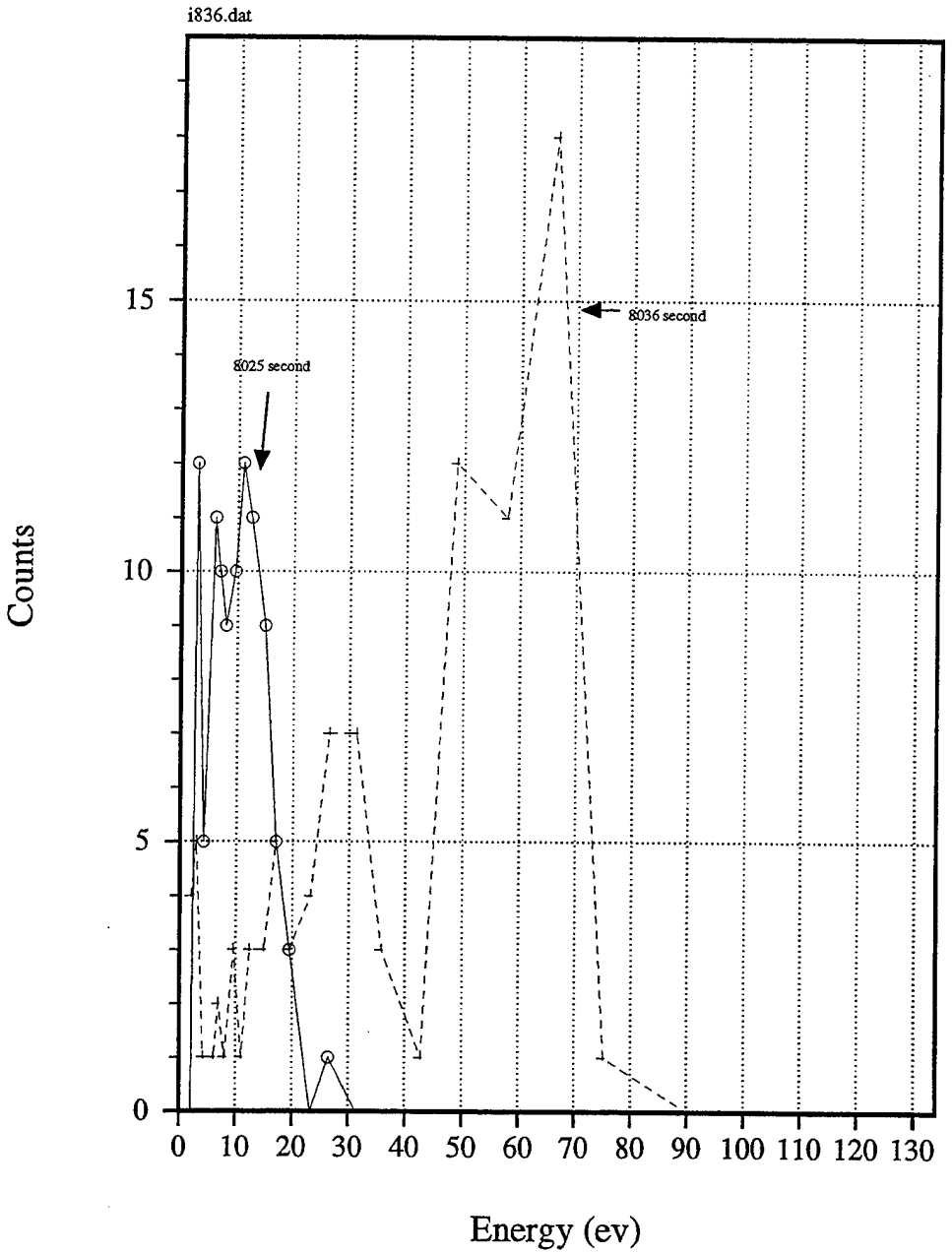

Figure 31. Ion Count Rate, -65 V and -130 V Bias

PD 3

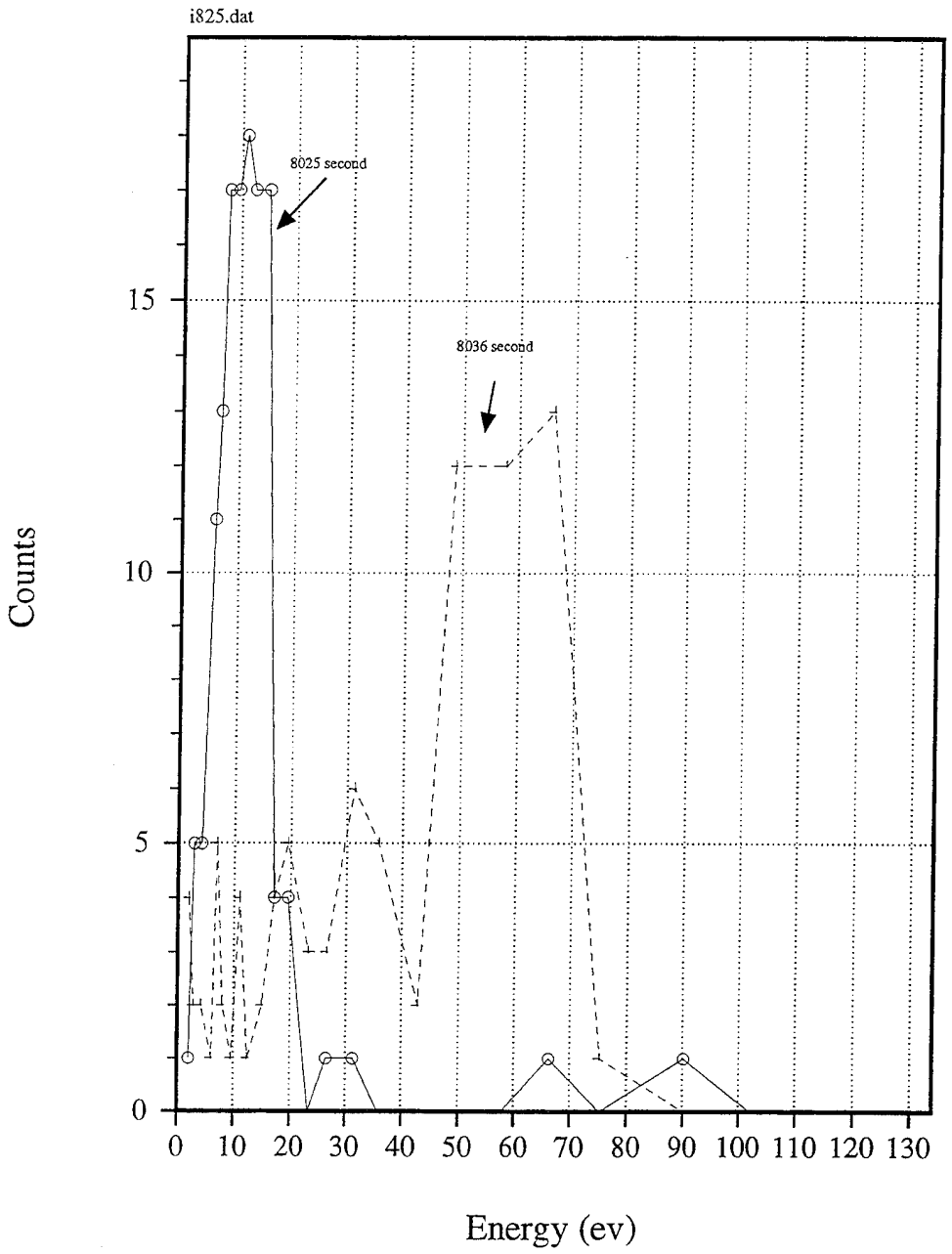

Figure 32. Ion Count Rate, -65 V and -130 V Bias

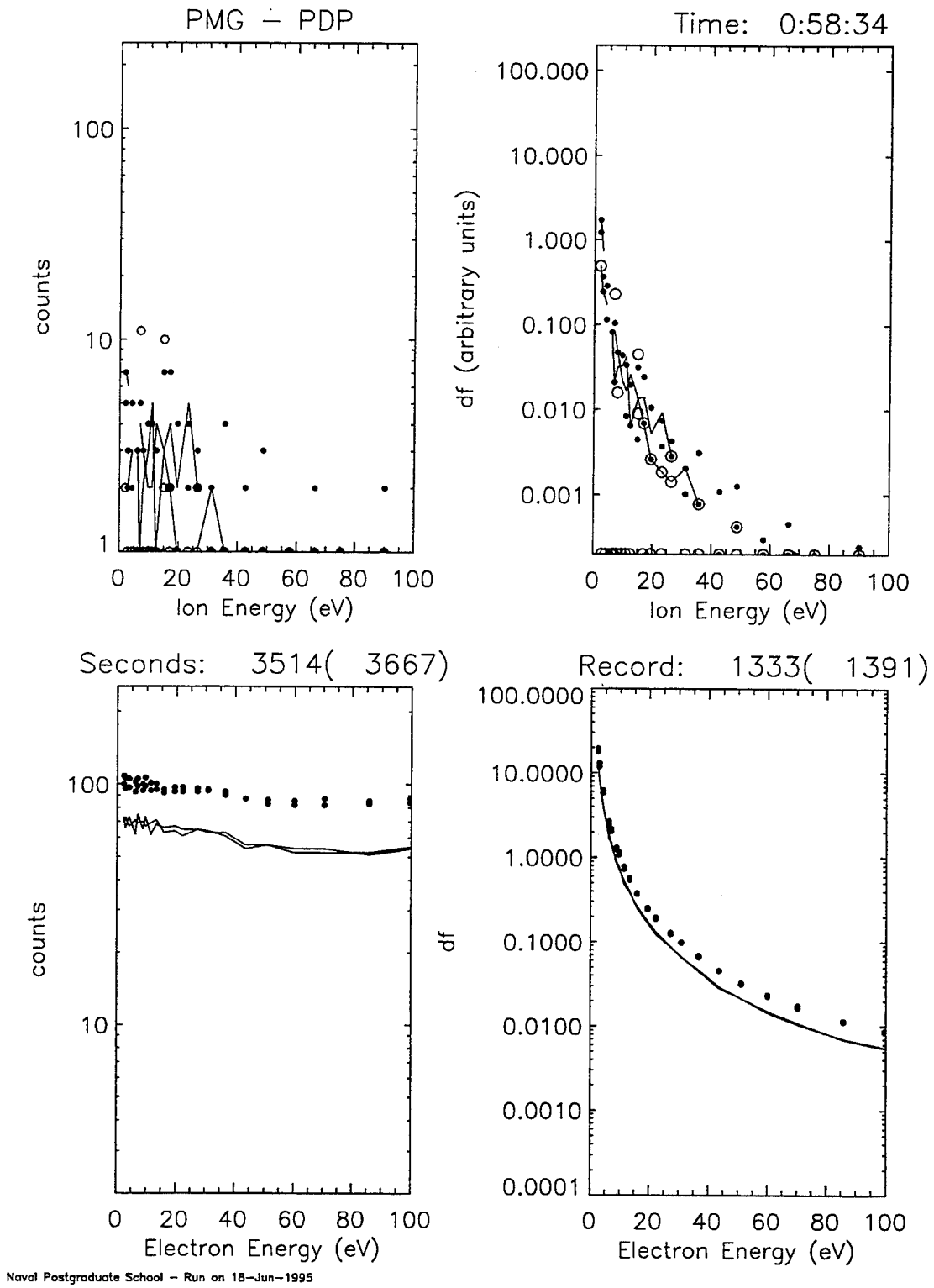

Figure 33. High Current Mode (3667s PMGT)

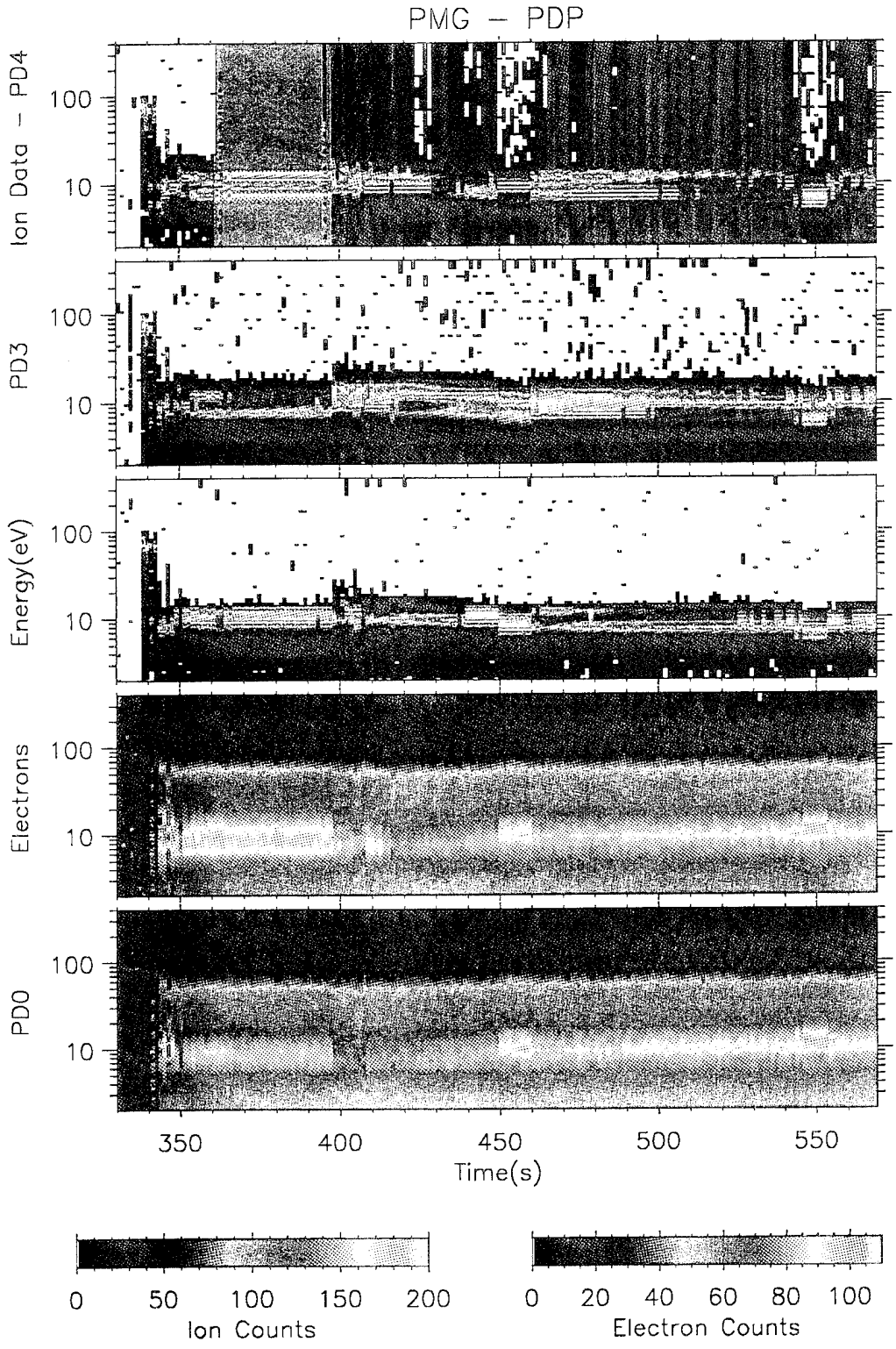

Figure 34. PDP Spectrogram from 330 to 570 Seconds PMGT

FEP HC Effects

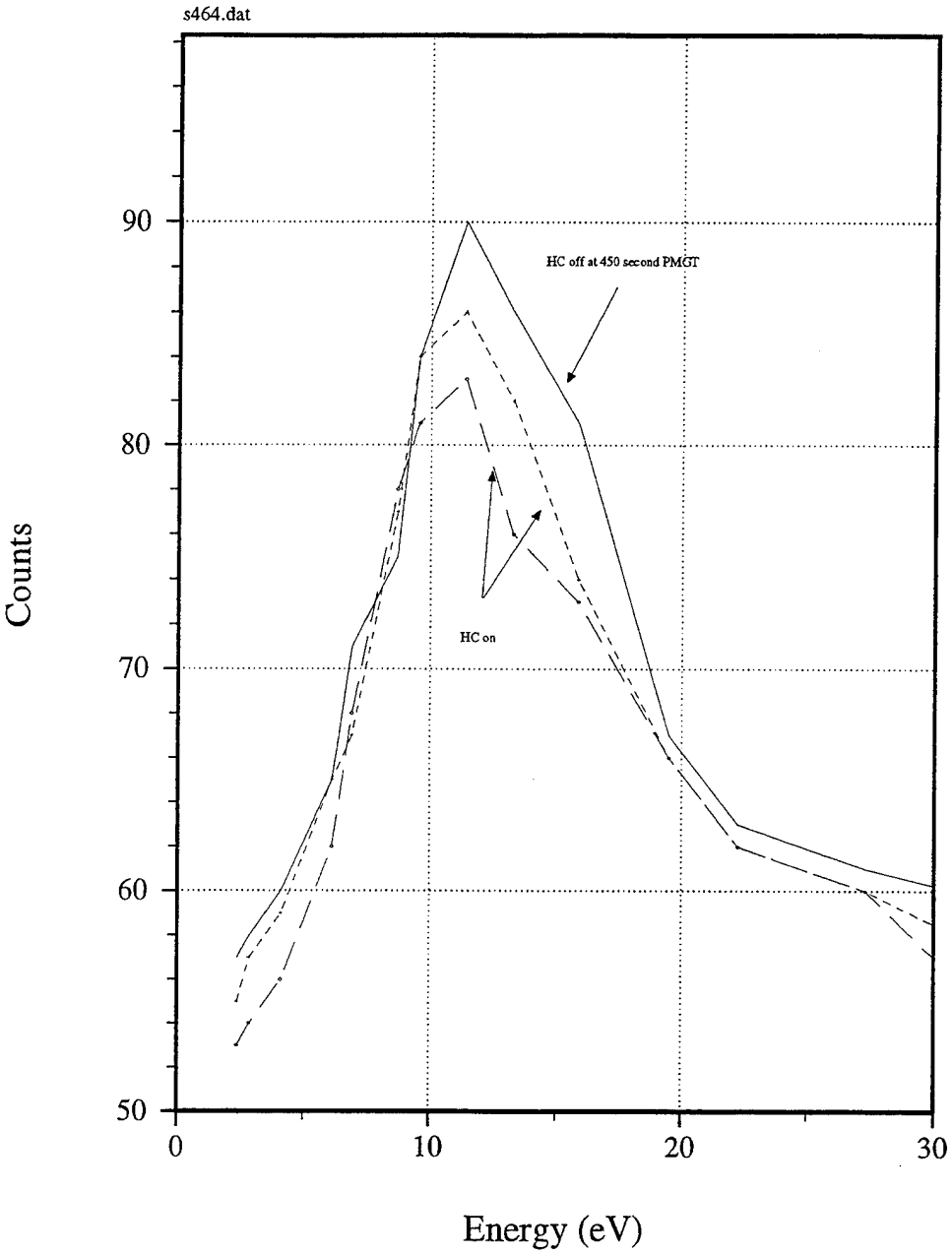

Figure 35. The FEP HC Effect (HC off at 450s PMGT)

FEP HC Effects

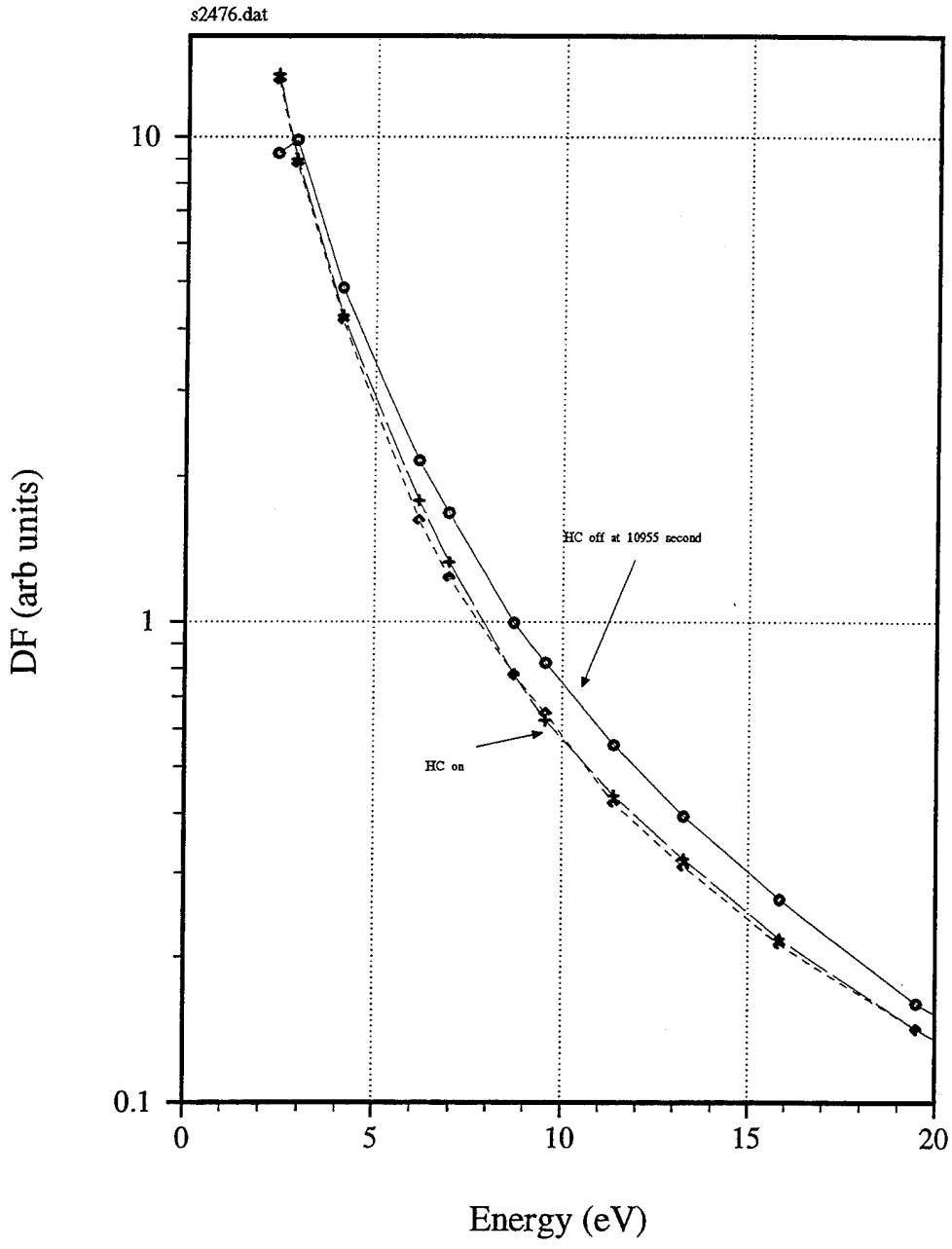

Figure 36. The FEP HC Effect (HC off at 10955s PMGT)

APPENDIX

During the PMG expetiment, the PDP provided approximately 2 oribits of useful data. The Appendix includes the spectrogram from the complete data set.

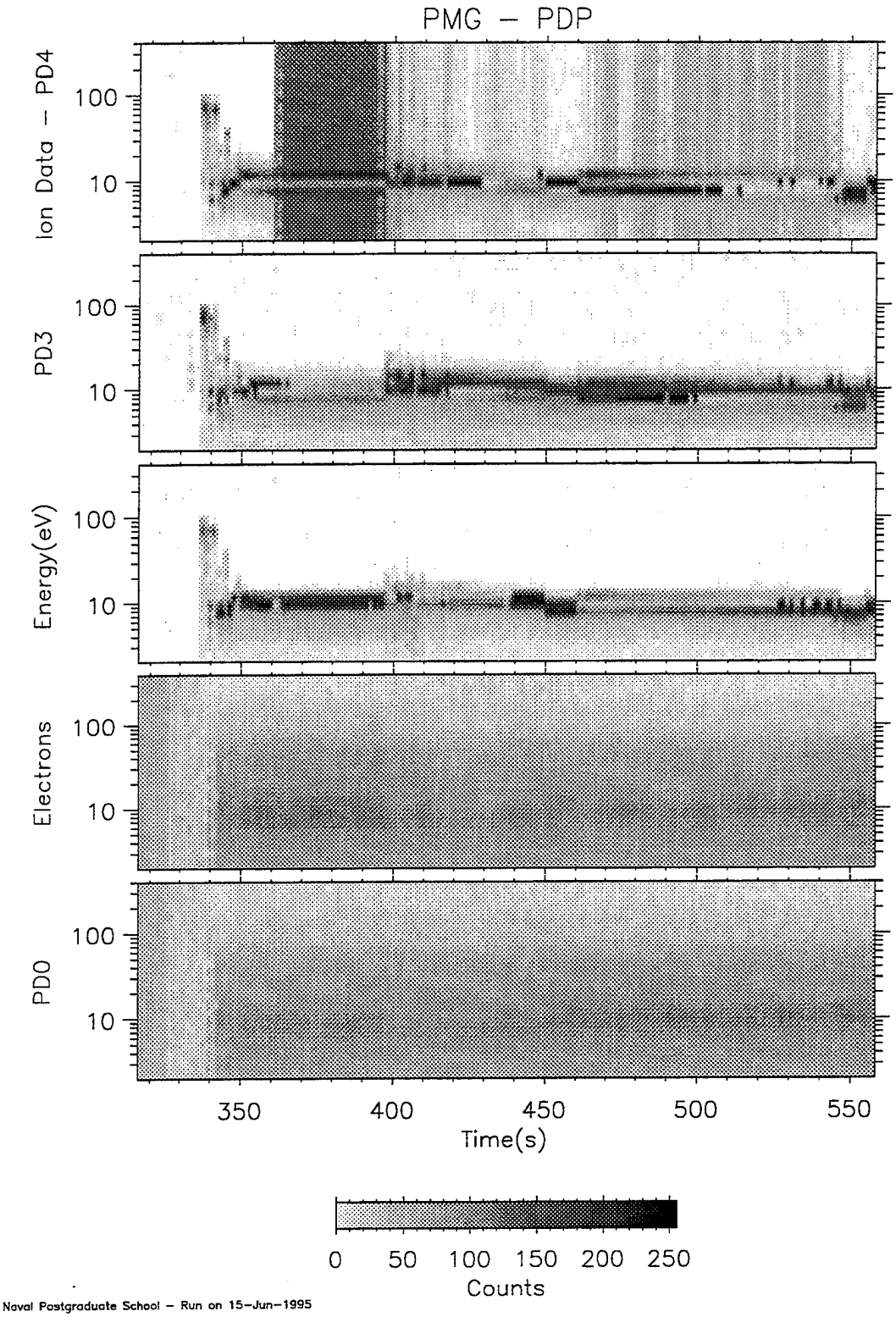
PMG – PDP
Ion Data – PD4
PD3
Energy(eV)
Electrons
PD0
100
10
350
400
450
500
550
Time(s)
0
50
100
150
200
250
Counts
Naval Postgraduate School – Run on 15–Jun–1995

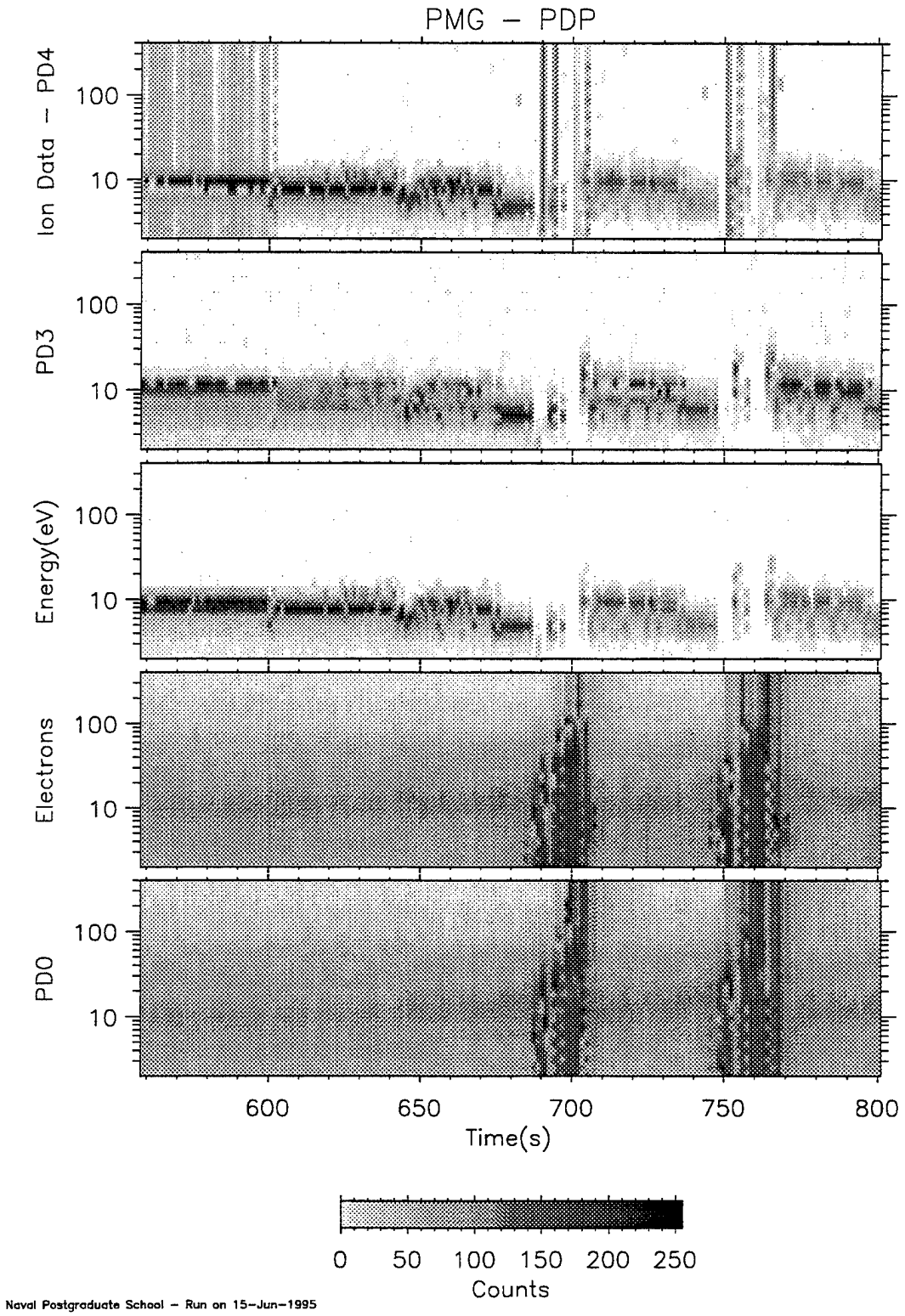
PMG – PDP
Ion Data – PD4
PD3
Energy(eV)
Electrons
PD0
100
10
600
650
700
750
800
Time(s)
0
50
100
150
200
250
Counts
Naval Postgraduate School – Run on 15–Jun–1995

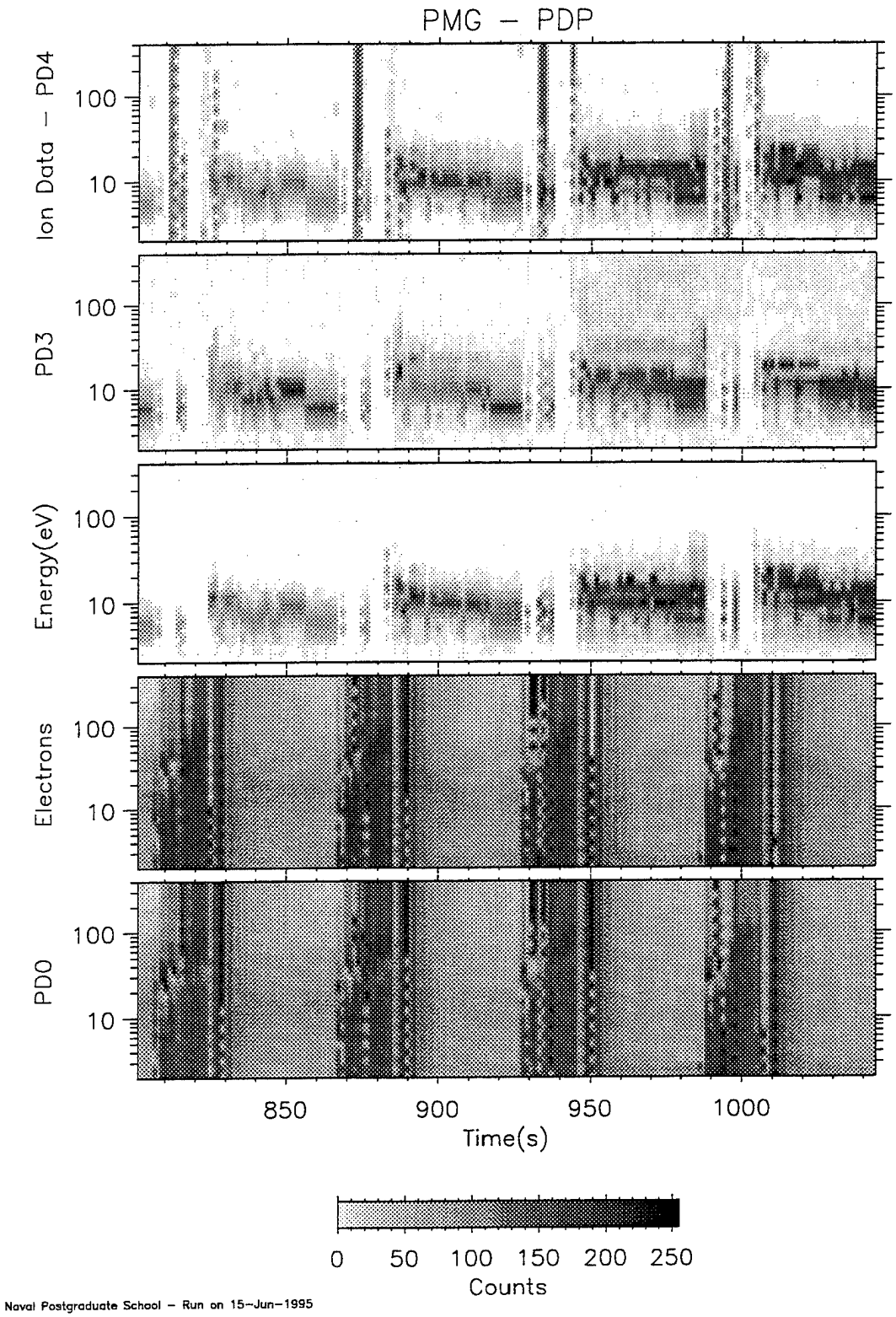
PMG – PDP
Ion Data – PD4
PD3
Energy(eV)
Electrons
PD0
100
10
850
900
950
1000
Time(s)
0
50
100
150
200
250
Counts
Naval Postgraduate School – Run on 15–Jun–1995

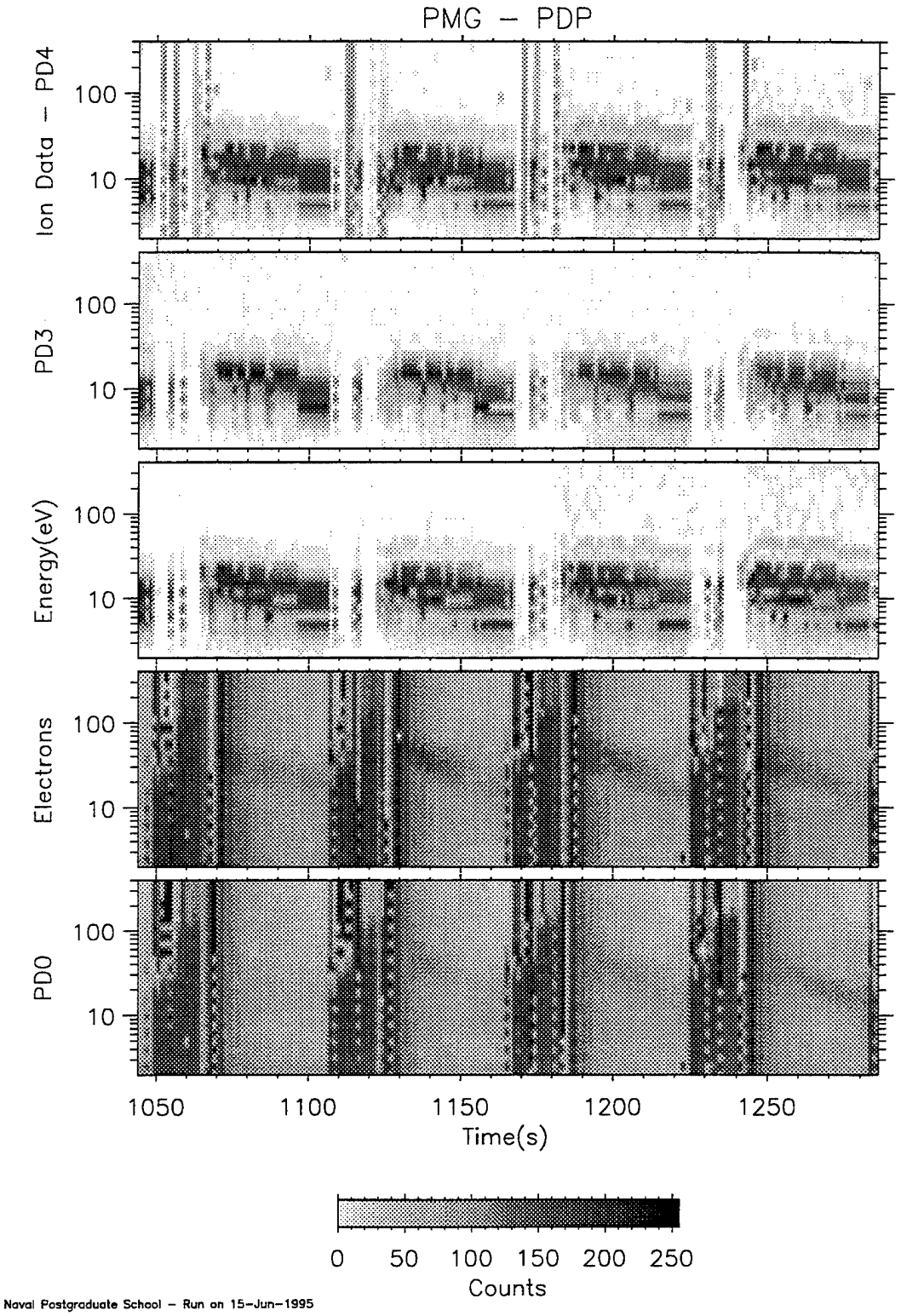
PMG – PDP
Ion Data – PD4
PD3
Energy(eV)
Electrons
PD0
100
10
1050
1100
1150
1200
1250
Time(s)
0
50
100
150
200
250
Counts
Naval Postgraduate School – Run on 15-Jun-1995

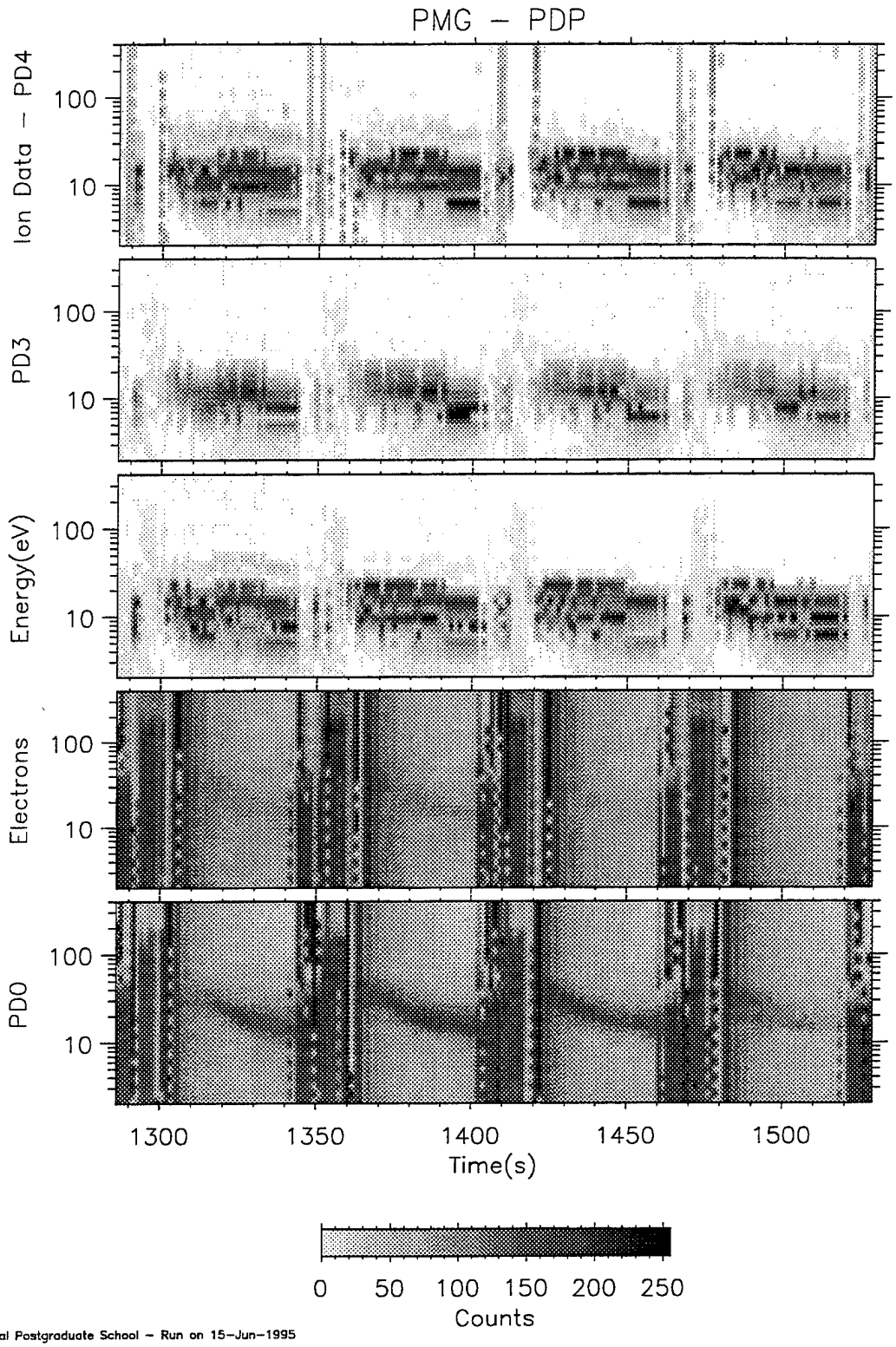
PMG – PDP
Ion Data – PD4
PD3
Energy(eV)
Electrons
PD0
100
10
1300
1350
1400
1450
1500
Time(s)
0
50
100
150
200
250
Counts
Naval Postgraduate School – Run on 15–Jun–1995

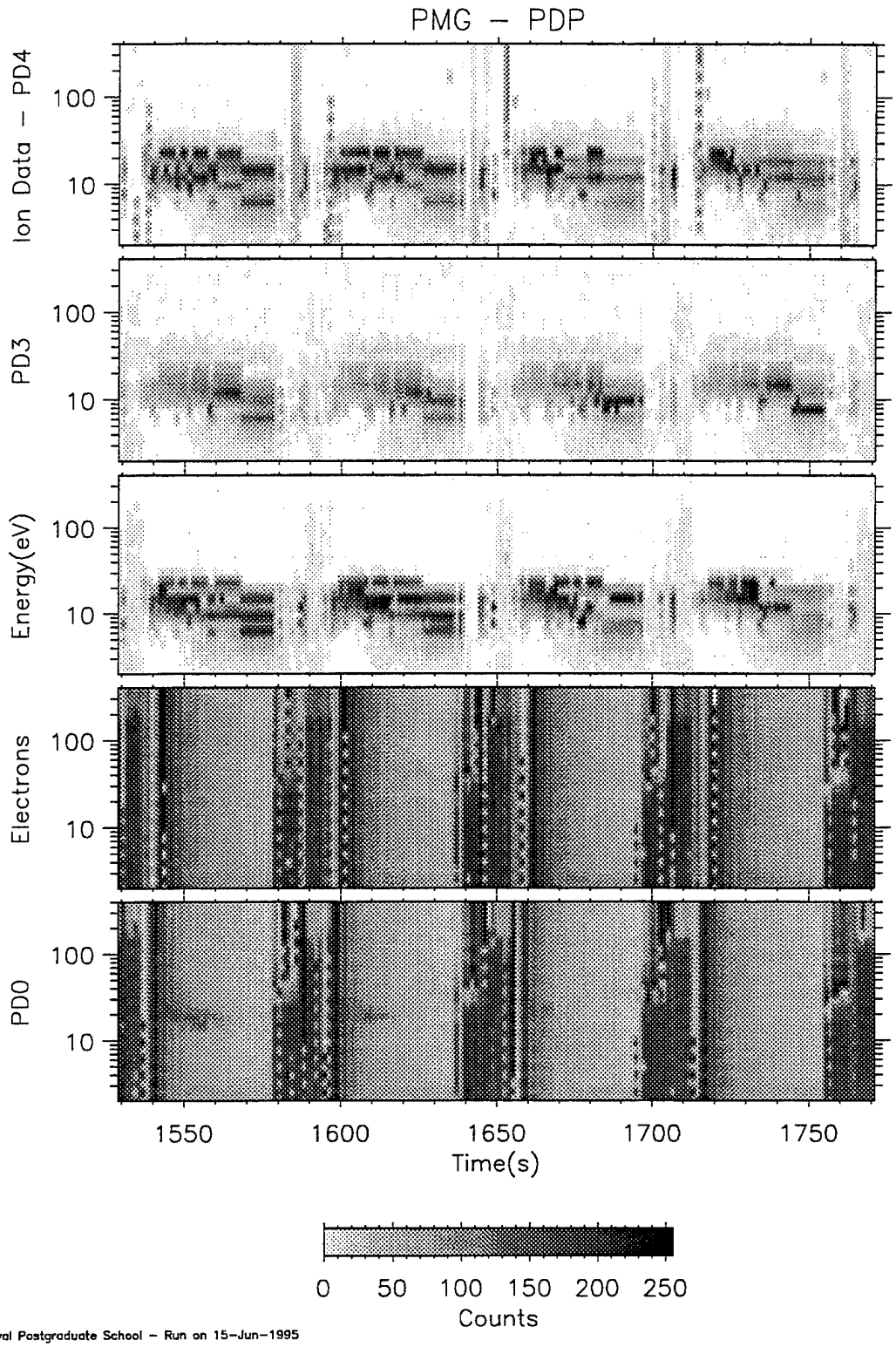
PMG – PDP
Ion Data – PD4
PD3
Energy(eV)
Electrons
PD0
100
10
1550
1600
1650
1700
1750
Time(s)
0
50
100
150
200
250
Counts
Naval Postgraduate School – Run on 15–Jun–1995

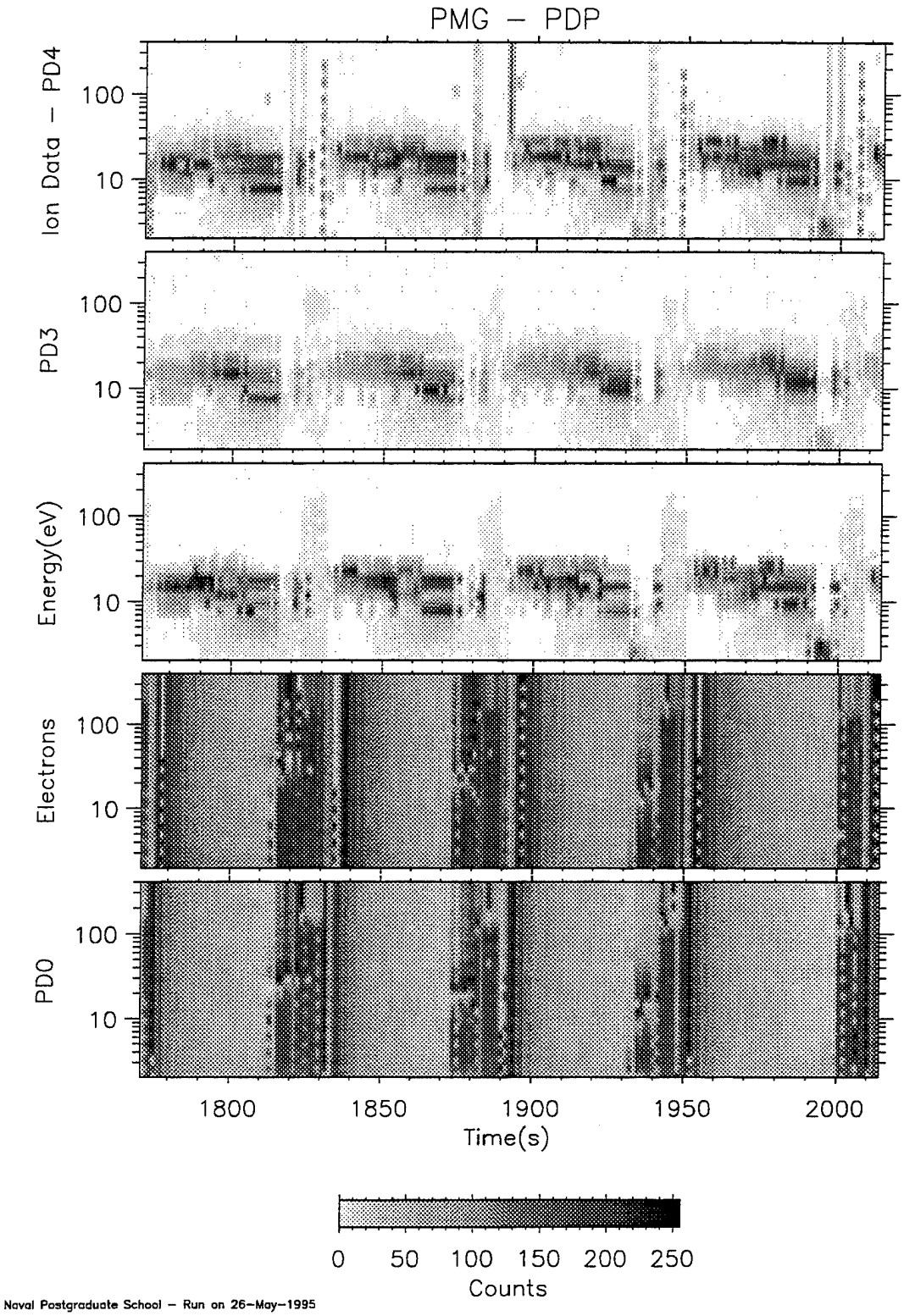
PMG – PDP
Ion Data – PD4
PD3
Energy(eV)
Electrons
PD0
100
10
1800
1850
1900
1950
2000
Time(s)
0
50
100
150
200
250
Counts
Naval Postgraduate School – Run on 26–May–1995

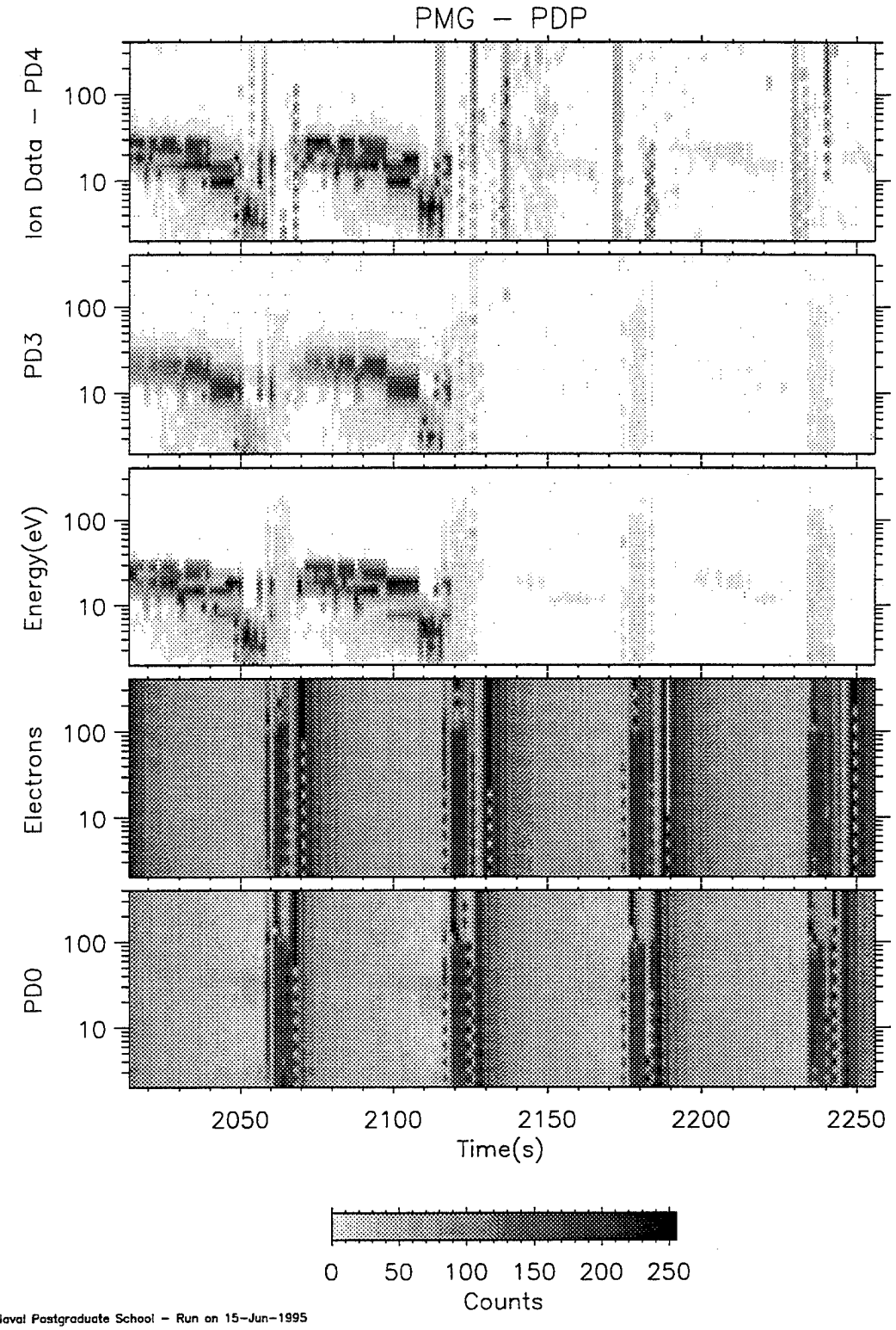
PMG – PDP
Ion Data – PD4
PD3
Energy(eV)
Electrons
PD0
100
10
2050
2100
2150
2200
2250
Time(s)
0
50
100
150
200
250
Counts
Naval Postgraduate School – Run on 15–Jun–1995

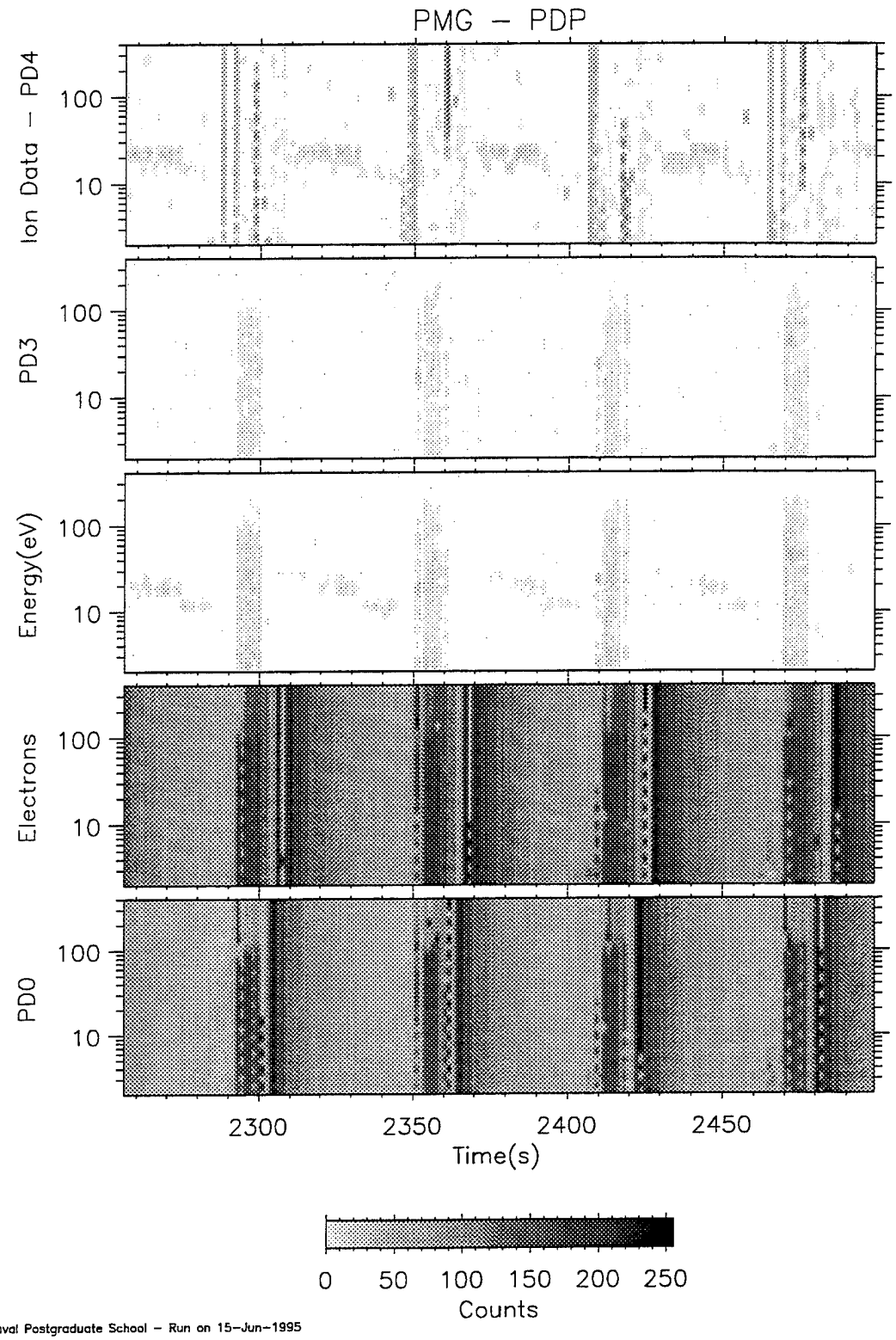
PMG – PDP
Ion Data – PD4
PD3
Energy(eV)
Electrons
PD0
100
10
2300
2350
2400
2450
Time(s)
0
50
100
150
200
250
Counts
Naval Postgraduate School – Run on 15–Jun–1995

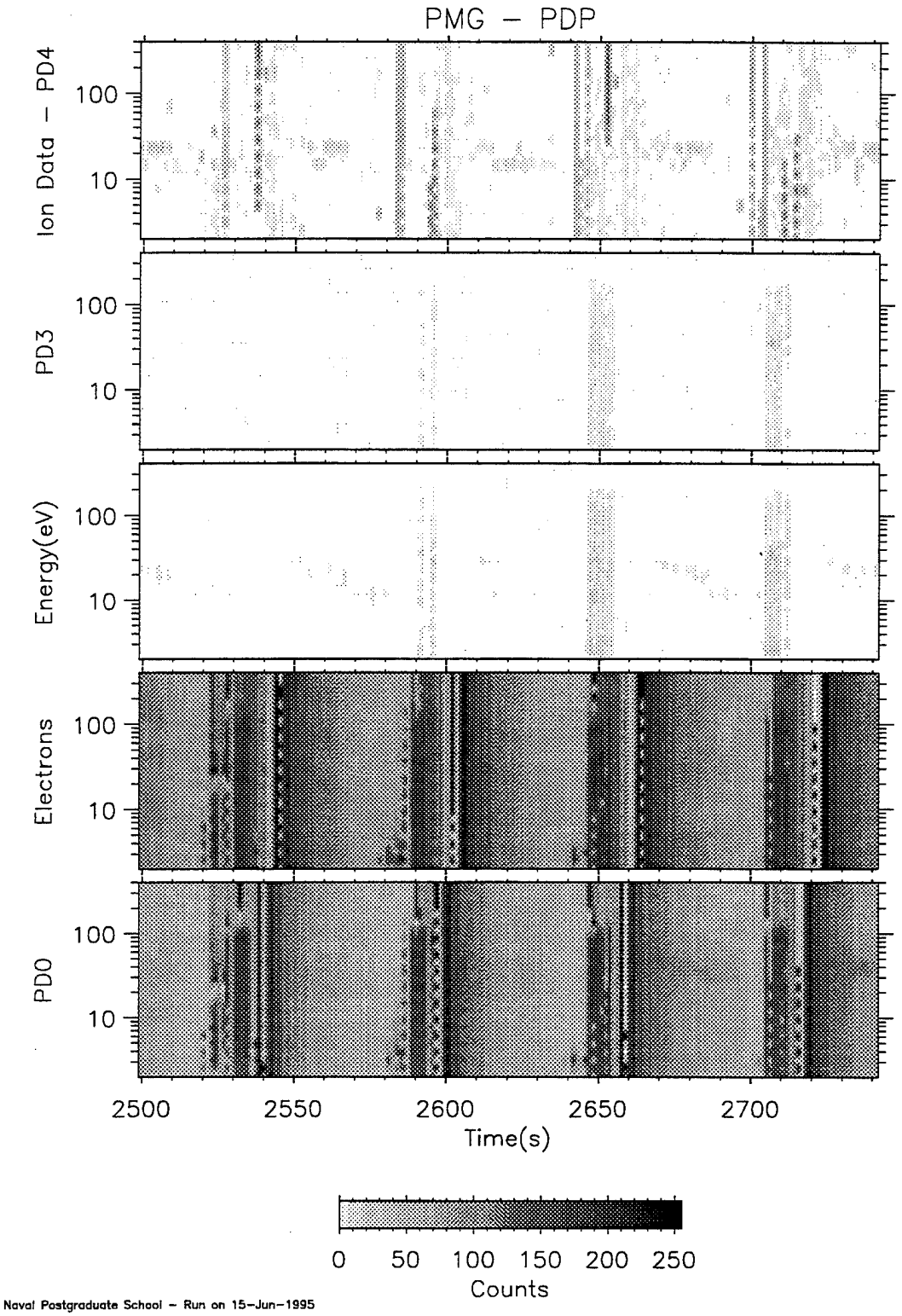
PMG – PDP
Ion Data – PD4
PD3
Energy(eV)
Electrons
PD0
100
10
2500
2550
2600
2650
2700
Time(s)
0
50
100
150
200
250
Counts
Naval Postgraduate School – Run on 15–Jun–1995

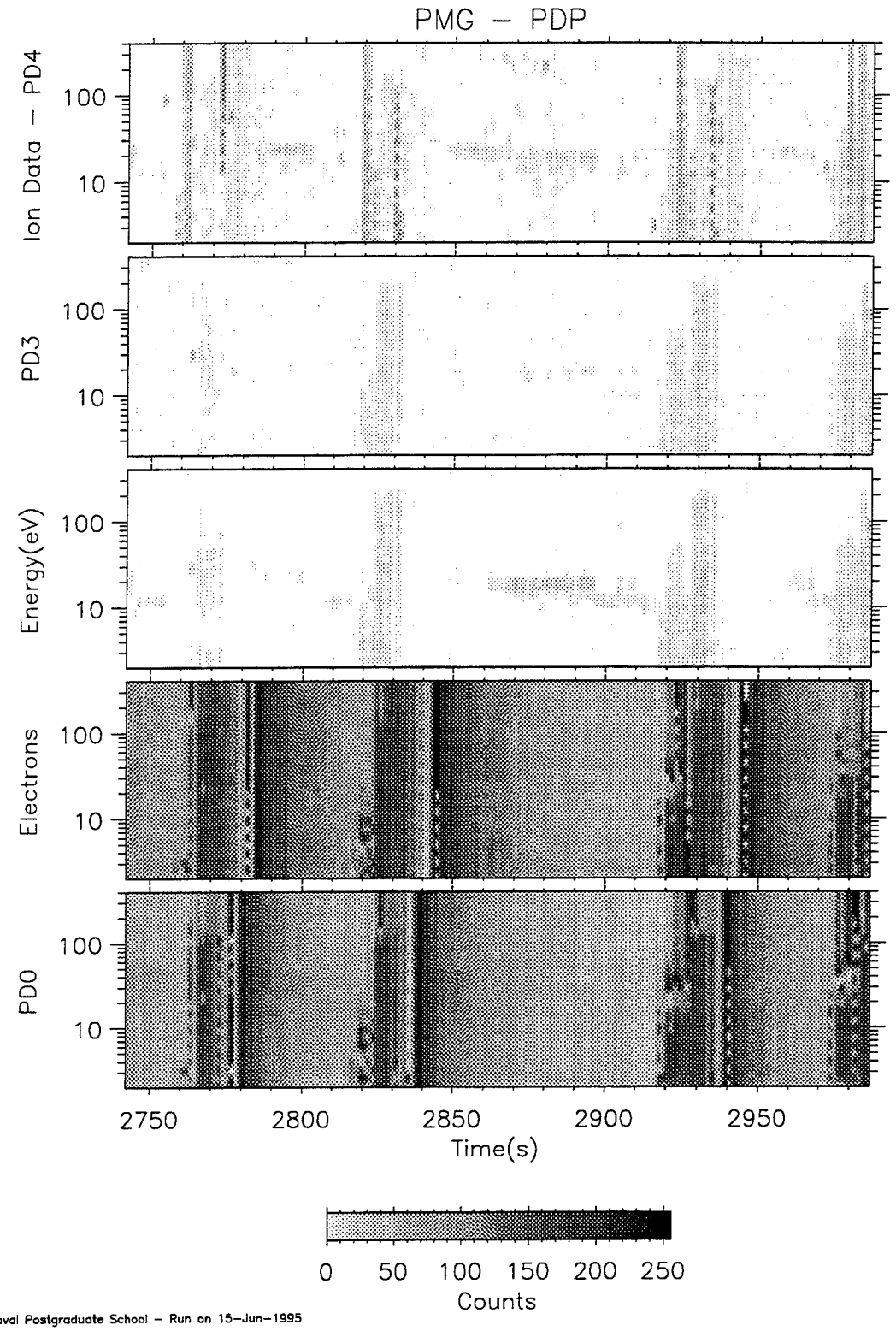
PMG – PDP
Ion Data – PD4
PD3
Energy(eV)
Electrons
PD0
100
10
2750
2800
2850
2900
2950
Time(s)
0
50
100
150
200
250
Counts
Naval Postgraduate School – Run on 15–Jun–1995

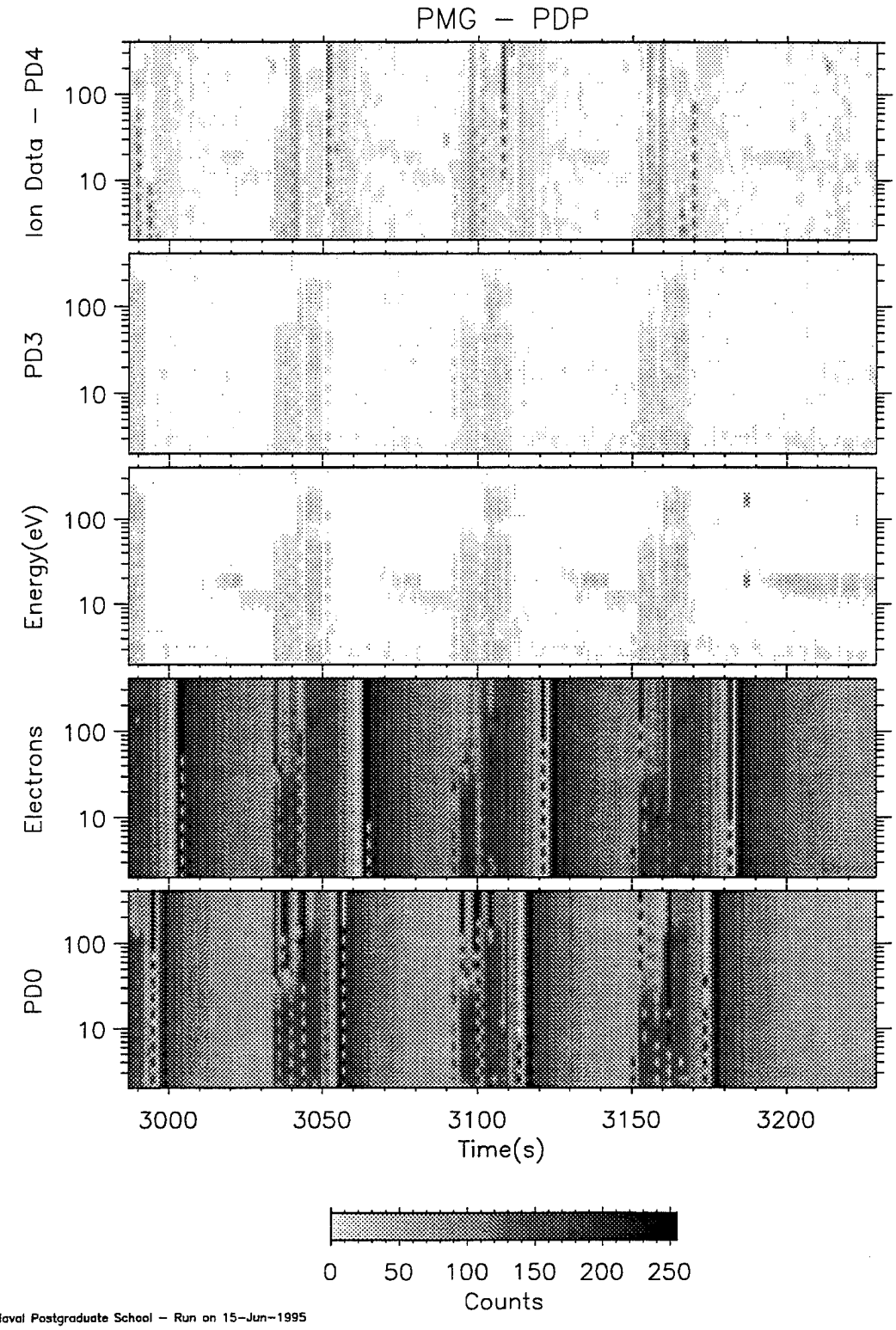
PMG – PDP
Ion Data – PD4
PD3
Energy(eV)
Electrons
PD0
100
10
3000
3050
3100
3150
3200
Time(s)
0
50
100
150
200
250
Counts
Naval Postgraduate School – Run on 15–Jun–1995

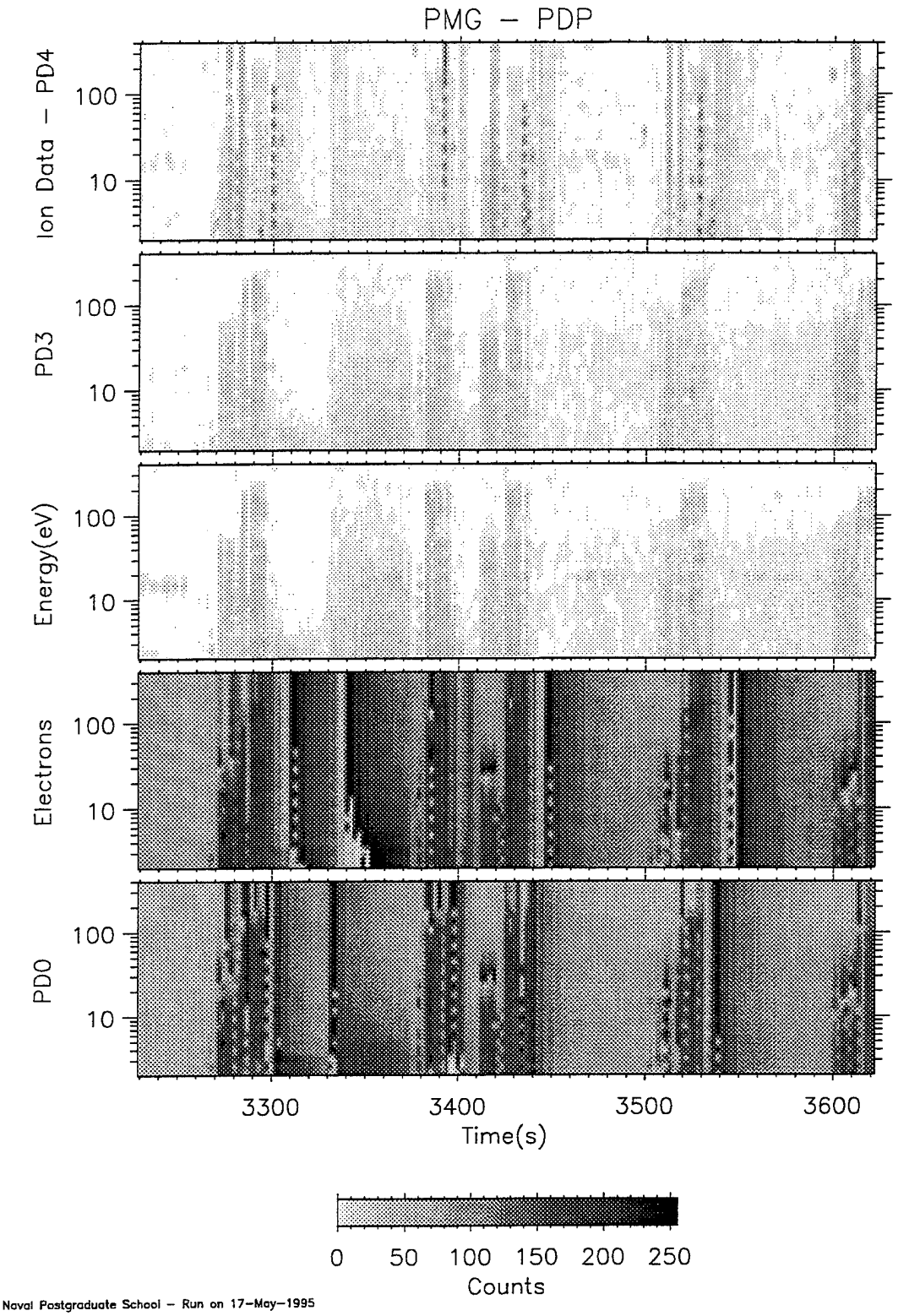
PMG – PDP
Ion Data – PD4
PD3
Energy(eV)
Electrons
PD0
100
10
3300
3400
3500
3600
Time(s)
0
50
100
150
200
250
Counts
Naval Postgraduate School – Run on 17–May–1995

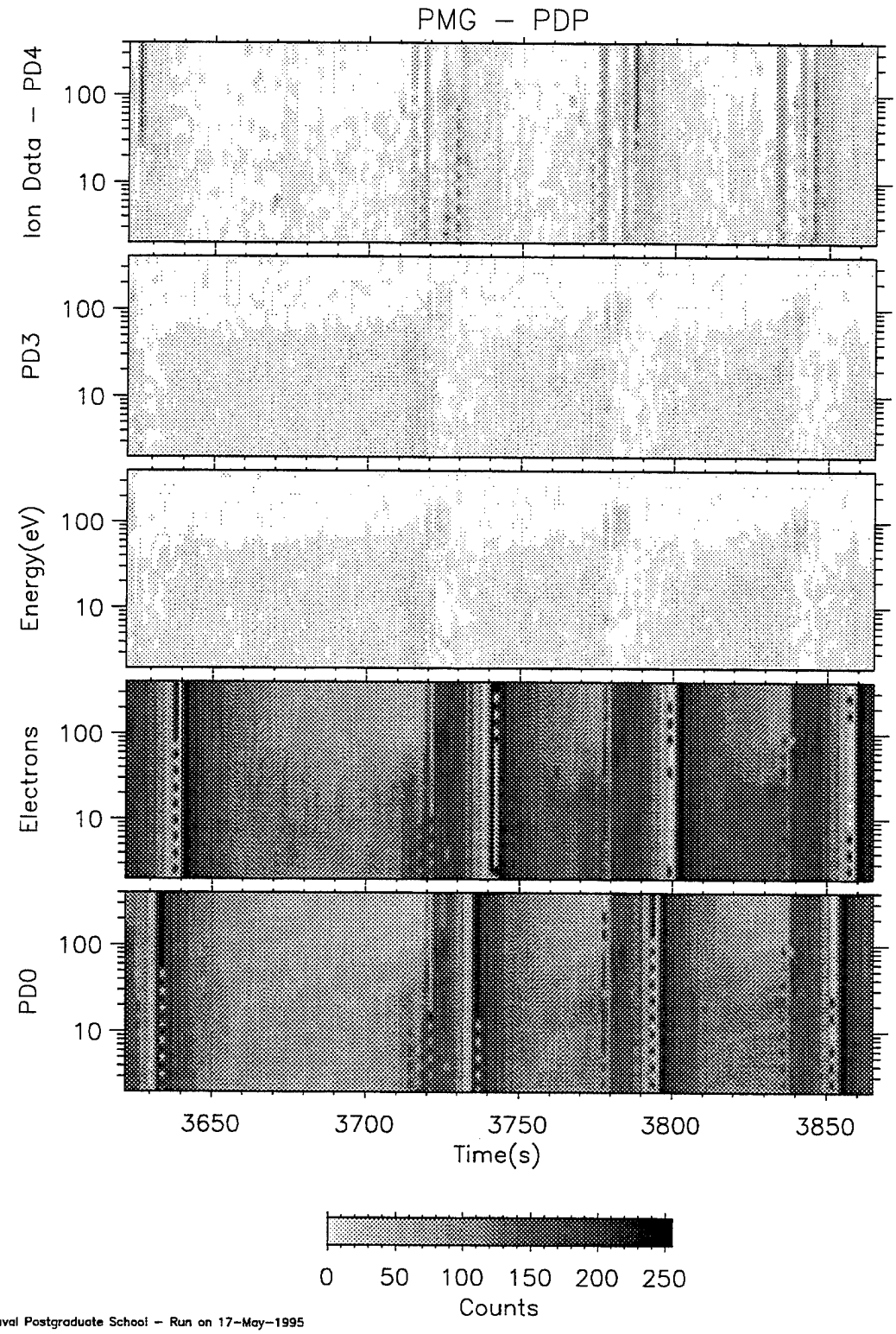
PMG – PDP
Ion Data – PD4
PD3
Energy(eV)
Electrons
PD0
100
10
3650
3700
3750
3800
3850
Time(s)
0
50
100
150
200
250
Counts
Naval Postgraduate School – Run on 17–May–1995

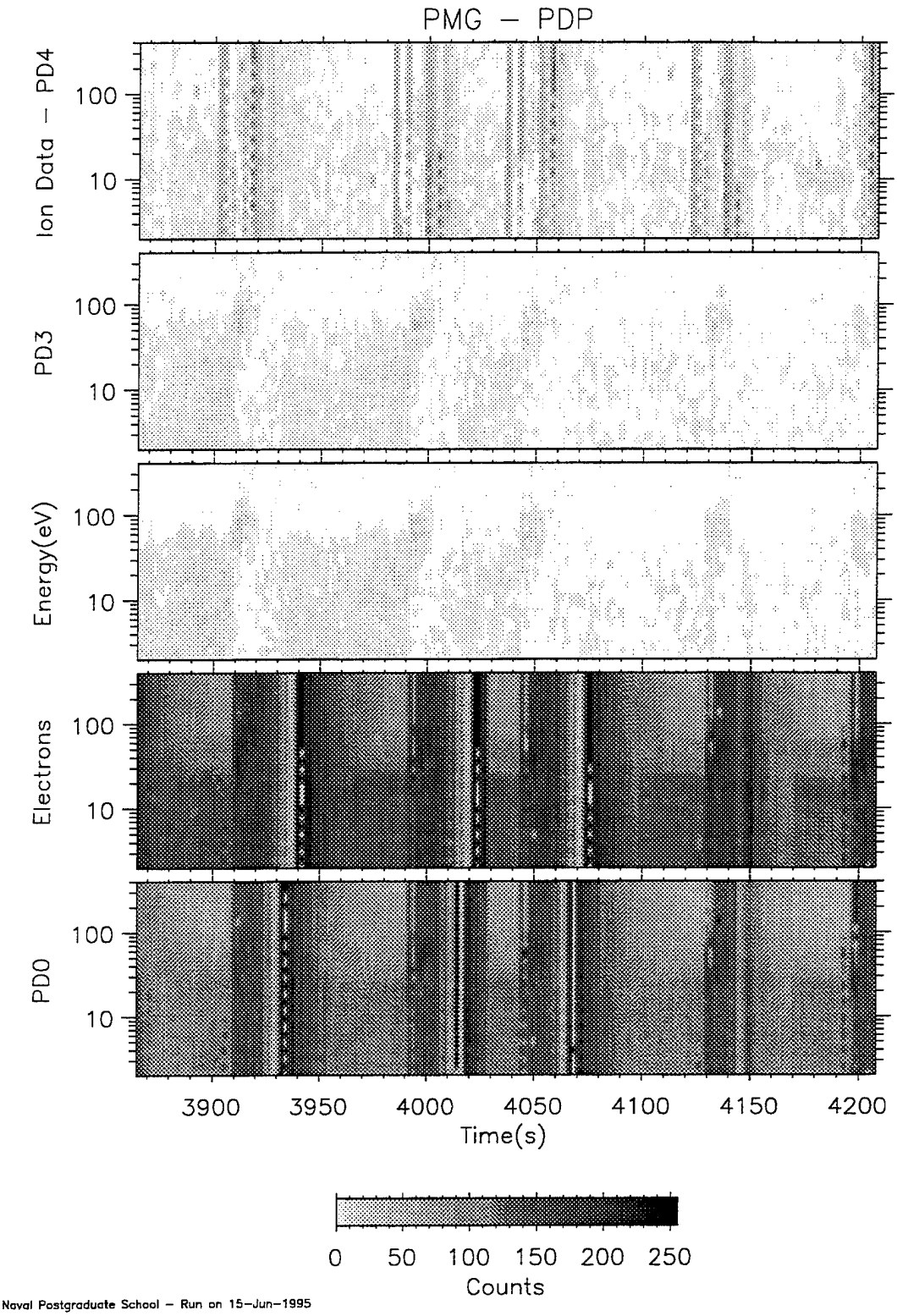
PMG – PDP
Ion Data – PD4
PD3
Energy(eV)
Electrons
PD0
100
10
3900
3950
4000
4050
4100
4150
4200
Time(s)
0
50
100
150
200
250
Counts
Naval Postgraduate School – Run on 15–Jun–1995

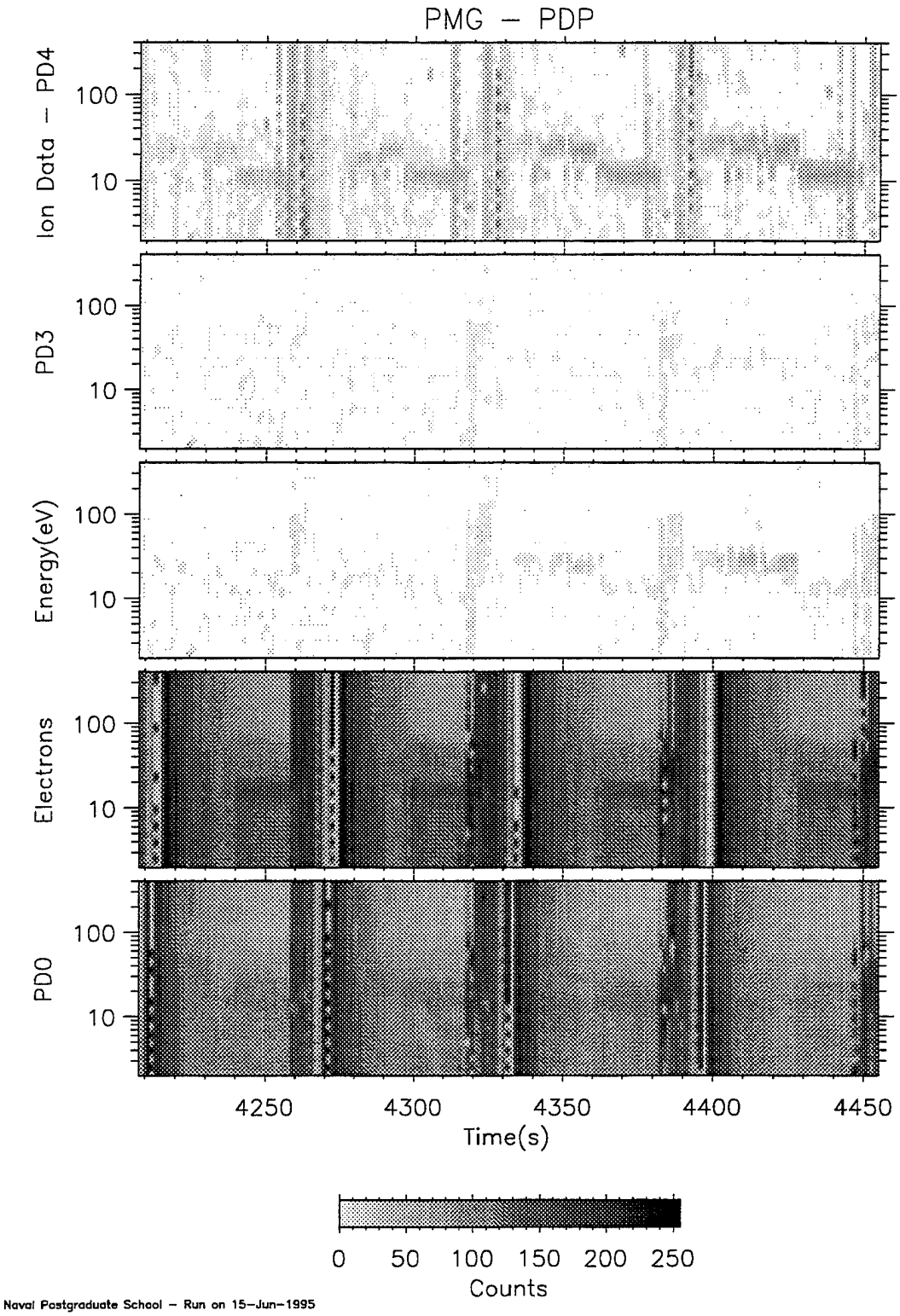
PMG – PDP
Ion Data – PD4
PD3
Energy(eV)
Electrons
PD0
100
10
4250
4300
4350
4400
4450
Time(s)
0
50
100
150
200
250
Counts
Naval Postgraduate School – Run on 15–Jun–1995

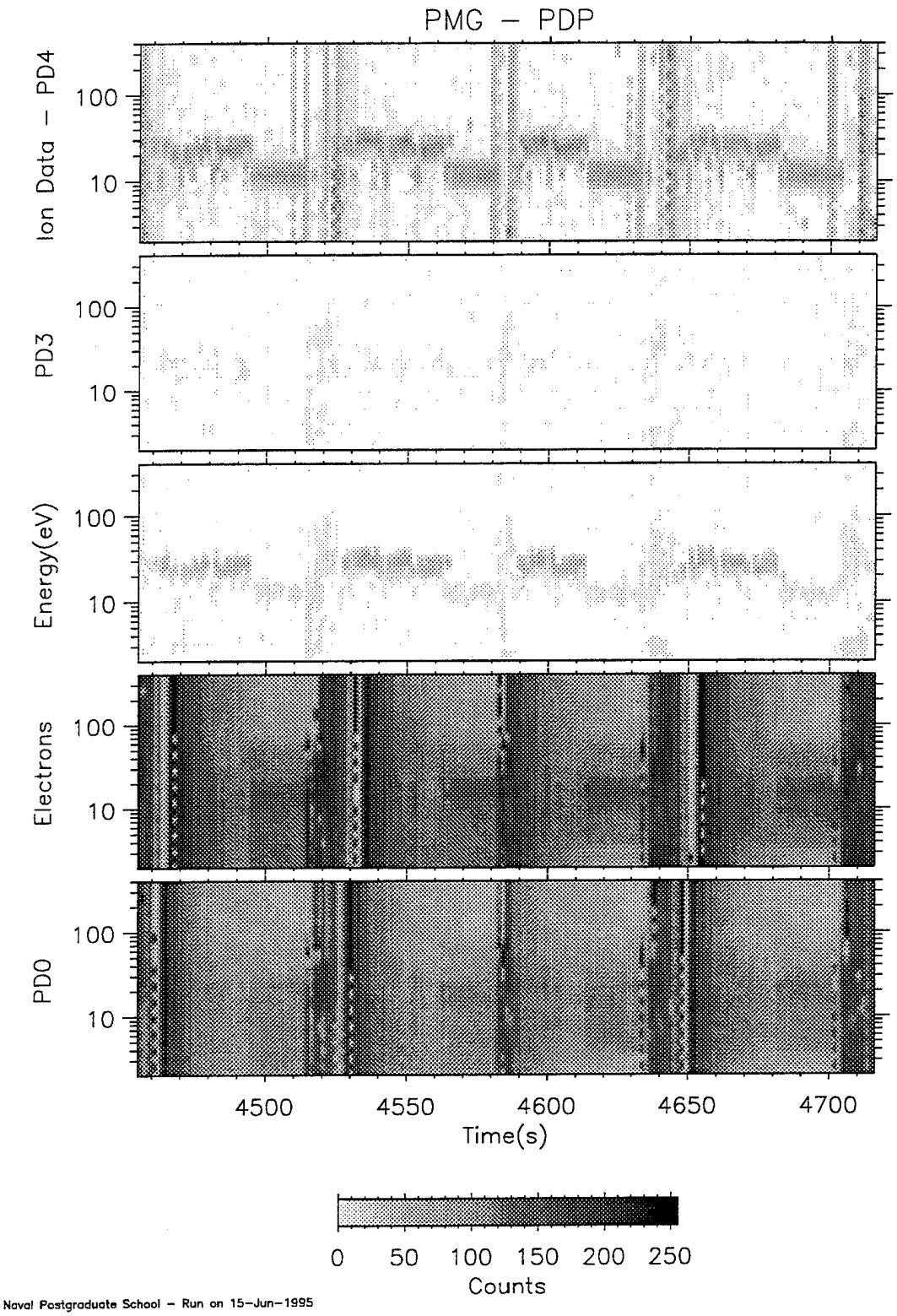
PMG – PDP
Ion Data – PD4
PD3
Energy(eV)
Electrons
PD0
100
10
4500
4550
4600
4650
4700
Time(s)
0
50
100
150
200
250
Counts
Naval Postgraduate School – Run on 15–Jun–1995

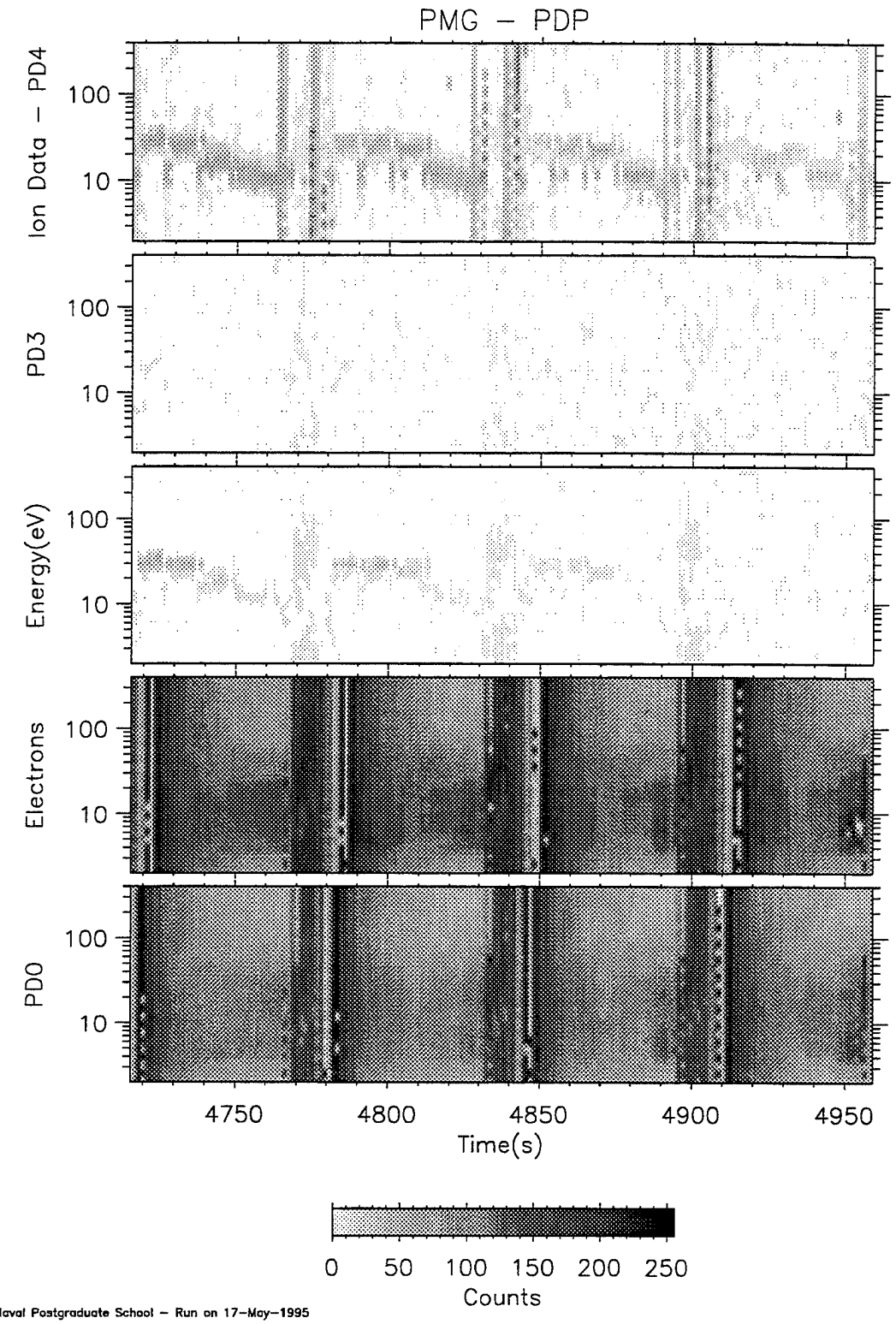
PMG – PDP
Ion Data – PD4
PD3
Energy(eV)
Electrons
PD0
100
10
4750
4800
4850
4900
4950
Time(s)
0
50
100
150
200
250
Counts
Naval Postgraduate School – Run on 17–May–1995

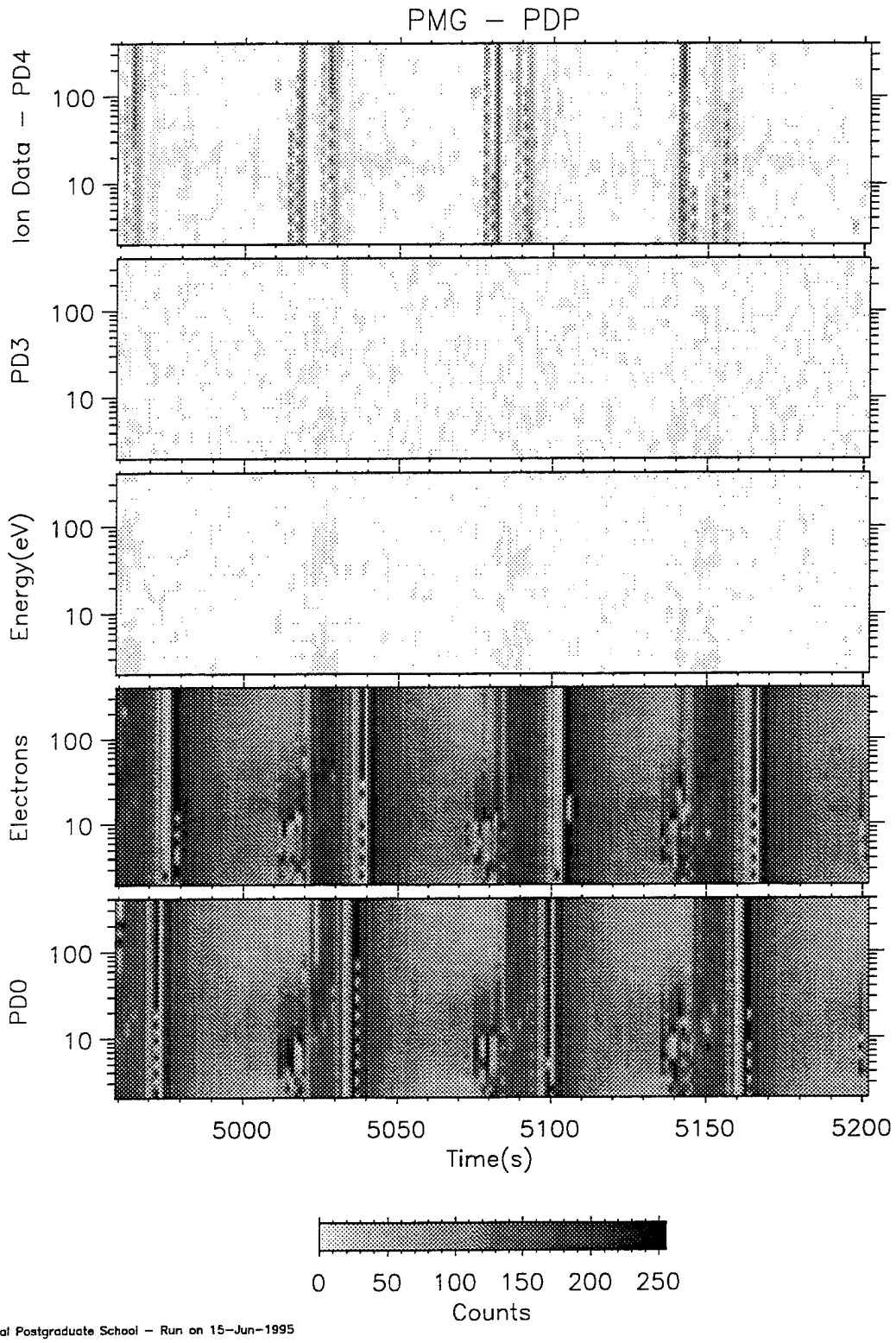
PMG – PDP
Ion Data – PD4
PD3
Energy(eV)
Electrons
PD0
100
10
5000
5050
5100
5150
5200
Time(s)
0
50
100
150
200
250
Counts
Naval Postgraduate School – Run on 15–Jun–1995

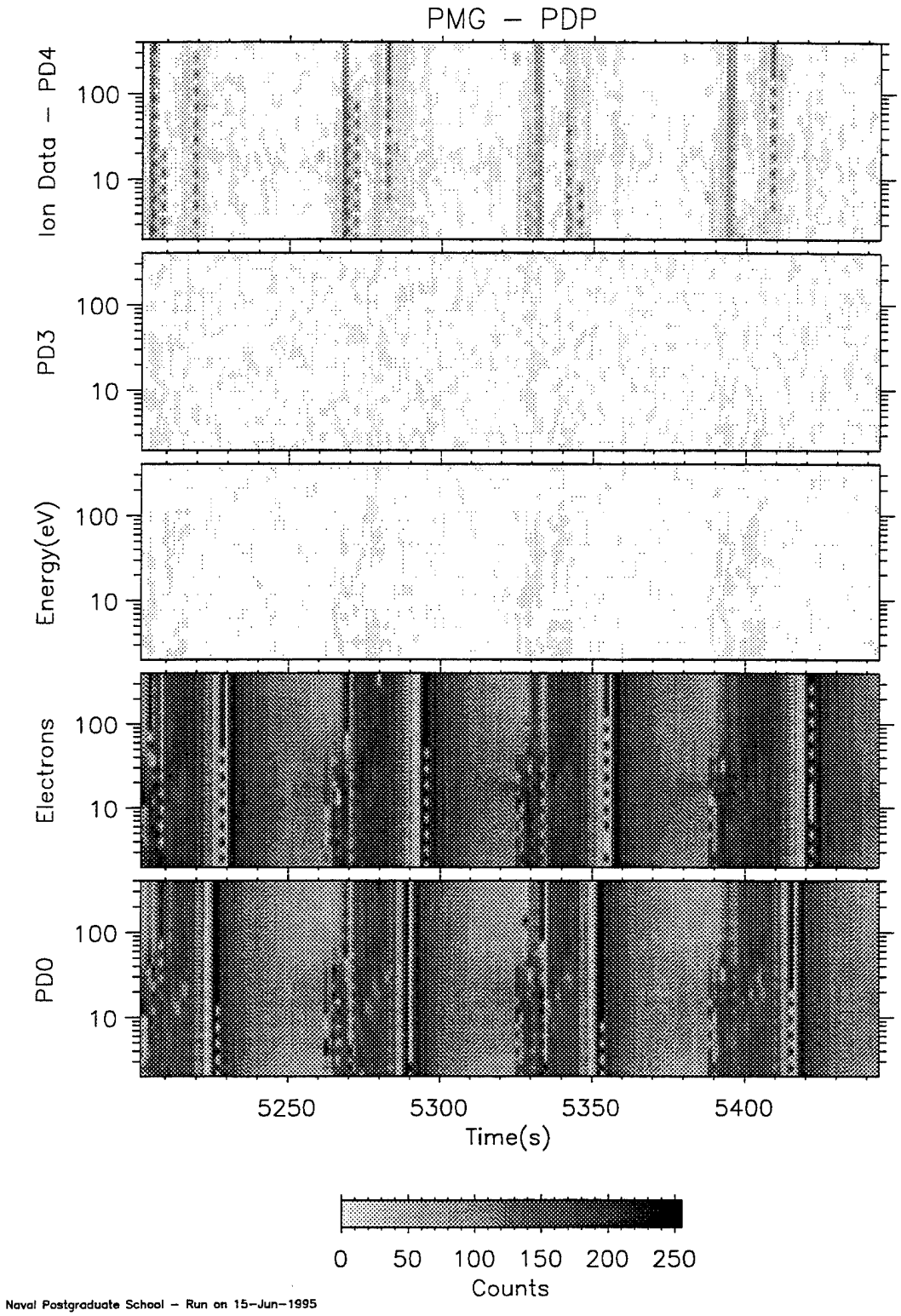
PMG – PDP
Ion Data – PD4
PD3
Energy(eV)
Electrons
PD0
100
10
5250
5300
5350
5400
Time(s)
0
50
100
150
200
250
Counts
Naval Postgraduate School – Run on 15–Jun–1995

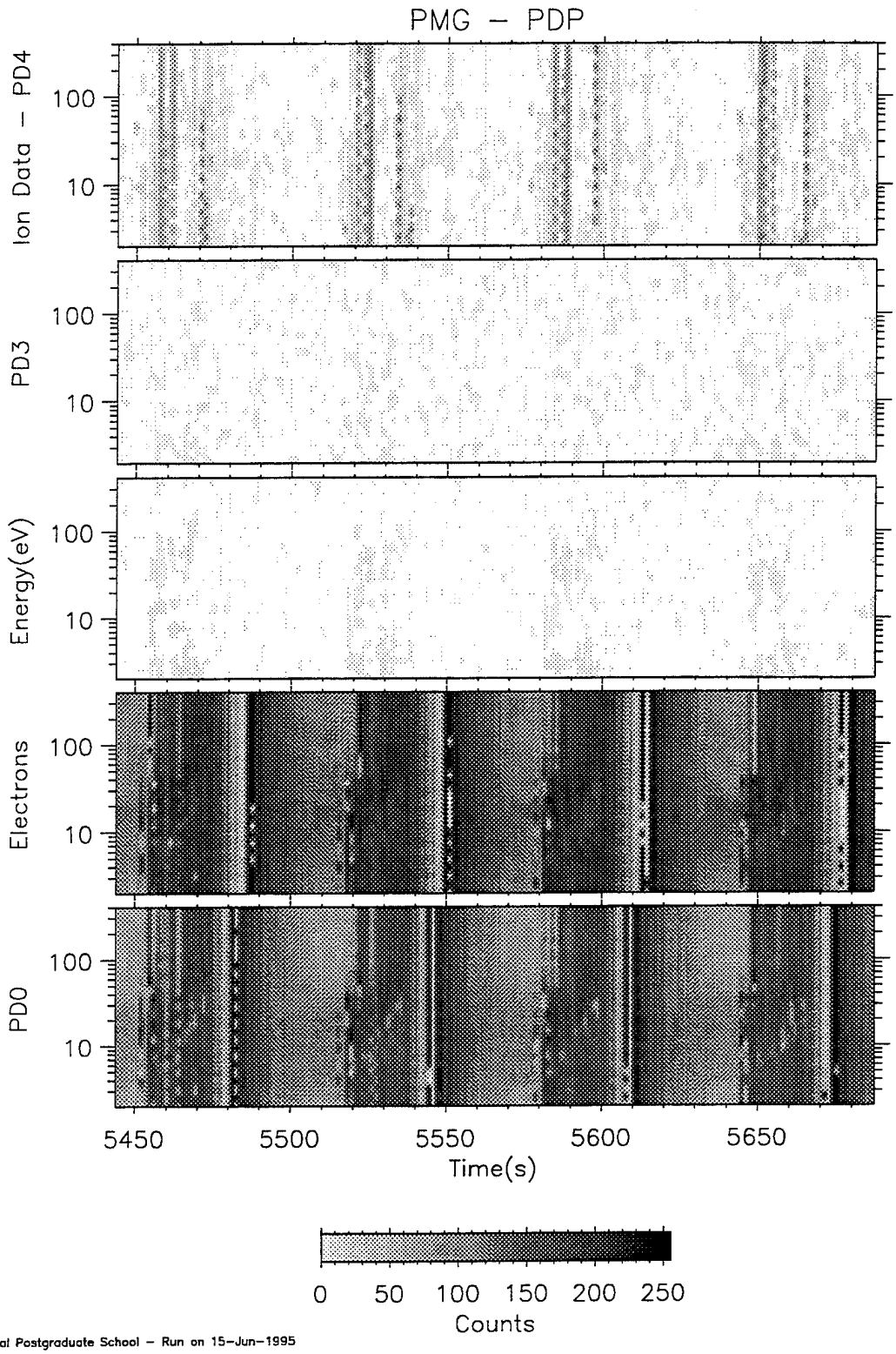
PMG – PDP
Ion Data – PD4
PD3
Energy(eV)
Electrons
PD0
100
10
5450
5500
5550
5600
5650
Time(s)
0
50
100
150
200
250
Counts
Naval Postgraduate School – Run on 15–Jun–1995

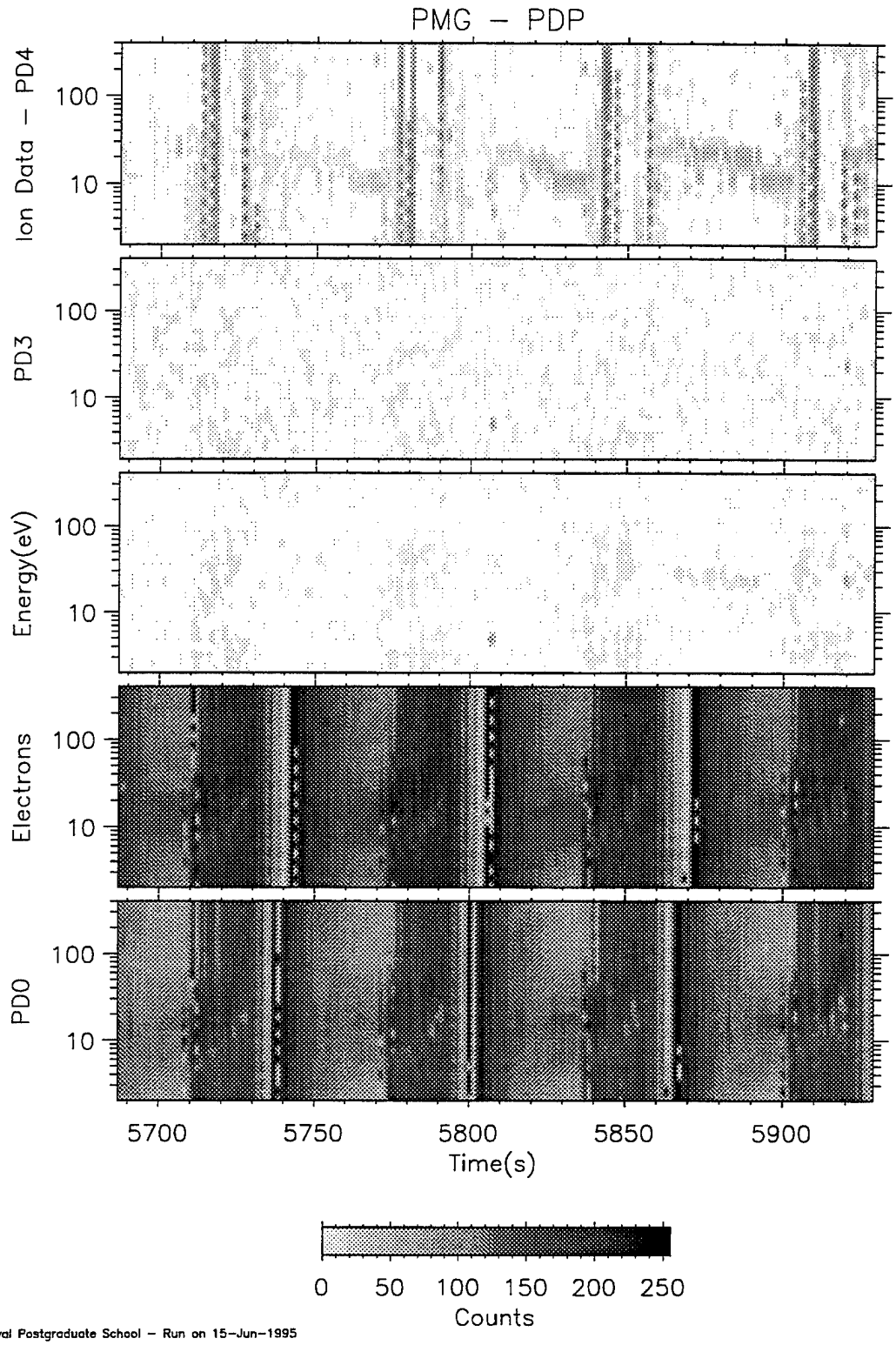
PMG – PDP
Ion Data – PD4
PD3
Energy(eV)
Electrons
PD0
100
10
5700
5750
5800
5850
5900
Time(s)
0
50
100
150
200
250
Counts
Naval Postgraduate School – Run on 15–Jun–1995

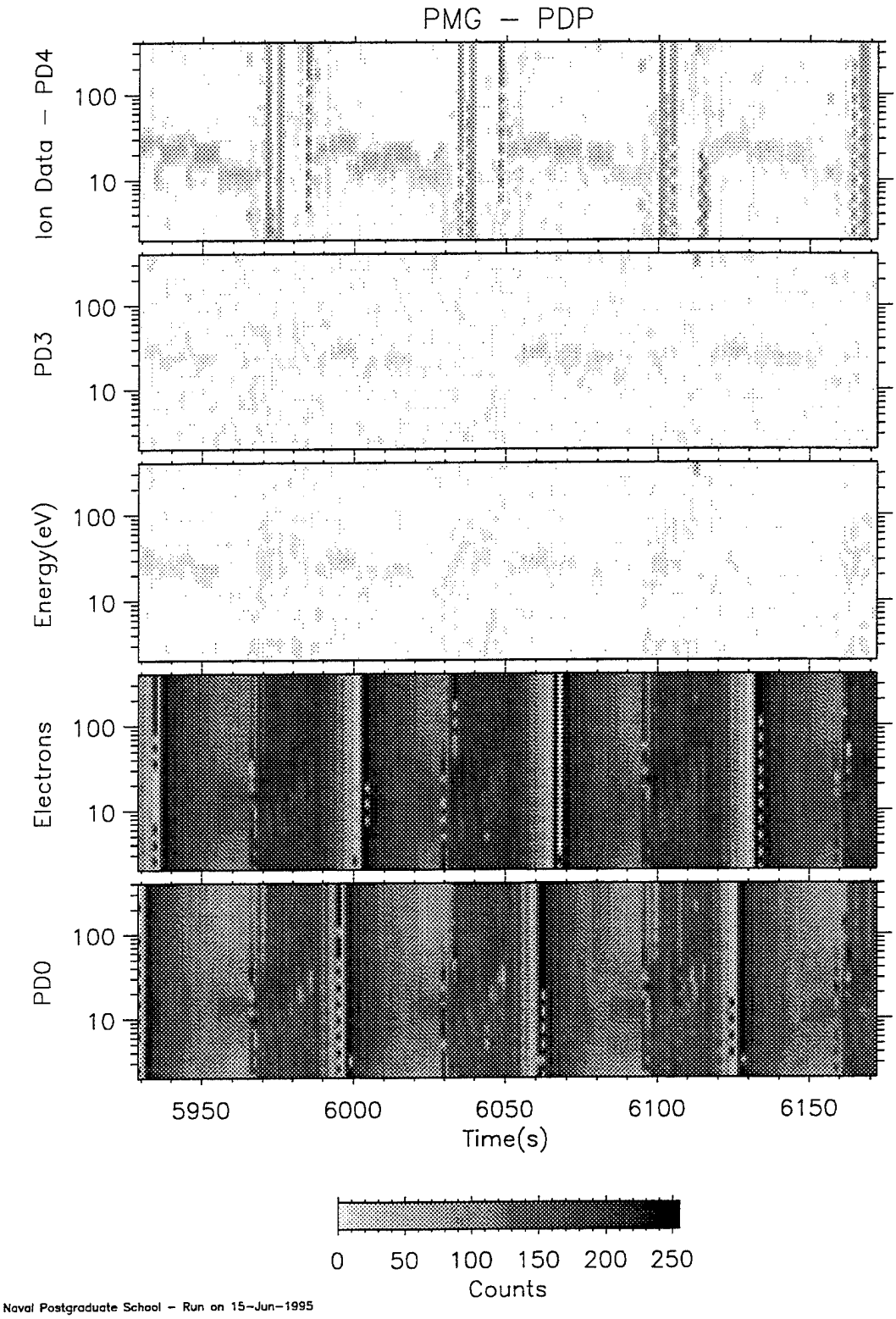
PMG – PDP
Ion Data – PD4
PD3
Energy(eV)
Electrons
PD0
100
10
5950
6000
6050
6100
6150
Time(s)
0
50
100
150
200
250
Counts
Naval Postgraduate School – Run on 15–Jun–1995

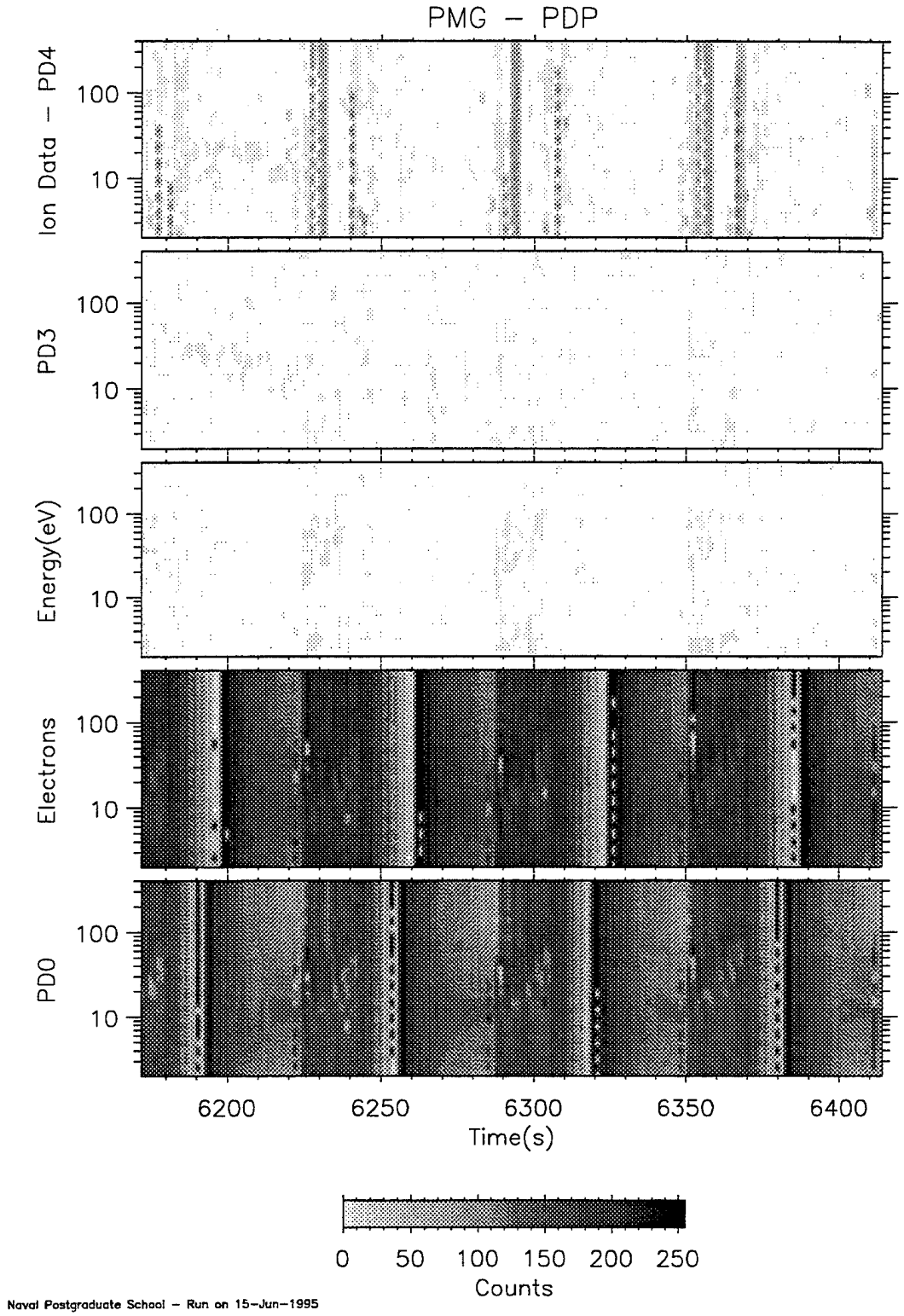
PMG – PDP
Ion Data – PD4
PD3
Energy(eV)
Electrons
PD0
100
10
6200
6250
6300
6350
6400
Time(s)
0
50
100
150
200
250
Counts
Naval Postgraduate School – Run on 15–Jun–1995

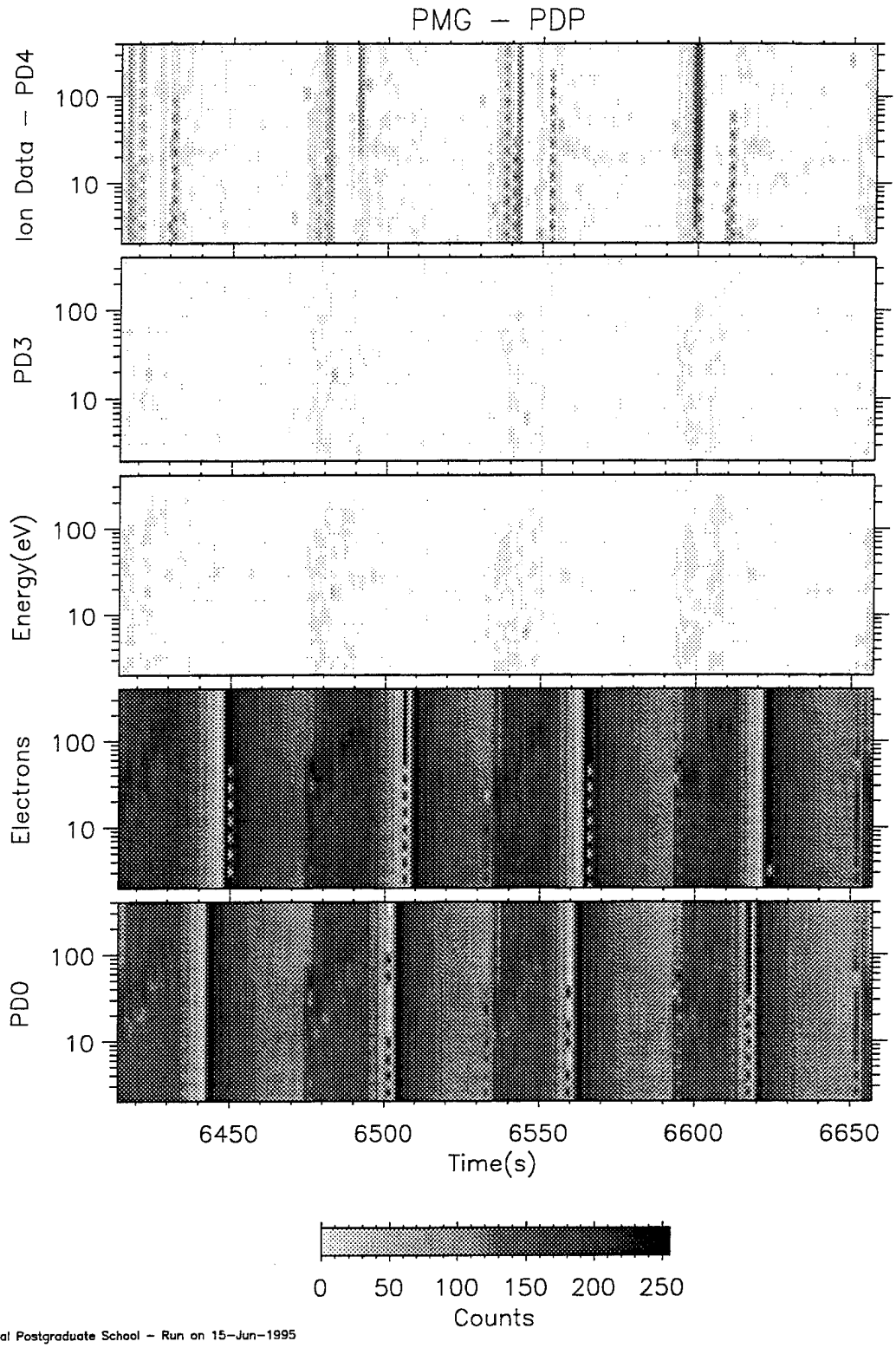
PMG – PDP
Ion Data – PD4
PD3
Energy(eV)
Electrons
PD0
100
10
6450
6500
6550
6600
6650
Time(s)
0
50
100
150
200
250
Counts
Naval Postgraduate School – Run on 15–Jun–1995

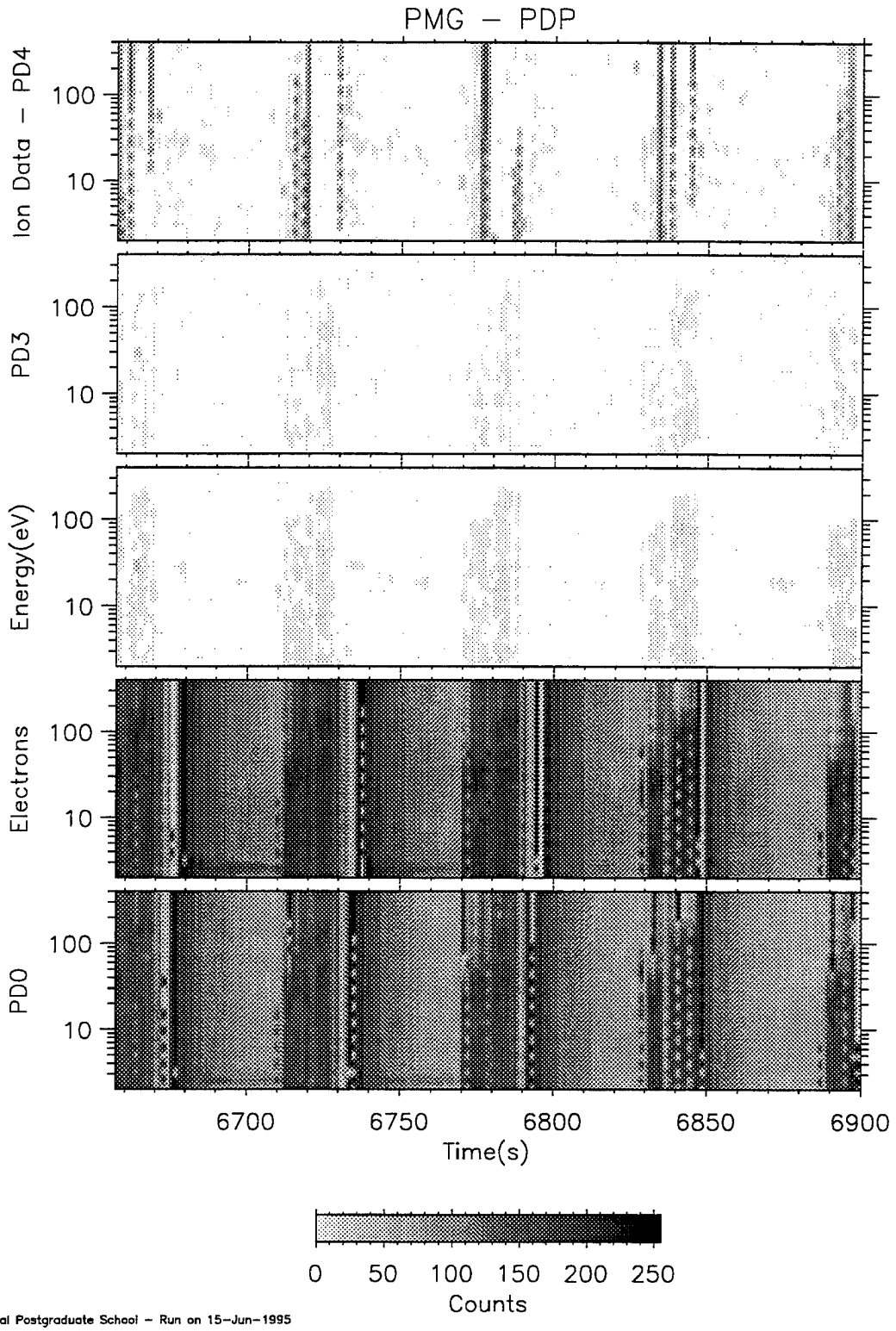
PMG – PDP
Ion Data – PD4
PD3
Energy(eV)
Electrons
PD0
100
10
6700
6750
6800
6850
6900
Time(s)
0
50
100
150
200
250
Counts
Naval Postgraduate School – Run on 15–Jun–1995

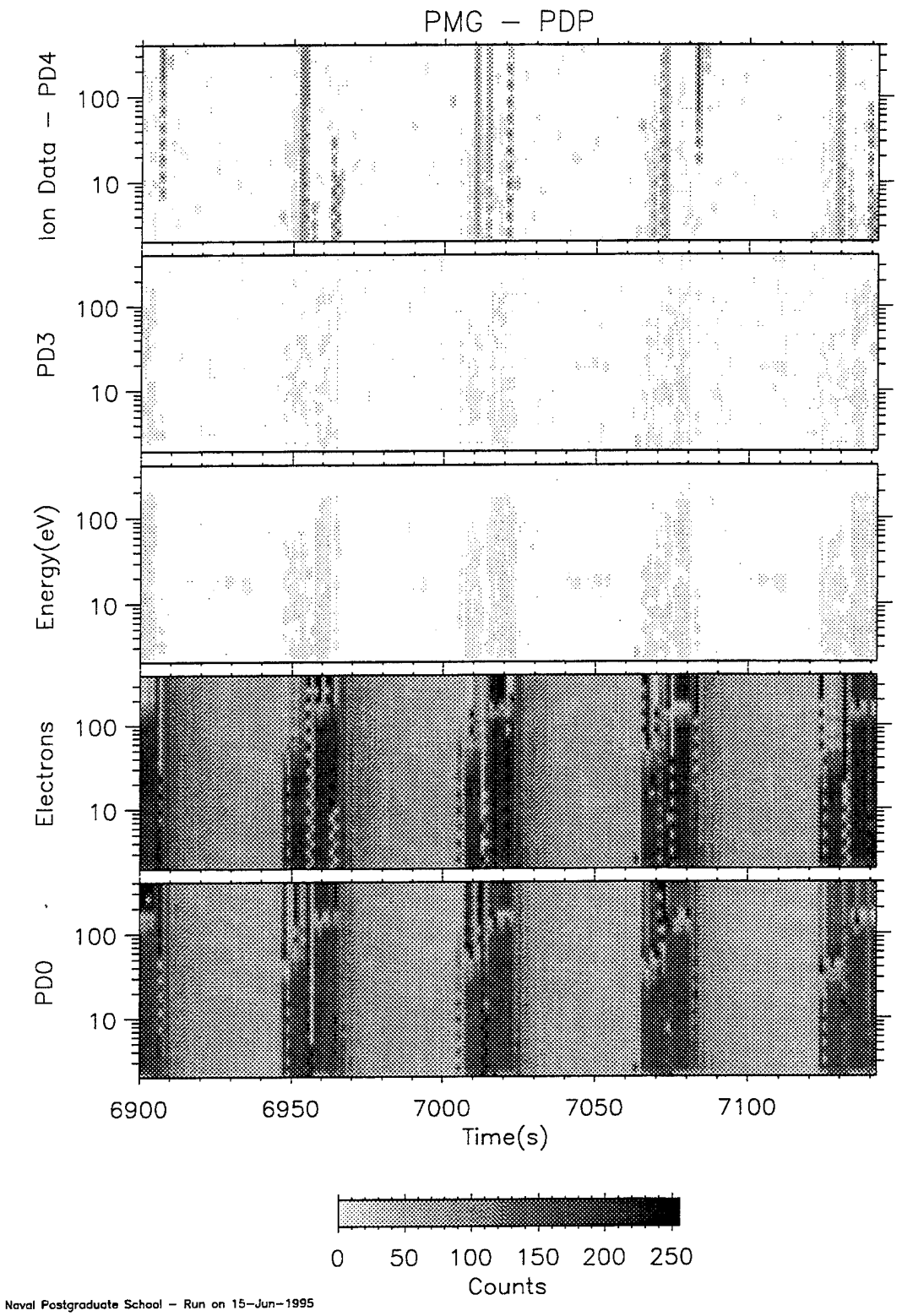
PMG – PDP
Ion Data – PD4
PD3
Energy(eV)
Electrons
PD0
100
10
6900
6950
7000
7050
7100
Time(s)
0
50
100
150
200
250
Counts
Naval Postgraduate School – Run on 15–Jun–1995

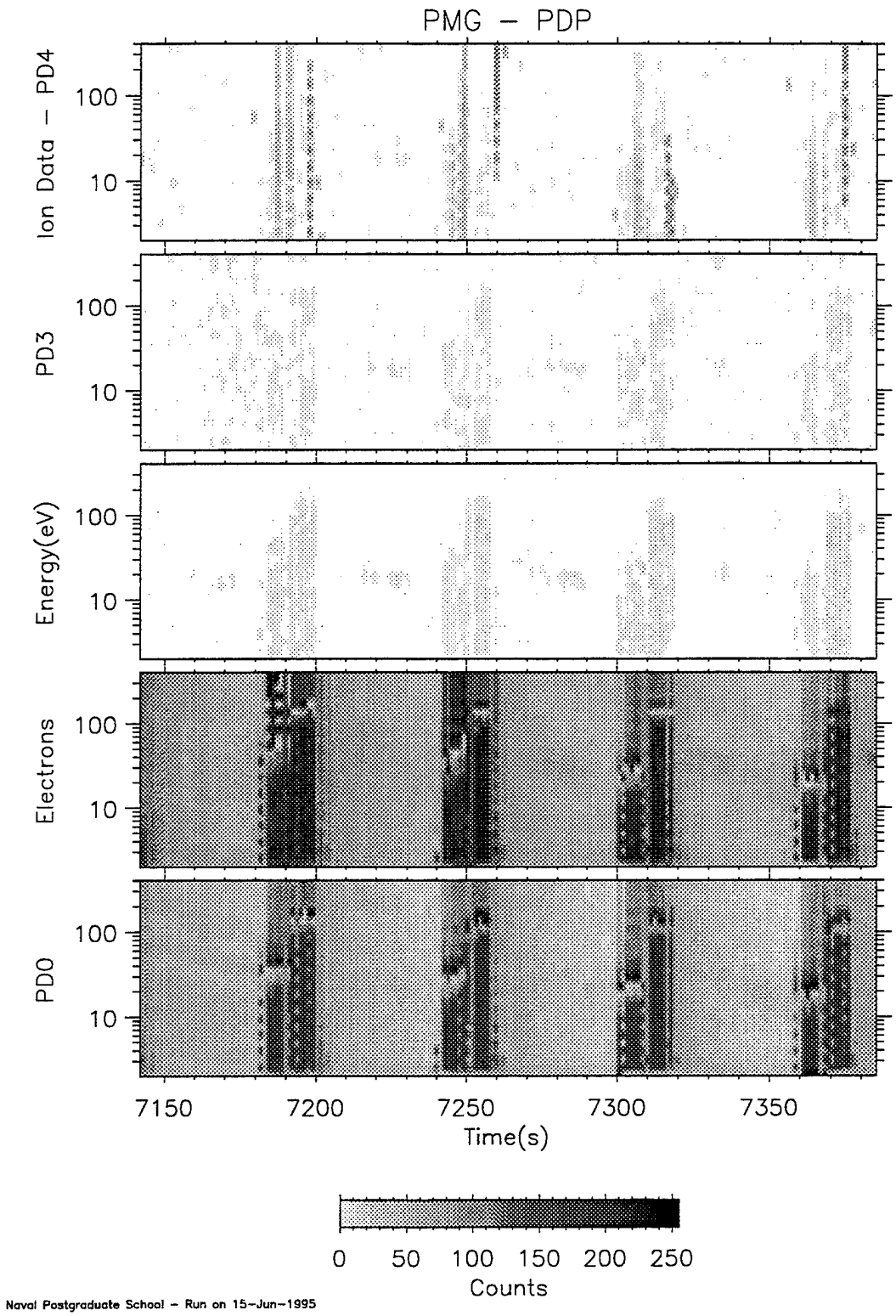
PMG – PDP
Ion Data – PD4
PD3
Energy(eV)
Electrons
PD0
100
10
7150
7200
7250
7300
7350
Time(s)
0
50
100
150
200
250
Counts
Naval Postgraduate School – Run on 15–Jun–1995

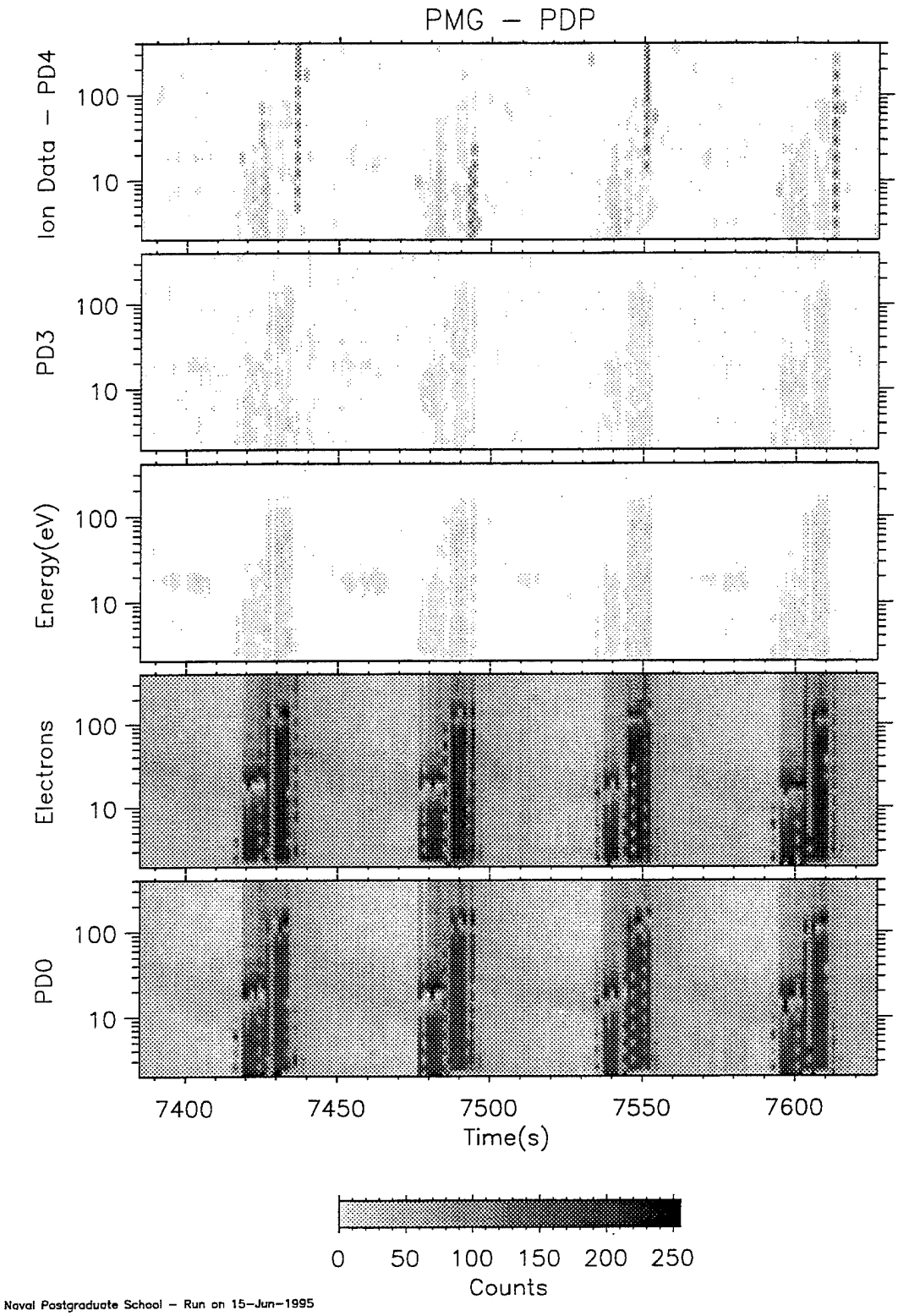
PMG – PDP
Ion Data – PD4
PD3
Energy(eV)
Electrons
PD0
100
10
7400
7450
7500
7550
7600
Time(s)
0
50
100
150
200
250
Counts
Naval Postgraduate School – Run on 15–Jun–1995

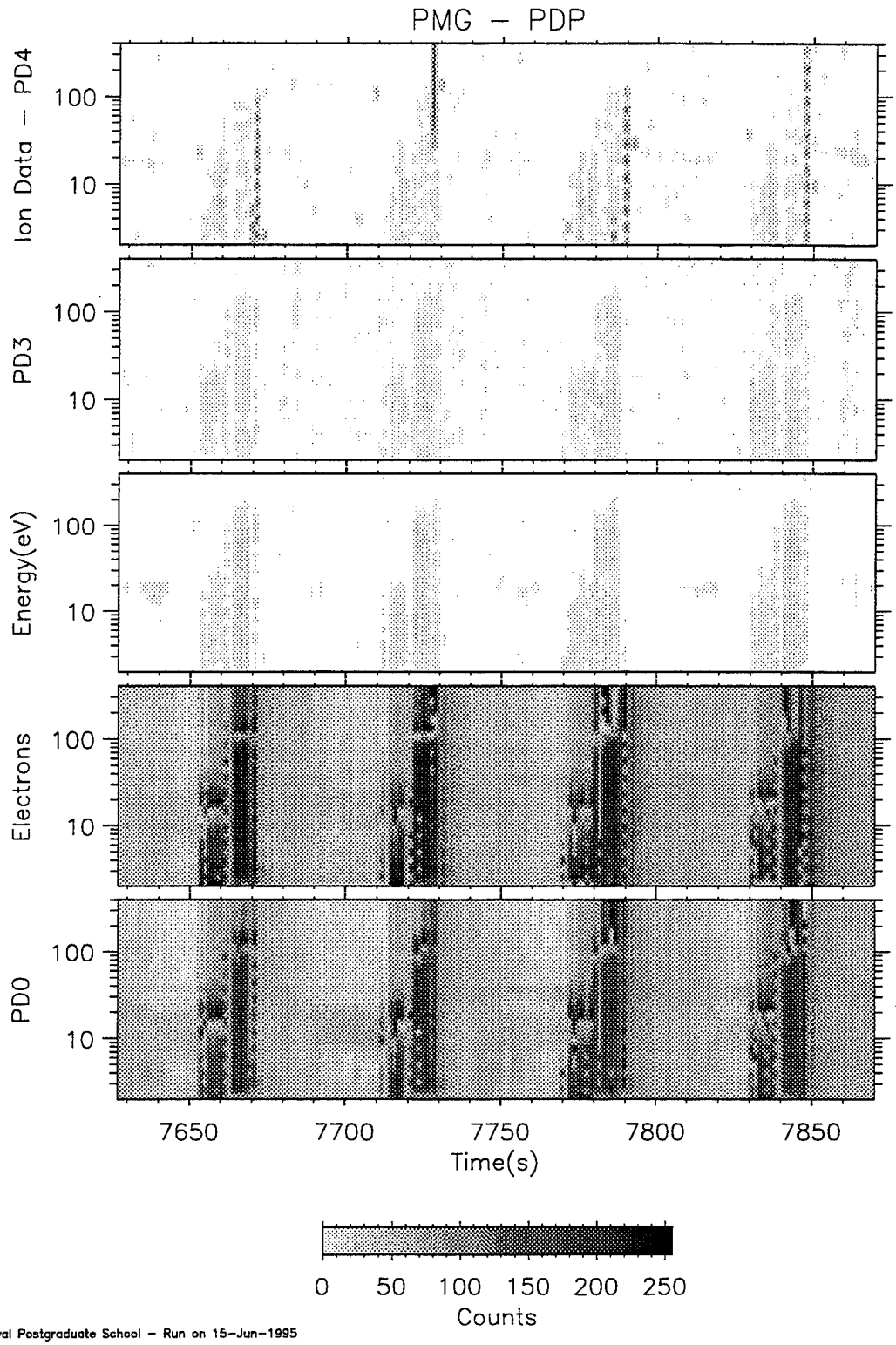
PMG – PDP
Ion Data – PD4
PD3
Energy(eV)
Electrons
PD0
100
10
7650
7700
7750
7800
7850
Time(s)
0
50
100
150
200
250
Counts
Naval Postgraduate School – Run on 15–Jun–1995

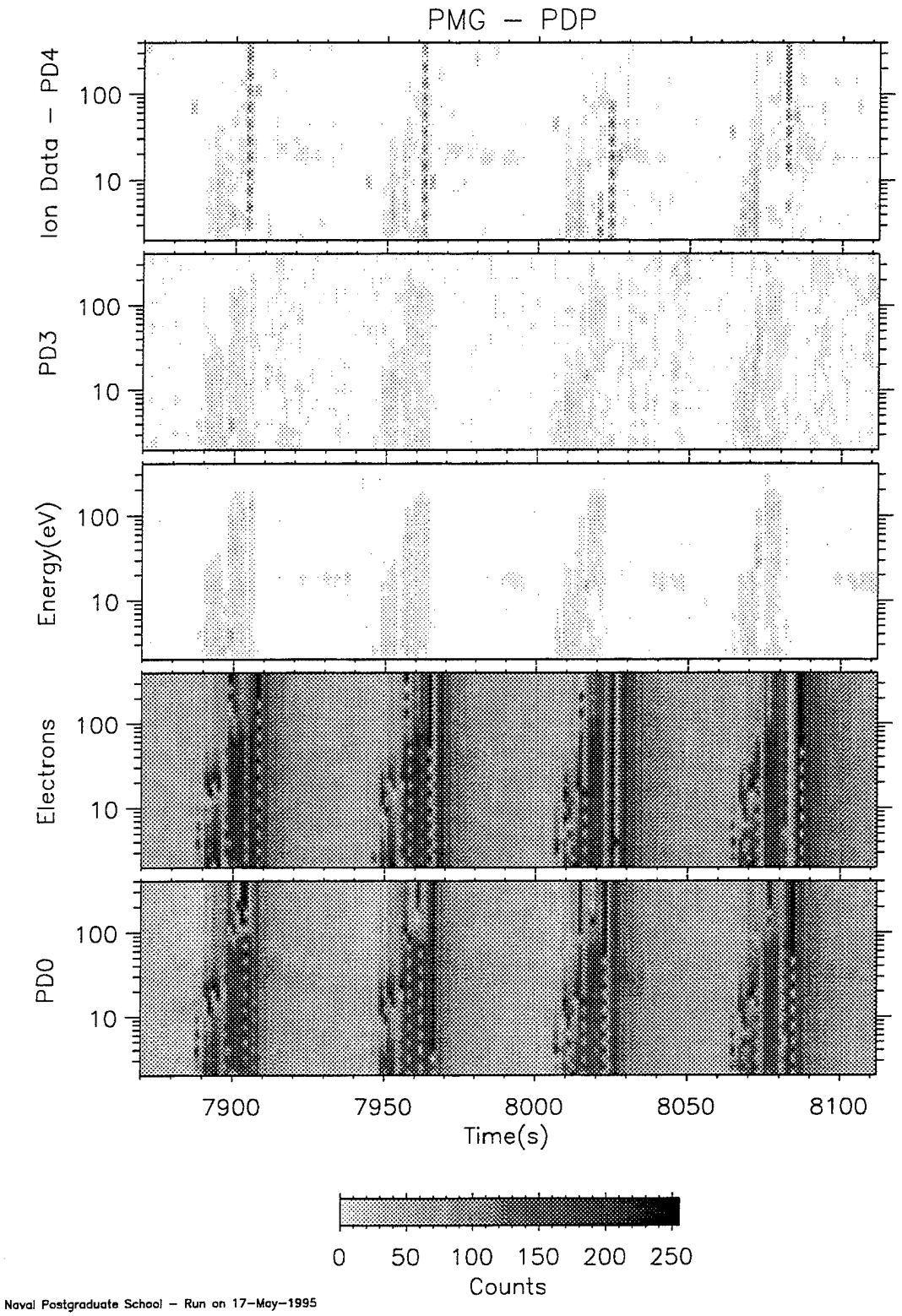
PMG – PDP
Ion Data – PD4
PD3
Energy(eV)
Electrons
PD0
100
10
7900
7950
8000
8050
8100
Time(s)
0
50
100
150
200
250
Counts
Naval Postgraduate School – Run on 17–May–1995

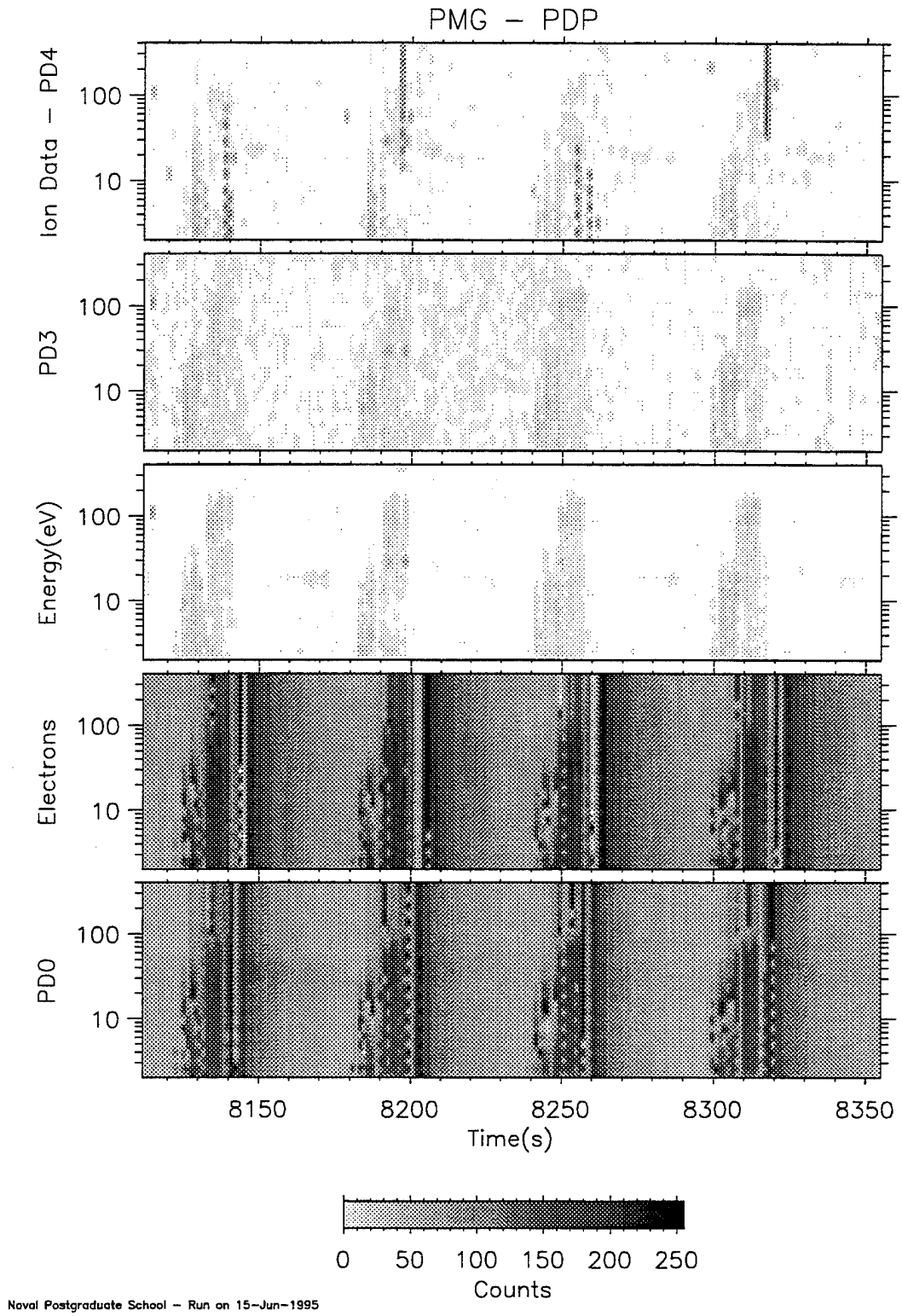
PMG – PDP
Ion Data – PD4
PD3
Energy(eV)
Electrons
PD0
100
10
8150
8200
8250
8300
8350
Time(s)
0
50
100
150
200
250
Counts
Naval Postgraduate School – Run on 15–Jun–1995

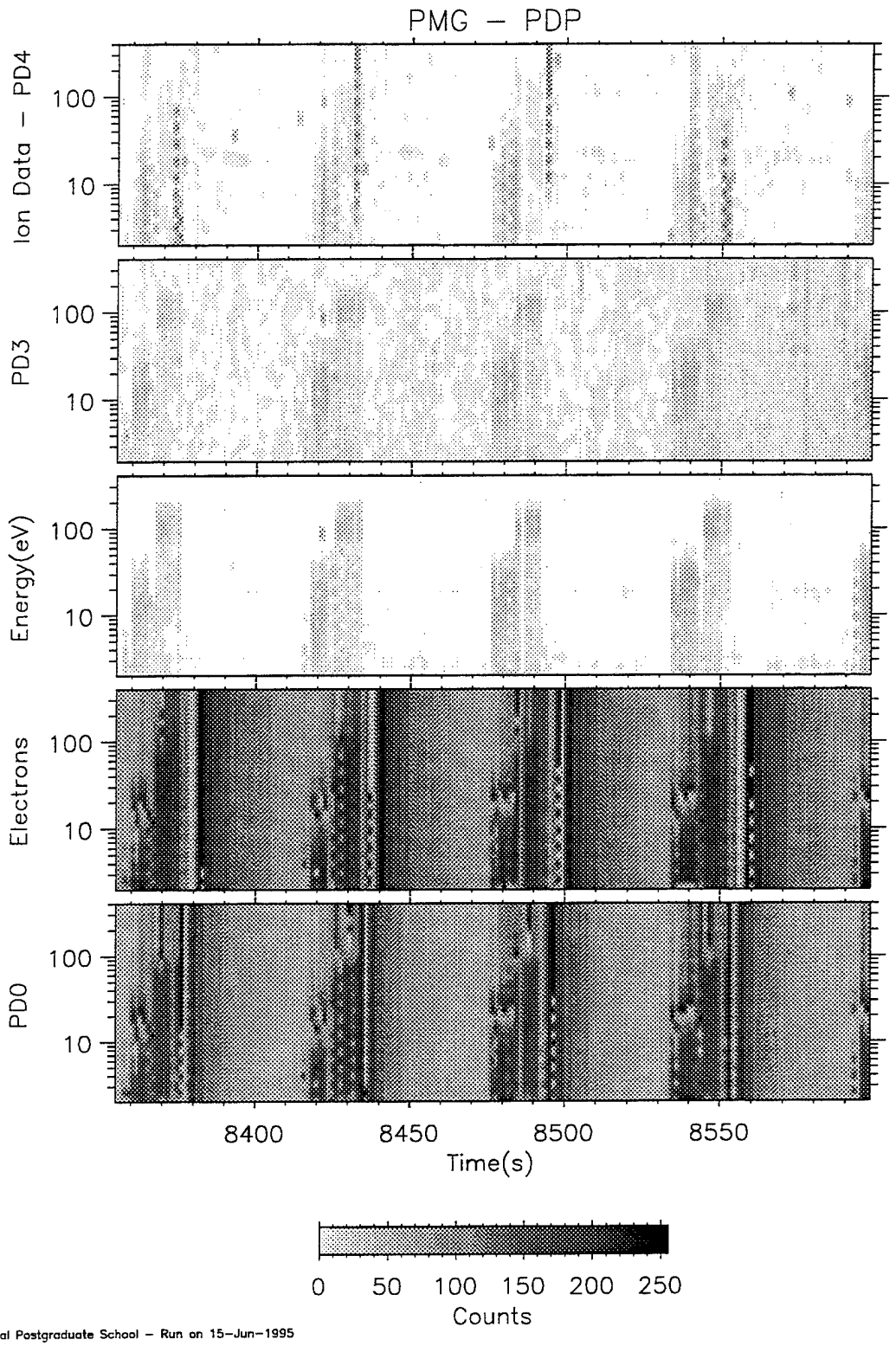
PMG – PDP
Ion Data – PD4
PD3
Energy(eV)
Electrons
PD0
100
10
8400
8450
8500
8550
Time(s)
0
50
100
150
200
250
Counts
Naval Postgraduate School – Run on 15–Jun–1995

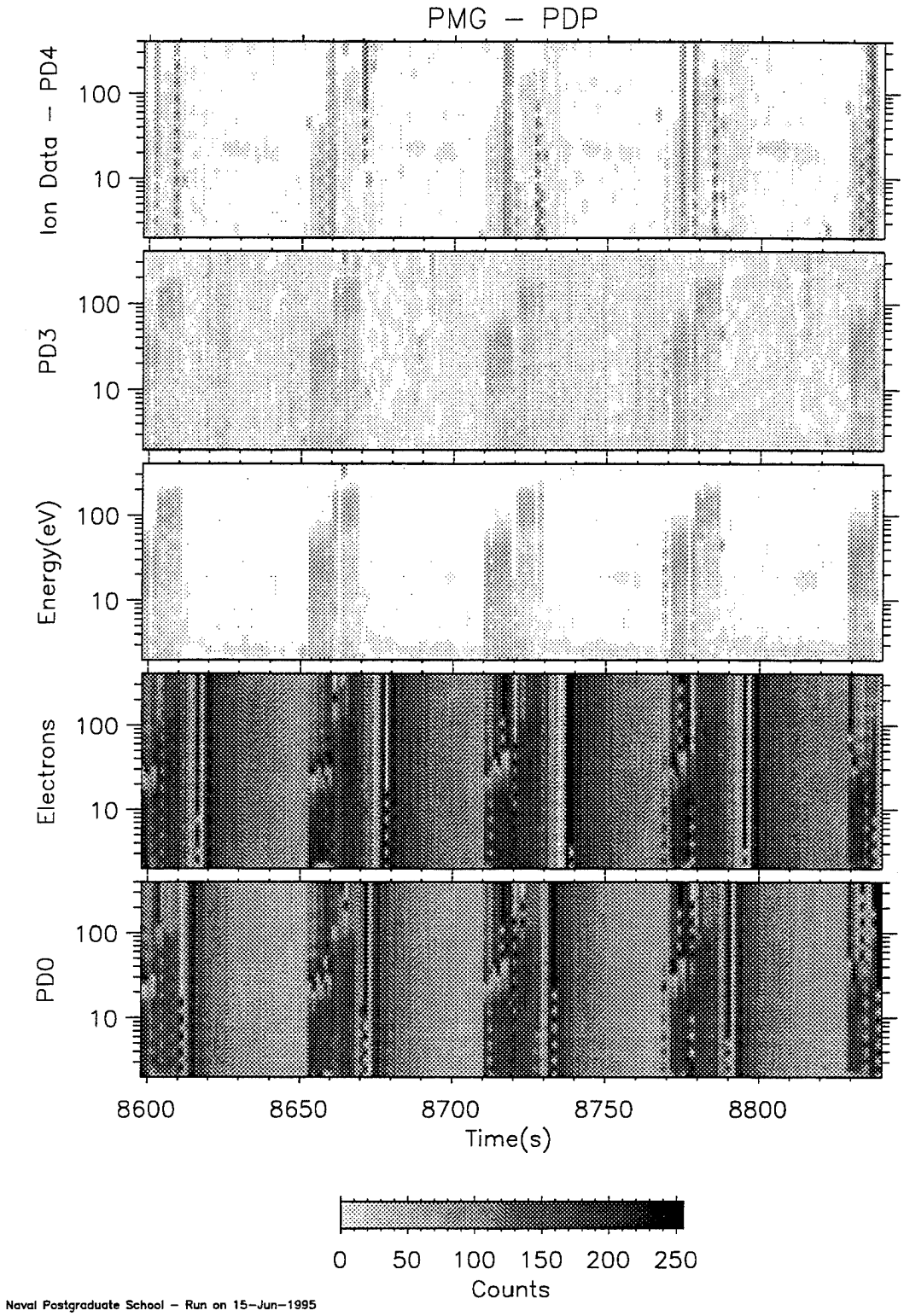
PMG – PDP
Ion Data – PD4
PD3
Energy(eV)
Electrons
PD0
100
10
8600
8650
8700
8750
8800
Time(s)
0
50
100
150
200
250
Counts
Naval Postgraduate School – Run on 15–Jun–1995

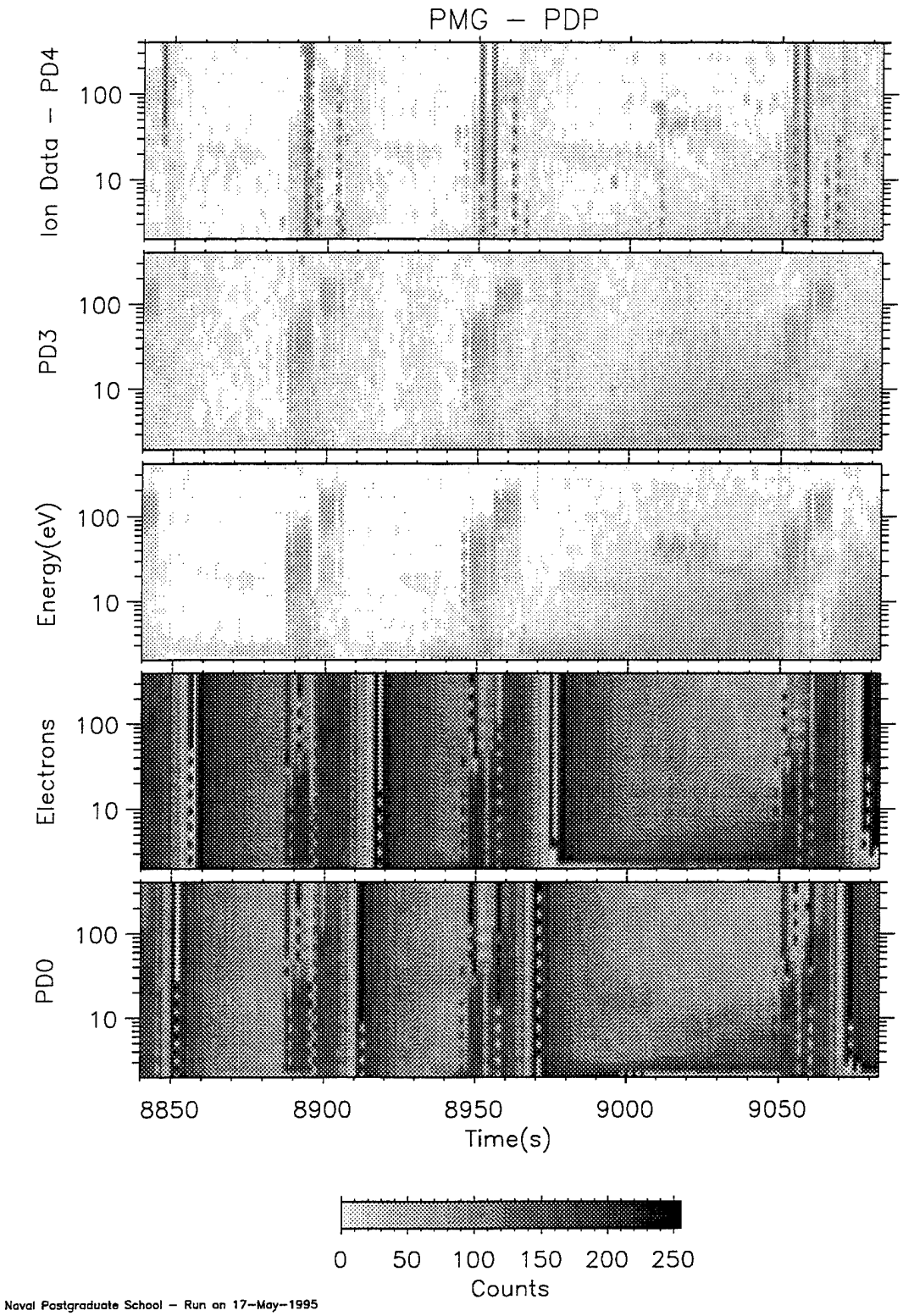
PMG – PDP
Ion Data – PD4
PD3
Energy(eV)
Electrons
PD0
100
10
8850
8900
8950
9000
9050
Time(s)
0
50
100
150
200
250
Counts
Naval Postgraduate School – Run on 17–May–1995

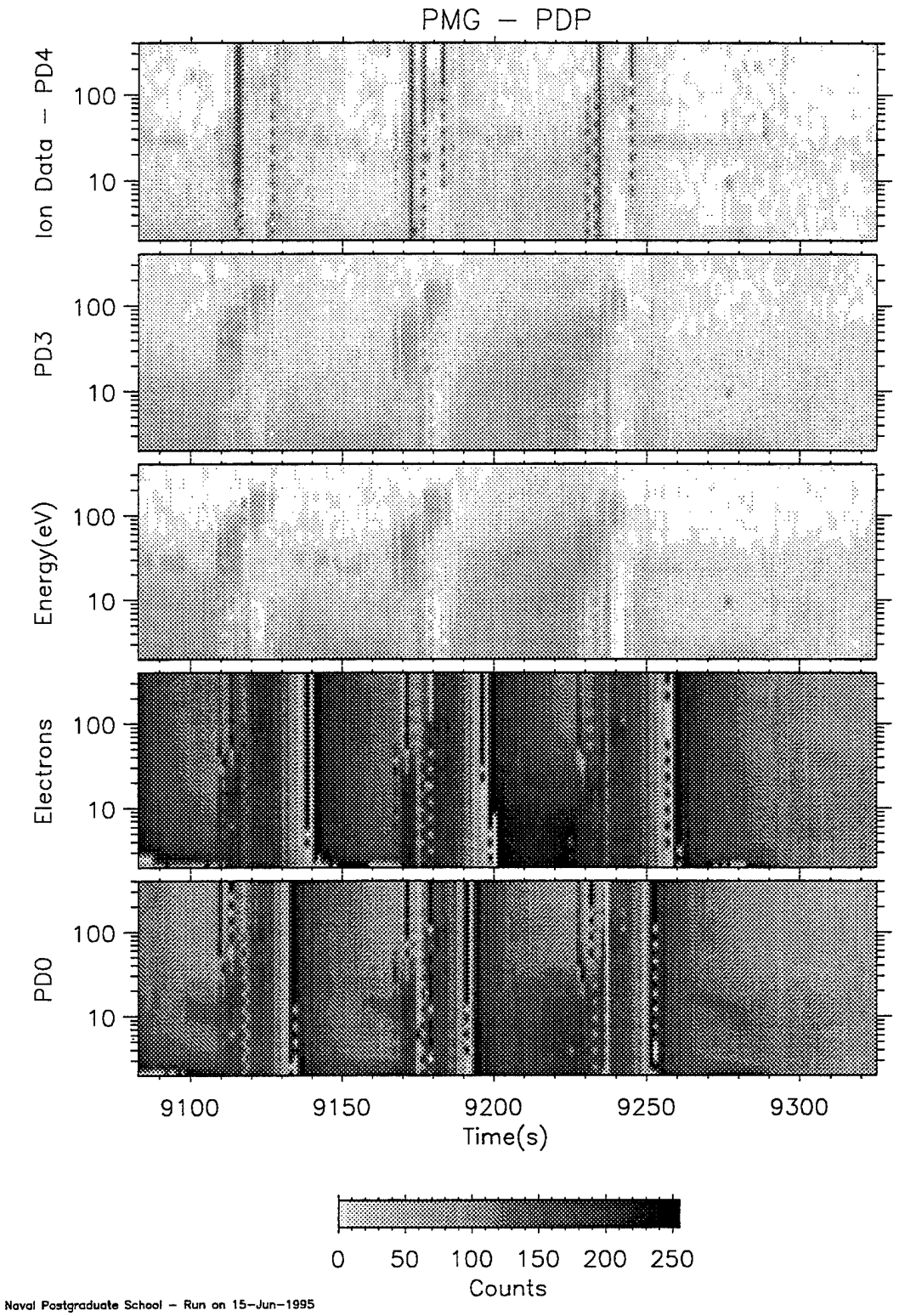
PMG – PDP
Ion Data – PD4
PD3
Energy(eV)
Electrons
PD0
100
10
9100
9150
9200
9250
9300
Time(s)
0
50
100
150
200
250
Counts
Naval Postgraduate School – Run on 15–Jun–1995

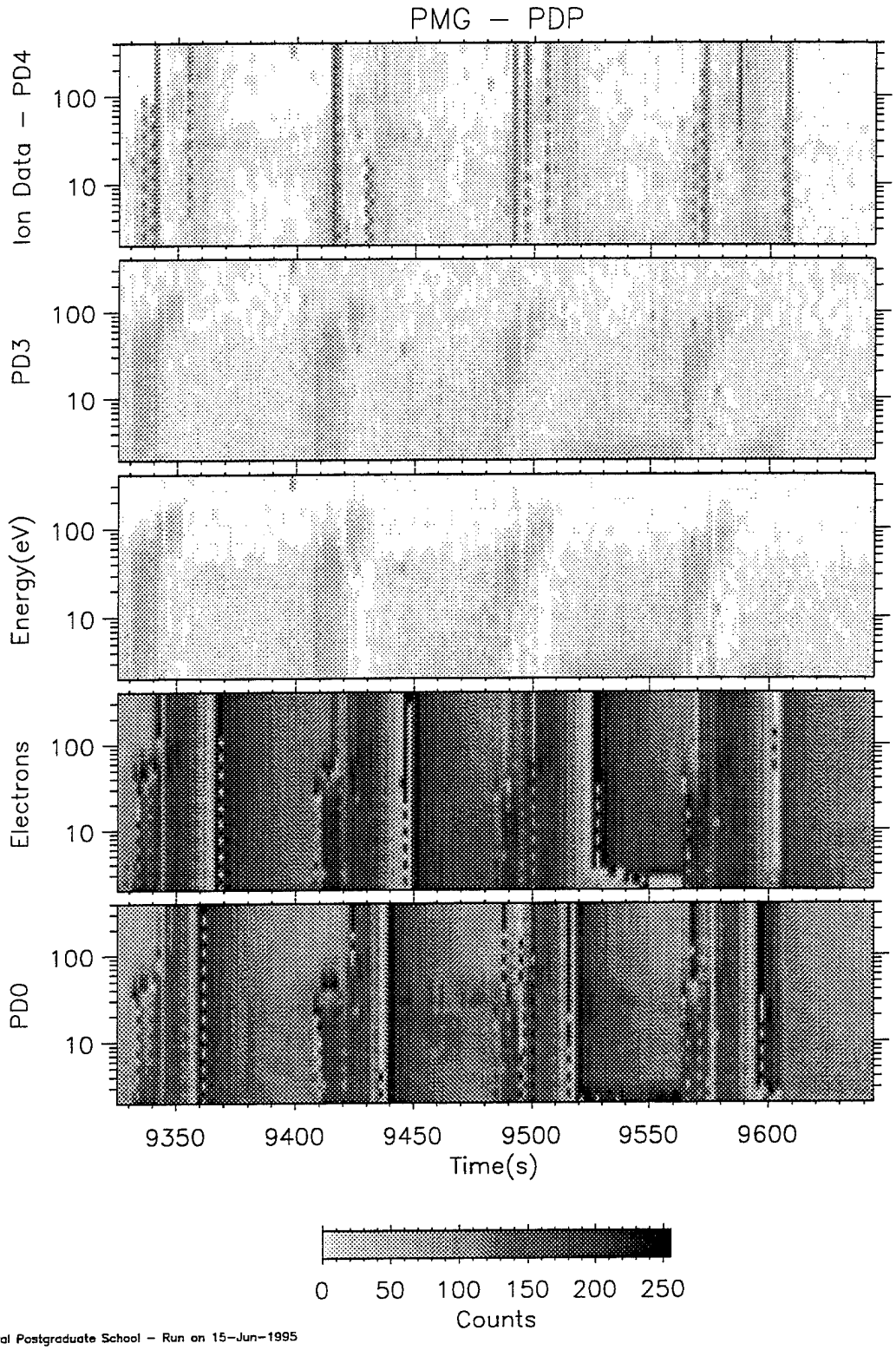
PMG – PDP
Ion Data – PD4
PD3
Energy(eV)
Electrons
PD0
100
10
9350
9400
9450
9500
9550
9600
Time(s)
0
50
100
150
200
250
Counts
Naval Postgraduate School – Run on 15–Jun–1995

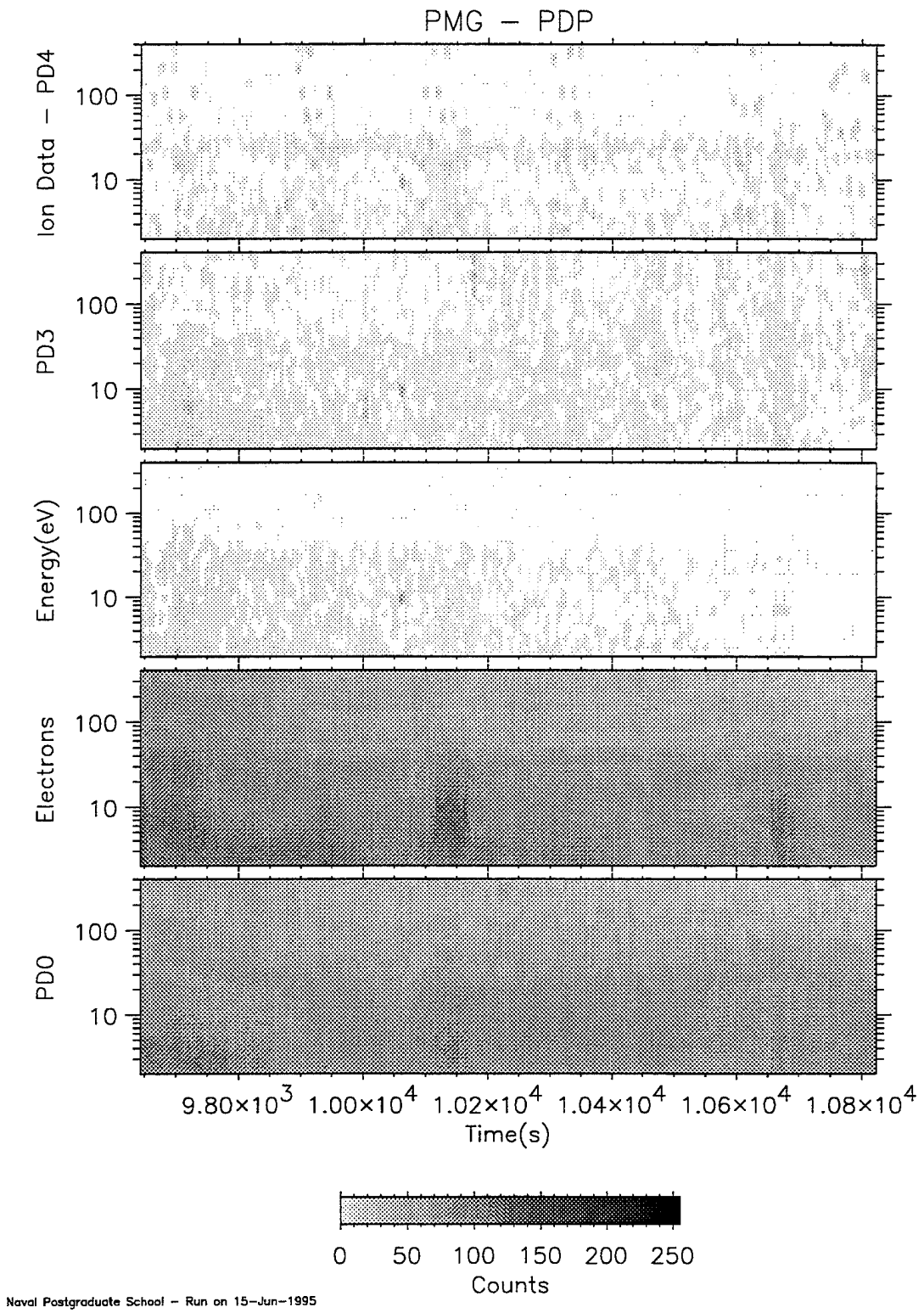
PMG – PDP
Ion Data – PD4
PD3
Energy(eV)
Electrons
PD0
100
10
9.80×10^3
1.00×10^4
1.02×10^4
1.04×10^4
1.06×10^4
1.08×10^4
Time(s)
0
50
100
150
200
250
Counts
Naval Postgraduate School – Run on 15–Jun–1995

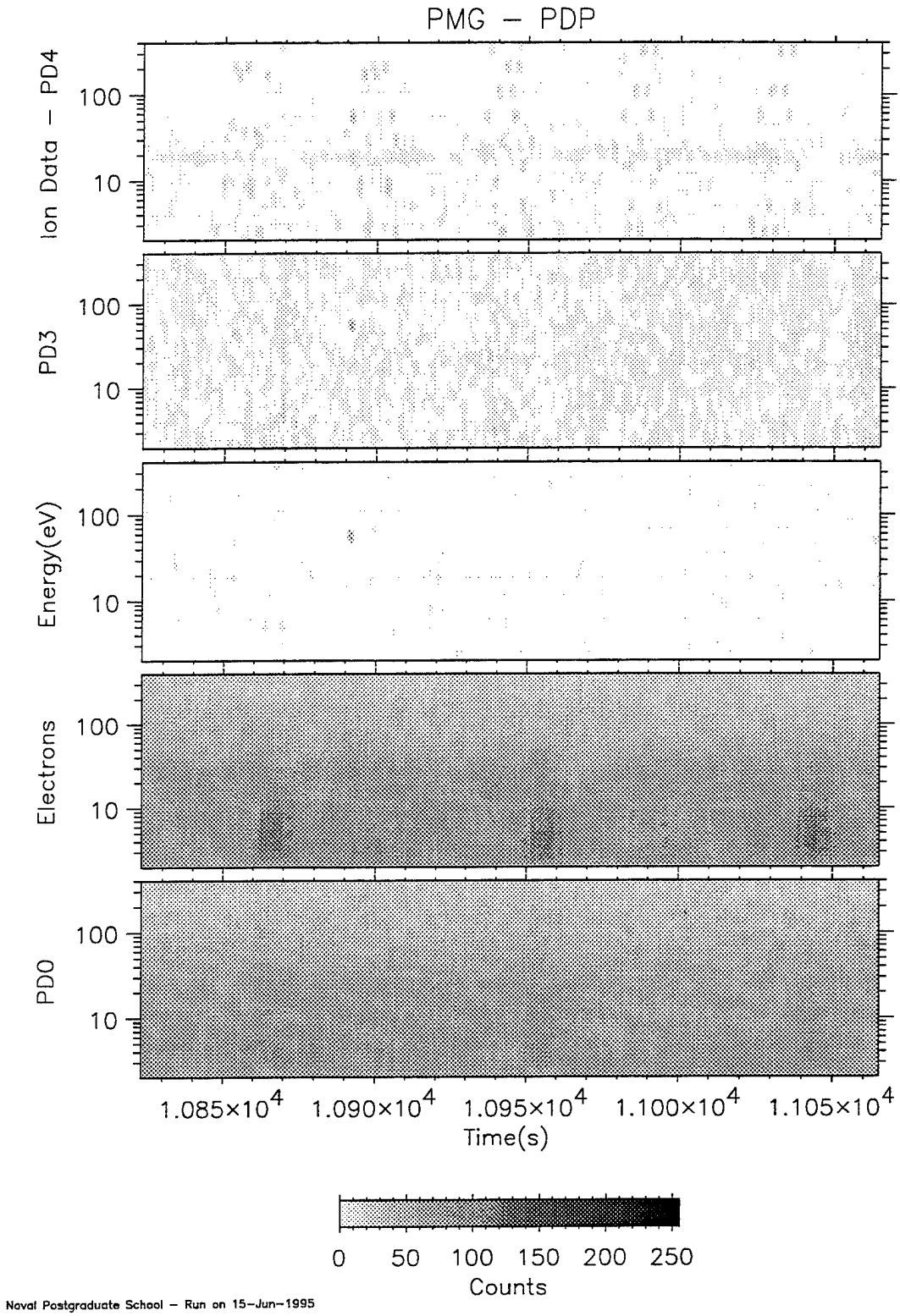
PMG – PDP
Ion Data – PD4
PD3
Energy(eV)
Electrons
PD0
100
10
1.085×10^4
1.090×10^4
1.095×10^4
1.100×10^4
1.105×10^4
Time(s)
0
50
100
150
200
250
Counts
Naval Postgraduate School – Run on 15–Jun–1995

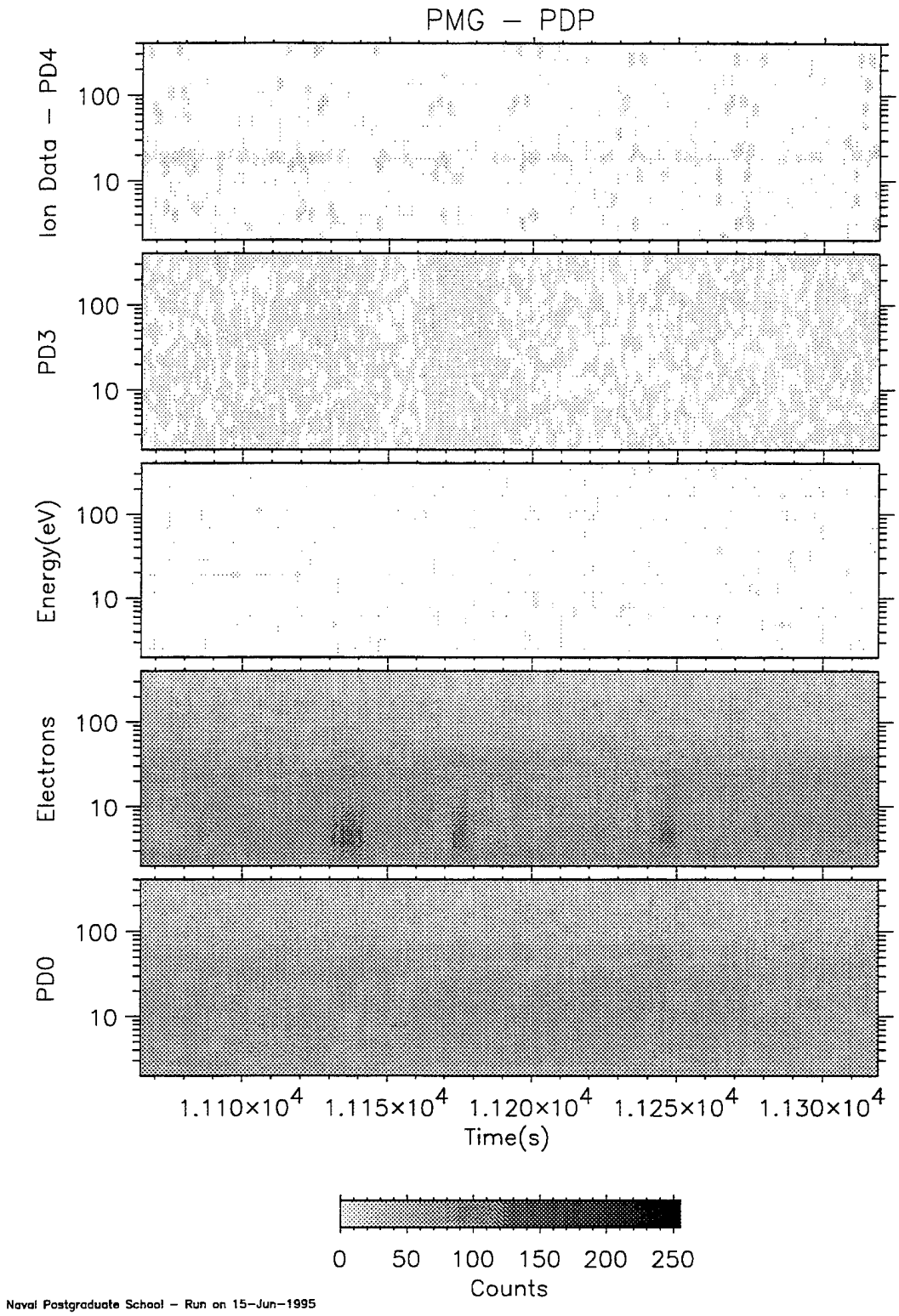
PMG – PDP
Ion Data – PD4
PD3
Energy(eV)
Electrons
PD0
100
10
1.110×10^4
1.115×10^4
1.120×10^4
1.125×10^4
1.130×10^4
Time(s)
0
50
100
150
200
250
Counts
Naval Postgraduate School – Run on 15–Jun–1995

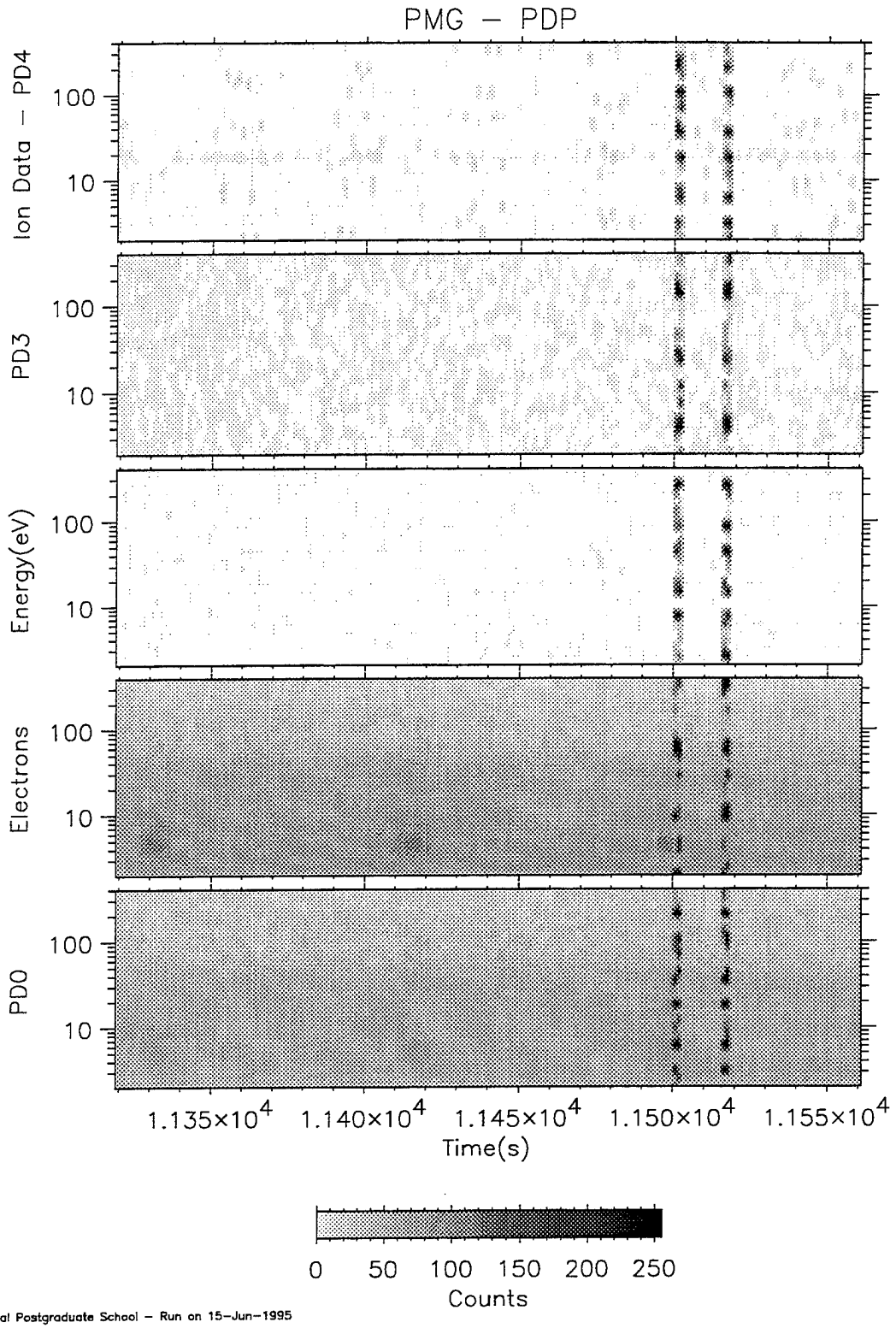
PMG – PDP
Ion Data – PD4
PD3
Energy(eV)
Electrons
PD0
100
10
1.135×10^4
1.140×10^4
1.145×10^4
1.150×10^4
1.155×10^4
Time(s)
0
50
100
150
200
250
Counts
Naval Postgraduate School – Run on 15–Jun–1995

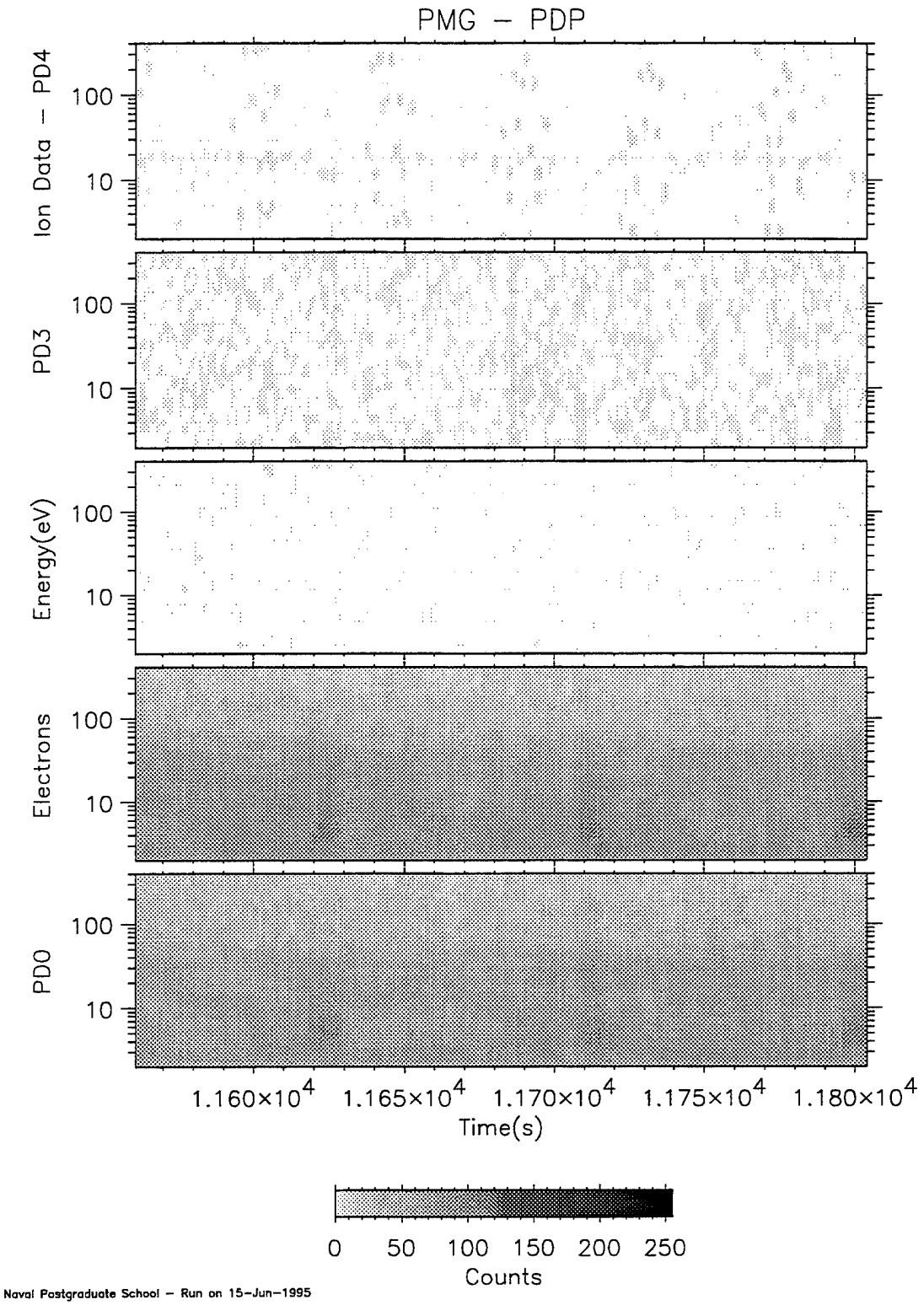
PMG – PDP
Ion Data – PD4
PD3
Energy(eV)
Electrons
PD0
100
10
1.160×10^4
1.165×10^4
1.170×10^4
1.175×10^4
1.180×10^4
Time(s)
0
50
100
150
200
250
Counts
Naval Postgraduate School – Run on 15–Jun–1995

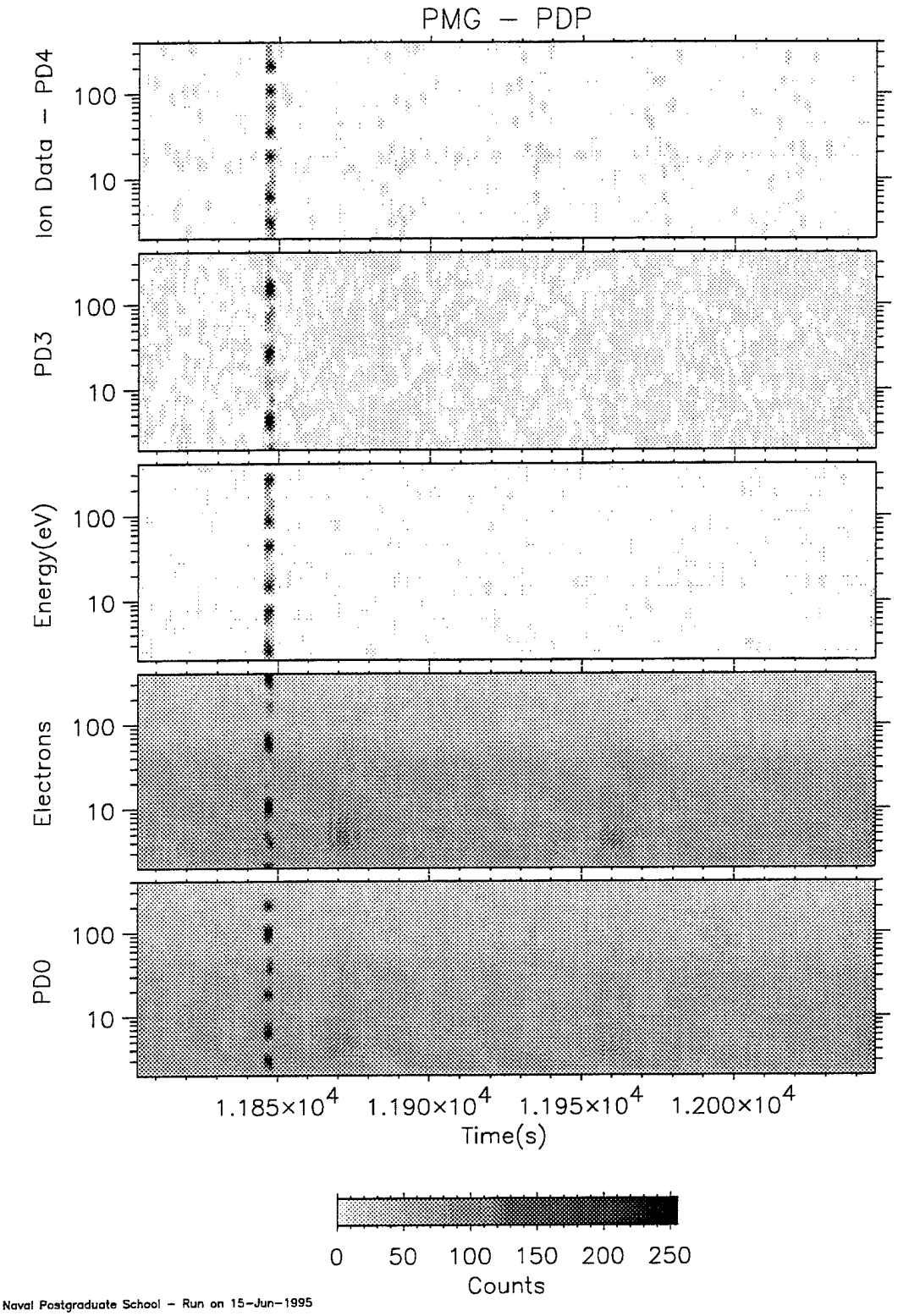
PMG – PDP
Ion Data – PD4
PD3
Energy(eV)
Electrons
PD0
100
10
1.185×10^4
1.190×10^4
1.195×10^4
1.200×10^4
Time(s)
0
50
100
150
200
250
Counts
Naval Postgraduate School – Run on 15–Jun–1995

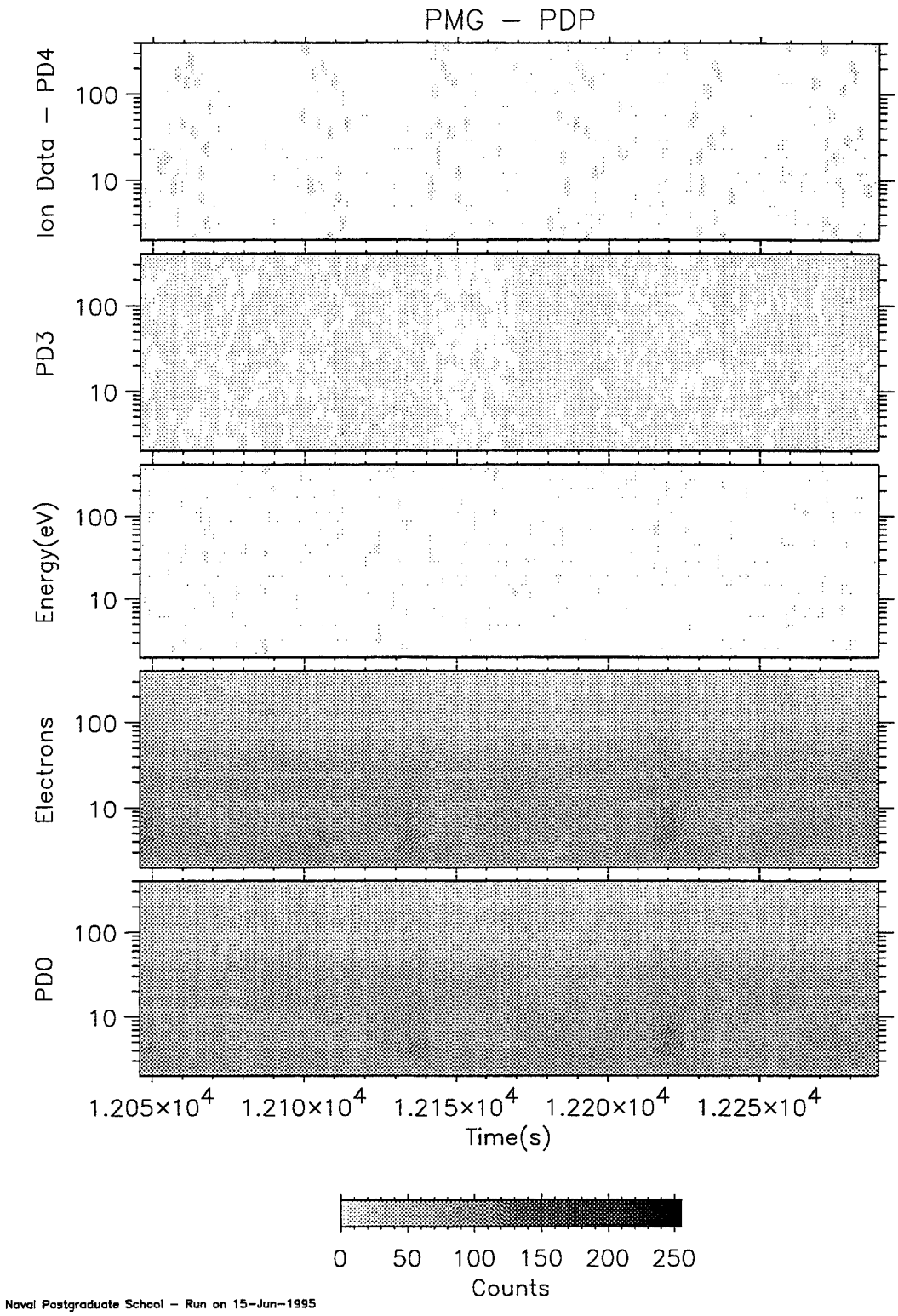
PMG – PDP
Ion Data – PD4
PD3
Energy(eV)
Electrons
PD0
100
10
1.205×10^4
1.210×10^4
1.215×10^4
1.220×10^4
1.225×10^4
Time(s)
0
50
100
150
200
250
Counts
Naval Postgraduate School – Run on 15–Jun–1995

LIST OF REFERENCES

Bekey, I., "Tether Propulsion", Washington, D. C.; P. A. Penzo, Jet Propulsion Laboratory, Pasadena, California, 1986.

Chang, C. J., "The Electrodynamic Behavior of Tether", Master Thesis, Naval Postgraduate School, June, 1994.

Chen, Francis F., "Introduction to Plasma Physics and Controlled Fusion, Volume 1: Plasma Physics", 1984.

Chlouber, D. Jost, R. J. Mccoy, J. E. Wilson, T. L., "Plasma Motor Generator (PMG) Deployment Profile and Tether Current Report", June 17, 1994.

Drell, S. D., "Drag and Propulsion of Large Satellites in the Ionosphere: An Alfven Propulsion Engine in Space", J. Geophys. Res., 70, 3131, 1965.

Gartenhaus, S., "Elements of Plasma Physics", Holt, Rinehart and Winston, Inc. 1964.

Grossi, M. D., "Historical Background Leading to the Tethered Satellite System" AIAA 24th Aerospace Sciences Meeting, January 6-9, 1986/ Reno, Nevada.

Hastings, D. E., "Theory of Plasma Contactors Used in the Ionosphere", MIT. Cambridge, Massachusetts, 1987.

Heinz, O. and Olsen, R. C., "Introduction to the Space Environment", Naval Postgraduate School, Monterey, California, 1994.

Katz, I. McCoy, J. E. Galofaro, J. and Ferguson, D. C., "Plasma Turbulence Enhanced Current Collection", Journal of Geophysical, Vol. 100, No. A2, pp. 1687-1690, February 1995.

Kerslake, W. R., "SERT II: Mission, Thruster Performance, and In-Flight Thrust Measurements", Journal of Spacecraft and Rockets, Vol. 8, No. 3, pp. 213-224, March 1971.

Lang, D. L. and Nolting, R. K., "Operation with Tethered Space Vehicles", Gemini Summary Conference, Manned Spacecraft Center, NASA sp-138, 1967.

Olsen, R. C., "Experiments in Charge Control at Geosynchronous Orbit", Journal of Spacecraft and Rocket, Vol. 22, No. 3, pp. 262, May-June 1985.

Park, D. E. and Katz, I., "Theory of Plasma Contactors for Electrodynamic Tethered Satellite Systems", Journal of Spacecraft, Vol. 24, No. 3, May-June 1987.

Rawlin, V. K. and Pawlik, E. V., "A Mercury Plasma-Bridge Neutralizer" Journal. Spacecraft, Vol. 5, NO. 7 1968.

Richmond, A. D., "The Ionosphere", "In the Solar Wind and the Earth" edited by S. I-Akasofu, and Y. Kamide,. Terra Scientific Co, Tokyo, 1987.

Sellen, J. M., "Synthesized Plasma Streams", The Review of Scientific Instruments, Vol. 36, No. 3, pp. 316-322, March 1965.

Stuart, D. G., "A Guidance Algorithm for Cooperative Tether-Mediated Orbital Rendezvous", pp. 31 - 45, MIT, 1987.

Thompson, G. C., "Design of ELF/VLF Satellite for Under the Ice Submarine Communications", Master Thesis, Naval Postgraduate School, September 1988.

Vannaroni, G., M. Dobrowolny, E. Melchioni, F. De Venuto, and R. Giovi, "Characterization of the Interaction Between a Hollow Cathode Source and an Ambient Plasma", J. Appl. Phys., October 1992.

Ward, J. W. and King, H. J., "Mercury Hollow Cathode Plasma Bridge Neutralizers" Journal. Spacecraft, Vol. 5, NO. 10 October 1968.

Yoon, S. I., "Definition Study and Model for a Tethered Sounding Rocket", Master Thesis, Naval Postgraduate School, December 1988.

INITIAL DISTRIBUTION LIST

1.	Defense Technical Information Center Cameron Station Alexandria, VA 22304-6165	2
2.	Dudley Knox Library Code 52 Naval Postgraduate School Monterey, CA 93943-5101	2
3.	Chairman Dr. William Boniface Colson Code PH Department of Physics Naval Postgraduate School Monterey, CA 93943	2
4.	Professor Richard Christopher Olsen Code PH/OS Department of Physics Naval Postgraduate School Monterey, CA 93943	5
5.	Naval Academy Library P. O. Box 90175 Tsoying, Kaohsiung, Taiwan, R. O. C.	2
6.	Jerry Jost System Planning Corp 18100 Upper Bay Road, Suite 208 Houston, TX 77058	1
7.	Jim McCoy NASA/JSC/SN3 Houston, TX 77058	1
8.	Nobie Stone NASA/MSFC Huntsville, Alabama 35812	1

9.	Jim Stanley NASA/JSC Houston, TX 77508	1
10.	Dr. Mario Grossi SAO Center for Astrophysics 60 Garden Cambridge, MA 02138	1
11.	Joe Carroll Tether Applications 1813 Gotham St Chula Vista, CA 91913	1
12.	Roy Torbert Space Science Center - IEDS Univ. of New Hampshire Durhum, NH 03824	1
13.	Dan Hastings Dept, of Aeronautics and Astronautics MIT Cambridge, MA 02139	1
14.	Ira Katz S-Cubed/Maxwell Laboratories P. O. Box 1620 La Jolla, CA 92038	1
15.	Myron Mandell S-Cubed/Maxwell Laboratories P. O. Box 1620 La Jolla, CA 92038	1
16.	Victoria Davis S-Cubed/Maxwell Laboratories P. O. Box 1620 La Jolla, CA 92038	1

17. J. R. Lilley — 1
S-Cubed/Maxwell Laboratories
P. O. Box 1620
La Jolla, CA 92038

18. Dale Ferguson — 1
NASA/Lewis Research Center
21000 Brookpark Rd
Cleveland, Ohio 44135

19. Carolyn Purvis — 1
NASA/Lewis Research Center
21000 Brookpark Rd
Cleveland, Ohio 44135

20. Cdr. Chi, Chia-hwa — 1
2F No 6, Lane 2014 Jo Lu 4th Rd
Kauoshing, TAIWAN